WL-TR-95-2079

LIQUID TRANSPORTED POWDER LUBRICANT STUDY

FINAL REPORT

Don W. Dareing, Ph.D., P.E.
The University of Southwestern Louisiana
Lafayette, LA, 70504

Michael Khonsari, Ph.D.
University of Pittsburgh
Pittsburgh, PA 15261

JUNE, 1995

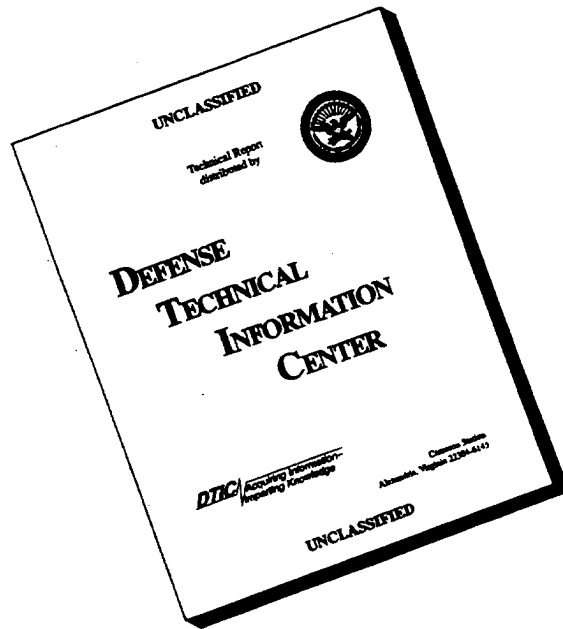FINAL REPORT FOR THE PERIOD March, 1992 - March, 1995

19960228 104

APPROVED FOR PUBLIC RELEASE; DISTRIBUTION UNLIMITED

AEROPROPULSION AND POWER DIRECTORATE
WRIGHT LABORATORY
AIR FORCE MATERIEL COMMAND
WRIGHT PATTERSON AFB OH 45433-7251
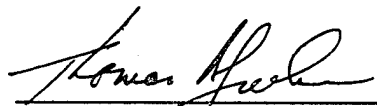
DTIC QUALITY INSPECTED 1

DISCLAIMER NOTICE

UNCLASSIFIED

Technical Report
distributed by

**DEFENSE
TECHNICAL
INFORMATION
CENTER**

DTIC Acquiring Information-
Imparting Knowledge

Cameron Station
Alexandria, Virginia 22304-6145

UNCLASSIFIED

THIS DOCUMENT IS BEST
QUALITY AVAILABLE. THE
COPY FURNISHED TO DTIC
CONTAINED A SIGNIFICANT
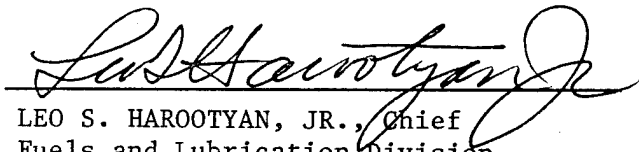NUMBER OF PAGES WHICH DO
NOT REPRODUCE LEGIBLY.

NOTICE

When government drawings, specifications, or other data are used for any purpose other than in connection with a definitely government-related procurement, the United States Government incurs no responsibility or any obligation whatsoever. The fact that the government may have formulated or in any way supplied the said drawings, specifications, or other data is not to be regarded by implication, or otherwise in any manner construed, as licensing the holder or any other person or corporation, or as conveying any rights or permission to manufacture, use, or sell any patented invention that may in any way be related thereto.

This report has been reviewed by the Office of Public Affairs (ASD/PA) and is releasable to the National Technical Information Service (NTIS). At NTIS, it will be available to the general public, including foreign nations.

This technical report has been reviewed and is approved for publication.

THOMAS A. JACKSON, Chief
Lubrication Branch
Fuels and Lubrication Division

LEO S. HAROOTYAN, JR., Chief
Fuels and Lubrication Division
Aero Propulsion and Power Directorate

If your address has changed, if you wish to be removed from our mailing list, or if the addressee is no longer employed by your organization, please notify **WL/POSL**, Wright-Patterson AFB OH 45433-7103 to help us maintain a current mailing list.

Copies of this report should not be returned unless return is required by security considerations, contractual obligations, or notice on a specific document.

REPORT DOCUMENTATION PAGE

1. AGENCY USE ONLY (Leave blank)	2. REPORT DATE June, 1995	3. REPORT TYPE AND DATES COVERED Final 3/92 – 3/95

4. TITLE AND SUBTITLE

Liquid Transported Powder Lubricant Study

5. FUNDING NUMBERS

C – F33615-92-C-2214
PE- 62203
PR- 3048
TA- 06
WU- AH

6. AUTHOR(S)

Don W. Dareing, Ph.D., P.E.
Michael Khonsari, Ph.D.

7. PERFORMING ORGANIZATION NAME(S) AND ADDRESS(ES)

The University of Southwestern Louisiana
Lafayette LA   70504-4170

The University of Pittsburgh
Pittsburgh PA   15261-5000

8. PERFORMING ORGANIZATION REPORT NUMBER

9. SPONSORING/MONITORING AGENCY NAME(S) AND ADDRESS(ES)

Aero Propulsion and Power Directorate
Wright Laboratory
Air Force Materiel Command
Wright-Patterson AFB OH   45433-7251

10. SPONSORING/MONITORING AGENCY REPORT NUMBER

WL-TR-95-2079

11. SUPPLEMENTARY NOTES

12a. DISTRIBUTION/AVAILABILITY STATEMENT

Approved for public release; distribution is unlimited.

12b. DISTRIBUTION CODE

13. ABSTRACT (Maximum 200 words)

Doubling the propulsion capacity of high efficiency gas turbine engines will require significant advances in engine lubricants and lubrication systems. Powder lubricants have bene identified as likely candidates for bearings required to operate at temperature levels well in excess of temperature capabilities of liquid lubricants. Powder lubricants can be delivered by either air or liquid carriers. This study deals with lubrication qualities of powder lubricant slurries where the carrier liquid is ethylene glycol. Traction coefficients, determined both experimentally and theoretically were the focus of this research. Experimental data was taken on the University of Southwestern Louisiana campus using a traction rig on loan from the USAF. Theoretical work was done primarily at the University of Pittsburgh.

Initial traction measurements were conducted on a standard petroleum based lubricant to provide a baseline check on the traction rig and instrumentation. The experimental results check out favorably with known results in the literature. Theoretical prediction of traction coefficients for this Newtonian fluid also correlated well with laboratory measurements. Ethylene glycol slurry data at approximately 100°F showed significantly lower traction coefficient levels than predicted theoretically. This was repeatable and deserves further investigation. Different results may be expected at elevated temperatures when the ethylene glycol is driven from the slurry.

14. SUBJECT TERMS

15. NUMBER OF PAGES

210

16. PRICE CODE

17. SECURITY CLASSIFICATION OF REPORT	18. SECURITY CLASSIFICATION OF THIS PAGE	19. SECURITY CLASSIFICATION OF ABSTRACT	20. LIMITATION OF ABSTRACT
UNCLASSIFIED	UNCLASSIFIED	UNCLASSIFIED	UL

EXECUTIVE SUMMARY

The Air Force and other government agencies, in concert with the turbine engine industry, are engaged in an initiative to double propulsion capability by 2003. Significant advances in turbine engine lubricants and lubrication systems will be required to enable the objectives of that initiative to be met. Air Force studies have identified the use of powder lubricants capable of operation at temperatures up to 1500 deg F, as a possible approach. One method of delivering powder lubricants to the bearing contact zone is via a liquid carrier. The objective of this program is to study and evaluate the performance of liquid transported powder lubricants under Hertzian contact pressures and at elevated temperatures. The evaluation of liquid transported powder lubricants in this study was based solely on the magnitude of traction coefficients.

The program focused on the use of ethylene glycol as the carrier for powder lubricants. The mathematical formulation for predicting fluid film behavior of lubricant slurries is fundamental to any powder lubricant but requires the knowledge of the rheological behavior of the particular slurry and the physical properties of the particular powder lubricant. In this study, the analysis focused primarily on graphite powder because it was the only powder lubricant used in the

experimental traction tests. The analytical part of the research was conducted by Dr. Michael Khonsari in the Mechanical Engineering Department at the University of Pittsburgh. Dr. Khonsari is uniquely qualified to address the multiphase aspects of this most difficult analytical problem; his work is summarized in Section 4 of this report and through a paper attached in the appendix. Dr. Khonsari also made significant input to the experimental portion of this study.

The experimental portion of the study was conducted at the University of Southwestern Louisiana (USL) under the direction of Dr. Don W. Dareing. The test rig used to measure traction coefficients was an Air Force rig which was moved from the Wright Laboratory to USL for use during this study. Initially all testing was to be conducted on this rig at the Wright Laboratory during summer months. By moving this rig to USL, testing could be done on a continuous basis. This proved to be a wise decision since traction testing was actually conducted and required on a continuous basis during the last 2 years of this 3 year project. One graduate student and one laboratory technician were dedicated to the traction test rig during this two year period. Discussion of rig instrumentation, operation of the rig, and surface preparation is given in Section 5.

The team approach between the two universities was very effective. While the analytical study and the experimental study were conducted separately, each study guided the other by means of; frequent phone conversations, fax transmittal of data, monthly/quarterly reports and on site visits by Dr. Khonsari who witnessed testing at USL on two occasions.

Traction testing and analytical predictions began with a standard Shell lubricant, which was a Newtonian fluid. Shell Turbo 68 was chosen because traction data were available in the literature and this data provided a good baseline check on the theory and the test rig. Khonsari's theoretical predictions check extremely well. Our experimental measurements did not exactly track the baseline data in the literature but nonetheless there was general agreement. The difference between our experimental data and the baseline data is believed to be related to the surface finish on the test disks, which is not accounted for in the theory. Several weeks were spent in refining our surface lapping procedures, recalibrating sensors, improving alignment of the disks centerlines, and retaking data. The experimental traction data were reproducible and many tests were conducted to support a high level of confidence in the test data.

Please note that one of the special aspects of this research is the assumption of line contact between the two rotating

disks. This condition was chosen to alleviate the already complex analytical elastohydrodynamic problem. Line contact eliminates the axial flow aspect of the analysis but complicates the experimental aspect of the project because of alignment.

Following an extended period of baseline testing and analysis, the project team then turned to predictions and measurements of traction coefficients of graphite slurries using ethylene glycol as the liquid carrier (see Sections 4 and 5). Theoretical predictions were based on assumed rheological behavior of the slurries at extreme pressures and on assumed physical properties of graphite at extreme pressures. Comparison of theoretical predictions with experimental measurements of traction coefficients shows a major difference between the two. The experimental data are about 1/10th the predicted value. The experimental data were consistently reproduced by testing over a 2-month period.

The level of the traction coefficients for the graphite slurry is low in comparison with typical EHD films and is on the order of what is typical of hydrodynamic films. The reason for this low level of friction may be due to molecular effects which are not covered in the theory. The fact that the level of friction is so low and is repeatable in the laboratory is significant and is worthy of further study.

Finally, the focus of this project is on liquid transported powder lubricants. Much effort was spent on the performance of the slurry itself between rotating disks associated with traction drives. At some temperature level, however, the liquid carrier boils away leaving the powder lubricant. Ethylene glycol, for example, boils at a temperature of 387 deg F at standard atmospheric pressure. At higher temperatures, the powder lubricant must perform by itself. Section 6 gives some insight as to the performance of dry graphite powder lubricants compressed to Hertzian pressure levels.

TABLE OF CONTENTS

ix

TABLE OF CONTENTS (continued)

LIST OF FIGURES

LIST OF FIGURES(Continued)

xiv

LIST OF TABLES

1.0   Introduction/Objective

The Air Force and other government agencies, in concert with the turbine engine industry, are engaged in an initiative to double propulsion capability by 2003. Significant advances in turbine engine lubricants and lubrication systems will be required to enable the objectives of that initiative to be met. Feasibility studies show that lubricants for these new engines will have to operate at temperatures up to 1000 deg F and in some cases well above this temperature level. This means that new lubricants and lubrication systems will have to be developed.

Table 1 (Wedeven and Harris, 1987) shows the temperature limitations of various liquid lubricants while Table 2 (Wedeven and Harris, 1987) shows the possible maximum operating temperatures of various powder lubricants; other powder lubricants not shown in this table are also being considered by the industry. One method of delivering powder lubricants to the bearing contact zone is via a liquid carrier.

1

Table 1

Temperature Limits for Sustained Operation

(Liquid Lubricants)

Lubricant	Temperature Limit	
	(deg F)	(deg C)
Standard mineral oils	250	120
Polyglycols	350	177
Ester	400	204
Super refined and synthetic mineral oils	450	230
Silicones	525	274

Table 2

Temperature Limits for Sustained Operation

(Common Solid Lubricants)

Lubricant	Temperature Limit	
	(deg F)	(deg C)
Molybdenum disulfide (MoS2)	750	400
Pure graphite	750	400
Graphite fluoride (CF)	1000	538
Graphite + additive	1250	675

One liquid being considered as a carrier for powder lubricants is ethylene glycol. A comprehensive description of the physical properties of ethylene glycol is given by Curme and Johnston (1952). This liquid has a clean burn and leaves little or no residue. The boiling point of ethylene glycol at atmospheric pressure is 387 degree F. This means that at operating temperatures below 387 deg F, the slurry would act as the lubricant while at operating temperatures above 387 deg F, only the powder lubricant would remain to provide lubrication to bearing surfaces.

The objective of this research is to evaluate the lubricating performance of graphite/ethylene glycol slurries in rolling contact applications by determining traction coefficients both experimentally and analytically. Experimental data were obtained with a traction rig donated to the University of Southwestern Louisiana (Lafayette) by Wright Laboratories for use specifically for this study. Analytical predictions of traction coefficients were made at the University of Pittsburgh by Professor Michael Khonsari and his students. Traction calculations are also made for dry graphite compacted within Hertzian contact regions.

2.0 Background on Rolling Contact Bearing Research

Key technical articles that form a basis for research on rolling contact bearings are identified and referenced throughout the report. This section introduces the overall problem of high temperature bearing applications.

2.1 Former Studies of High Speed, High Temperature Bearings

Bisson and Anderson (1964 a) identify key factors in the design and operation of high temperature bearings. They point out that bearing materials must have: adequate hot hardness, good oxidation resistance and good dimensional stability at high temperatures. When bearing temperatures exceed 1,000 deg F, ferrous base alloys become unsatisfactory. Super alloys containing base compositions of cobalt, chromium, and molybdenum can be used up to operating temperature of 1,500 deg F. Above 1,500 deg F, ceramic materials have to be used. Wedeven and Harris (1987) point out that extremely high shaft speed can produce inertial loading to bearing races that are of the same order of magnitude as applied bearing loads. For example it is not uncommon for shaft speeds in small gas turbine engines to operate at 50,000 rpms. At this speed level, load capacity is reduced considerably because of inertia forces. In this case operating speed becomes the bearings life limiting factor. Ceramic materials such as silicon nitride

(Si_3N_4) offer improved strength and density while also reducing inertial loading to 40 % of equal-size steel balls. Hot hardness or hardness at elevated temperature is an important material property of high temperature bearings. Hot hardness is not difficult to attain with ceramics. Values of Rc 70 can be reached at 2,000 deg F and higher. On the other hand, silicon nitride resistance to tension, torsion and bending is marginal. Care must be taken when mounting ceramic balls within steel races because differential thermal expansion and centrifugal loads induce tension stress.

2.2 Traction Testing of High Temperature Lubricants

Wedeven and Harris (1987) also give traction data for silicon nitride surfaces lubricated with and without graphite. As this work directly relates to the current research project. Their traction data are reproduced in Figure 1.

Wedeven, Pallini and Miller (1988) present the results of high temperature traction studies conducted on silicon nitride under various conditions of surface lubrication (graphite) and temperature (up to 1000 deg F). They point out that advantages of this ceramic as a rolling element material are:

    a)   low density

    b)   high temperature strength

    c)   high temperature hardness
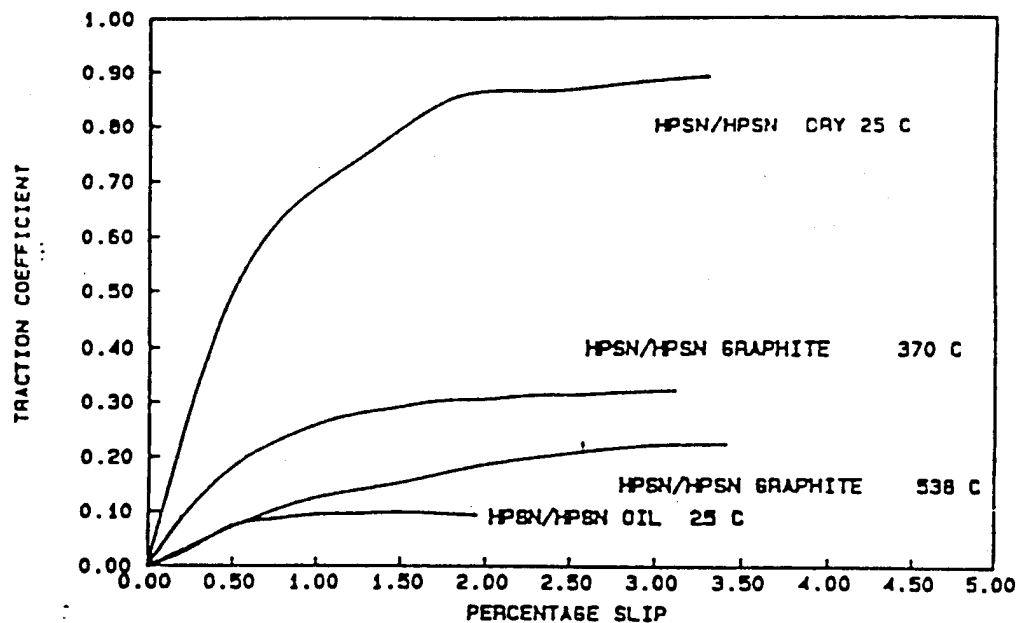
Figure 1 - Typical Traction Curves for Hot-Pressed
Silicon Nitride with and without lubrication
(Wedeven and Harris, 1987)

d) good corrosion resistance

e) high contact fatigue life

This paper focuses primarily on the wear and friction of ceramic materials. Conclusions from this work as reported by the authors are:

a) With unlubricated clean surfaces (Si_3N_4), very high maximum traction coefficients (1.0) are observed at room temperature which result in the formation of tensile stress cracks at the surface.

b) Very low traction coefficients (0.06) are found with the injection of distilled water giving EHD, micro-EHD or at least good boundary lubrication.

c) Lubrication at elevated temperatures with graphite impregnated with phosphate additives results in lower maximum traction coefficients.

d) The application of the solid lubricants by burnishing at elevated temperatures is not a benign mechanical process. The rubbing action of the graphite against silicon nitride can remove a significant amount of material by what appears to be a tribochemical and abrasive mechanism.

8

3.0 Overview of EHD Theory and Solution Methods

This section of the report puts the current research in historical perspective by reviewing the state of the art of Elastohydrodynamic theory, solution methodology and rheological models.

3.1 Newtonian Lubricants

3.1.1 Method of Solution

The evolution of the current theory of elasto-hydrodynamic lubrication of contact surfaces is documented extremely well by Dowson and Higginson (1966). The early analytical work by Martin (1916) which was based on rigid contacting surfaces and constant viscosity, did not predict film thicknesses that were significant compared with typical surface roughness.

Meldahl (1941) appears to be the first to examine the effects of surfaces deformation on fluid film pressure, but assumed constant viscosity. Gatcombe (1945) extended this work by examining the effects of pressure on viscosity within the Hertzian contact region. Others followed the work of Gatcombe and considered various viscosity-pressure functions as well

as surface deformation. However, iterative computations were long and tedious until the digital computer came along in the 1960's. Prior to the computer age, Ertel, whose work was published by Grubin (1949), developed an approximate solution to the EHD problem which showed that over most of the Hertzian pressure area the lubricating film is essentially constant.

Furthermore Ertel reasoned that if the film is a constant then the fluid film pressure distribution is the same as the Hertzian pressure without the film. The pressure prediction is in error only at the exit end of the film where the flow is restricted by the choking of the flow due to a natural reduction in film geometry.

This simple but clever mathematical manipulation gives much insight into the lubrication of Hertzian contact surfaces. The solution to the EHD problem is one of solving the hydrodynamic aspect simultaneously with the surface deformation aspect of the problem. The logical approach is to start with an assumed fluid pressure (say Hertzian) and calculate surface deformation and recalculate fluid pressures, etc. Early studies along these lines yielded EHD solutions only for lightly loaded contacting surfaces. At higher and more realistic loads, this procedure does not converge on a fluid pressure-surface deformation solution.

Dowson and Higginson (1959 and 1960) developed a method of solution based on the use of three basic numerical processes:

1) The integration of Reynolds' equation to give the pressure distribution for a known geometry.

2) The inverse solution of the Reynolds equation yielding the geometry which would engender a specified pressure-distribution.

3) The calculation of surface displacements.

In the hydrodynamic part of the calculation, process (1) is used in the long inlet sweep where the pressures are relatively low. In the high pressure region, process (2) is used. The overall computation consists essentially of a rapidly convergent iteration over the inlet side up to fairly high pressures, and successive modification of the remainder of the pressure curve to bring the results of (2) and (3) into agreement. Typical EHD pressure curves and surface deformations are given in Figure 2.

Taylor and O'Callaghan (1972) and Oh and Huebner (1973) formulate the EHD problem in terms of finite elements and also conclude that successive calculations of surface deformation, fluid pressure, etc. converges only for slightly loaded bearings. To overcome the divergence problem at the higher loads they average and limit nodal displacements and approach

11
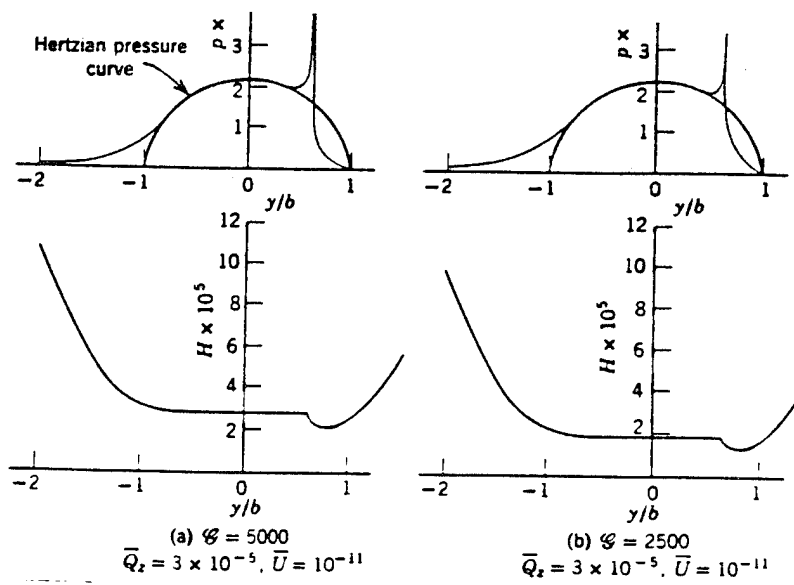
Figure 2 — Pressure Distribution and Film Thickness for Light Load Conditions (Dowson and Higginson, 1959)

the heavily loaded case from the lightly loaded side.

The finite element method offers an attractive approach to numerically handling the multiple aspects of this problem. The classic book by Zienkiewicz (1971) describes how this method can be adapted to handle nonstructural type problems. Two approaches are presented for setting up the numerical procedure. One approach depends on finding a functional to minimize. The other approach is based on the method of weighted residuals which does not require a functional.

Reddi (1969) was one of the first to apply the finite element method to the lubrication problem. This work was followed by that of Booker and Huebner (1972).

Huebner and Thornton (1982) give an outstanding presentation of the fundamentals of the finite method as applied to various engineering problems. They devote one chapter to the lubrication problem and show how Reynold's equation can be formulated for a numerical solution following the finite element method.

During the early stages of this research project, the fluid mechanics aspect of the problem was formulated in terms of the finite element method according to Huebner and Thornton (1982).

A computer program based on finite element was written during the first year of the study to handle the simultaneous solution to: (Kanumuru 1993)

  * Reynolds's equation of lubrication

  * pressure effects on viscosity

  * elastic deformation of the contacting surfaces.

The method of solution started by assuming rigid surfaces, constant viscosity throughout the film and an assumed minimum film thickness at $x = 0$. The iterative procedure built into the computer program progressed as follows:

  * calculate the pressure distribution based on rigid surfaces and a constant viscosity throughout the film.

  * calculate a viscosity distribution and surface deformations based on the initial pressure calculation.

  * solve Reynold's equation and determine the pressure distribution again using the new viscosity distribution and film thickness distribution.

  * recalculate viscosity and deflection distributions based on the latest pressure distribution and resolve Reynold's equation.

  * repeat the above steps until convergence is obtained on pressure, viscosity, and surface deformation distributions.

  * integrate under the pressure curve to determine the

corresponding applied load.

* compare this calculated load with the required applied load.

* adjust the value of the initially assumed input film thickness at x=0 based on the difference between the calculated load and the required applied load.

* repeat the above steps until the calculated load is acceptably close to the required applied load.

This method of solution worked for relatively light loads, but did not work for loads and contact stress levels normally associated with Hertzian contact, as was the case with the earlier scenario.

The smallest starting value for h_o that would lead to convergence for the select set of input data was 0.00025 inches; convergence was not achieved for ho = 0.0002 inches. The procedure described above converged to an applied load of N = 1602 lbs (see **Table 3, phase 1**). The corresponding pressure and film distribution are shown in **Figure 3**.

Applied load levels were increased by superimposing a disk translation, delta, onto the final displacement distribution at the end of the phase 1 calculation. Film shape distribution then became

$$h(x) = h_1(x) + h_2(x) + h_o + 2 d - delta \qquad (1)$$

15

as before. Convergence was achieved over the phase 2 set of calculations for a delta value of 0.00009 inches. This value of delta was determined by trial and error. Convergence was not achieved when delta was greater than 0.00009 inches. The corresponding pressure distribution and film shape are shown in Figure 4. The results from two additional sets of calculation (see Table 3, Phases 3 and 4) are shown in Figure 5 and 6.

Table 3

Convergence Data

Compliant Surfaces, Viscosity Varies with Pressure

Pure Rolling

$h_o = 0.00025$ inch

Viscosity Varying with Pressure

Phase   1.

N-load 1:	2,665.849805
N-load 2:	1,969.248386
N-load 3:	1,555.532329
N-load 4:	1,500.034222
N-load 5:	1,578.887874
N-load 6:	1,608.235093
N-load 7:	1,602.624101

Phase   2.

Delta:	0.000090
N-load 8:	2,322.996936
N-load 9:	2,391.996936
N-load 10:	2,294.532050
N-load 11:	2,167.433687

```
N-load 12:          2,119.261307

N-load 13:          2,183.020165


     Phase    3.

Delta 1:              0.000105

N-load 14:          2,406.779289

N-load 15:          2,431.184530

N-load 16:          2,356.986653

N-load 17:          2,268.447483

N-load 18:          2,253.290750

N-load 19:          2,327.864890


     Phase    4.

Delta 2:              0.000115

N-load 20:          2,495.311857

N-load 21:          2,500.901077

N-load 22:          2,417.529158

N-load 23:          2,324.178121

N-load 24;          2,321.547464

N-load 25:          2,432.336474
```
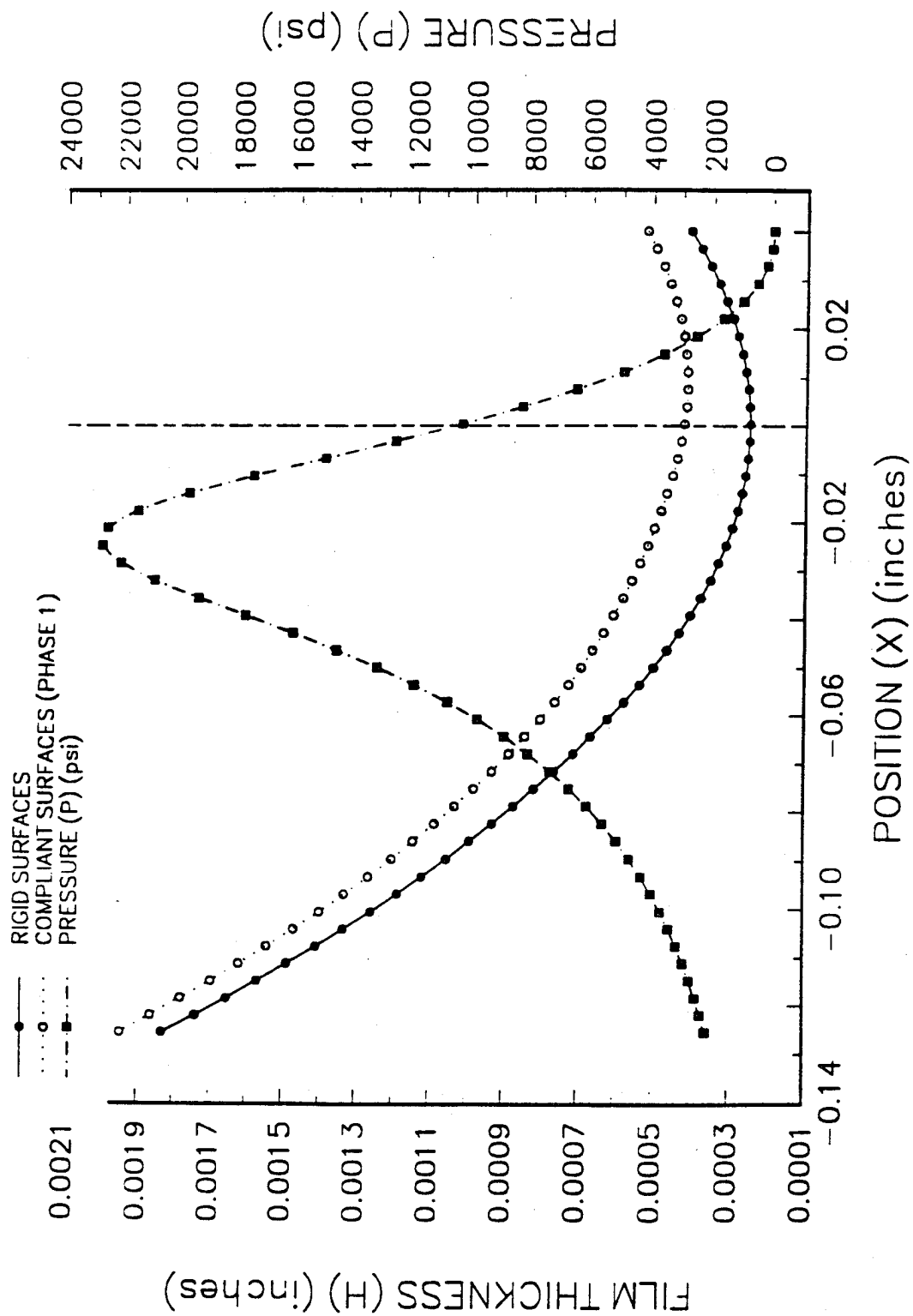
Figure 3.

ELASTO HYDRODYNAMIC RESPONSE.
(pure rolling; N_load = 1602 lb ; Phase 1).

RIGID SURFACES
COMPLIANT SURFACES (PHASE 1)
PRESSURE (P) (psi)

POSITION (X) (inches)

PRESSURE (P) (psi)

FILM THICKNESS (H) (inches)

19
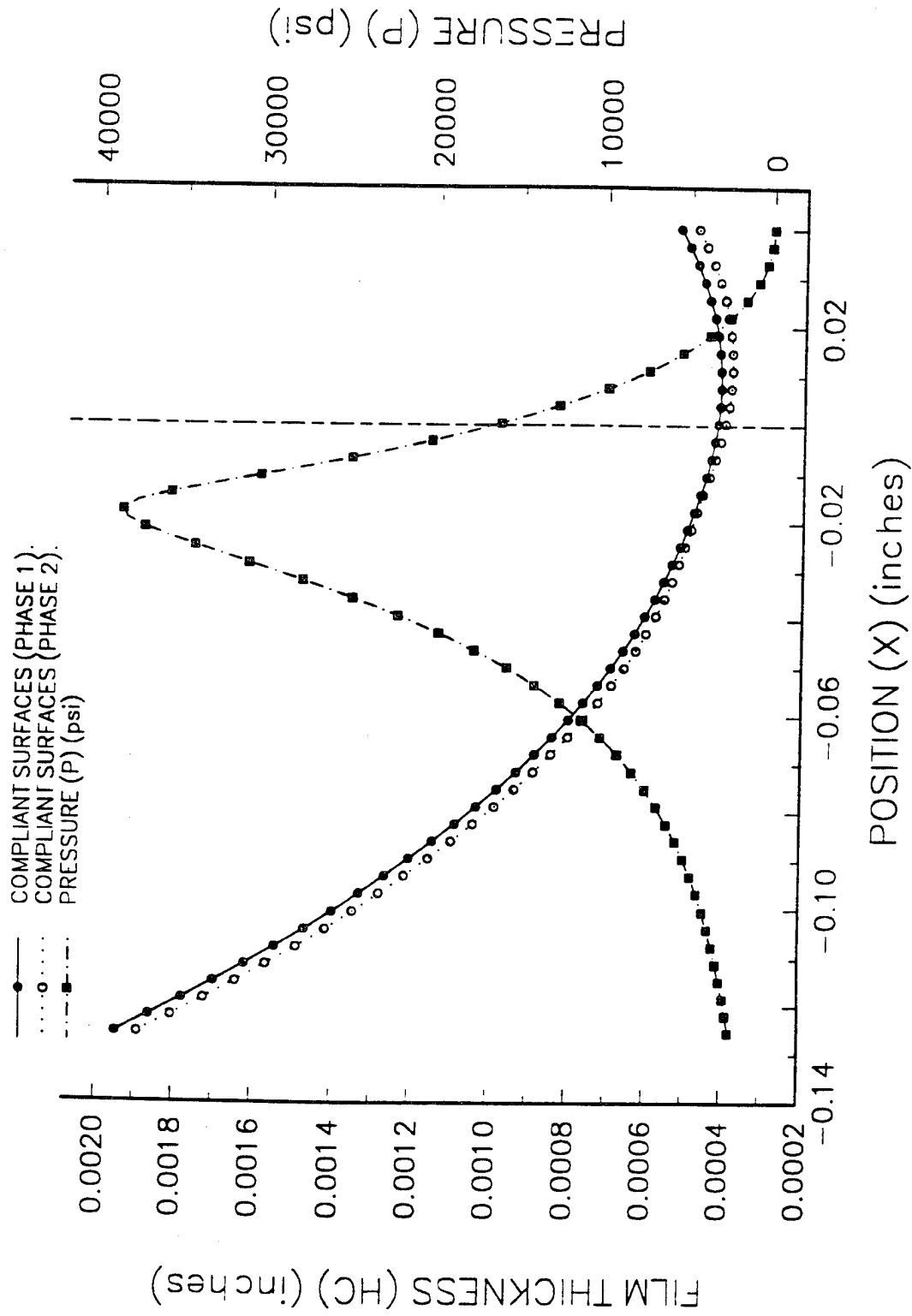
Figure 4.

ELASTO HYDRODYNAMIC RESPONSE.
(pure rolling; N_load = 2183 lb ; Phase 2).
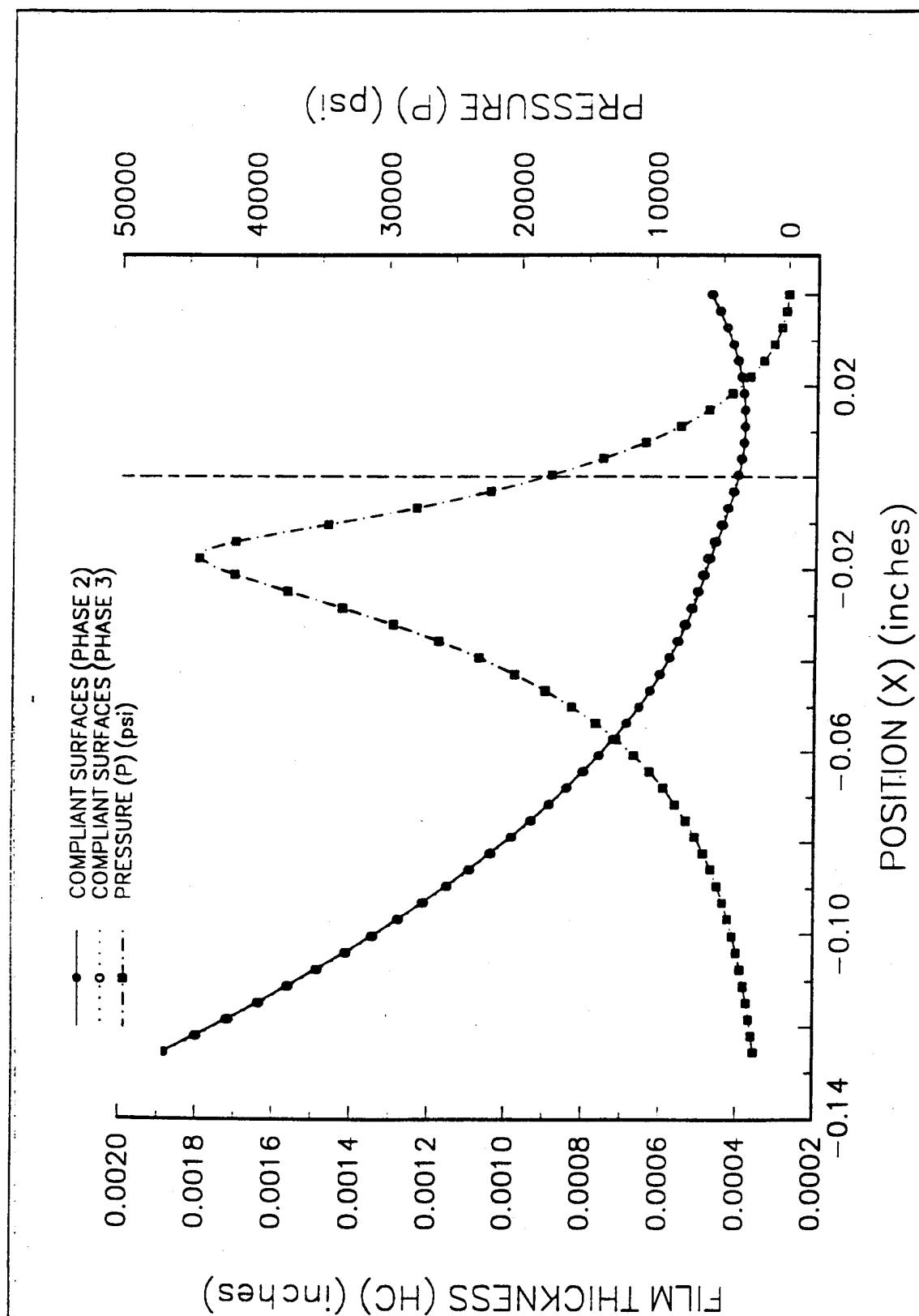
Figure 5.

ELASTOHYDRODYNAMIC RESPONSE.
(pure rolling; N_load = 2327 lb; Phase 3).
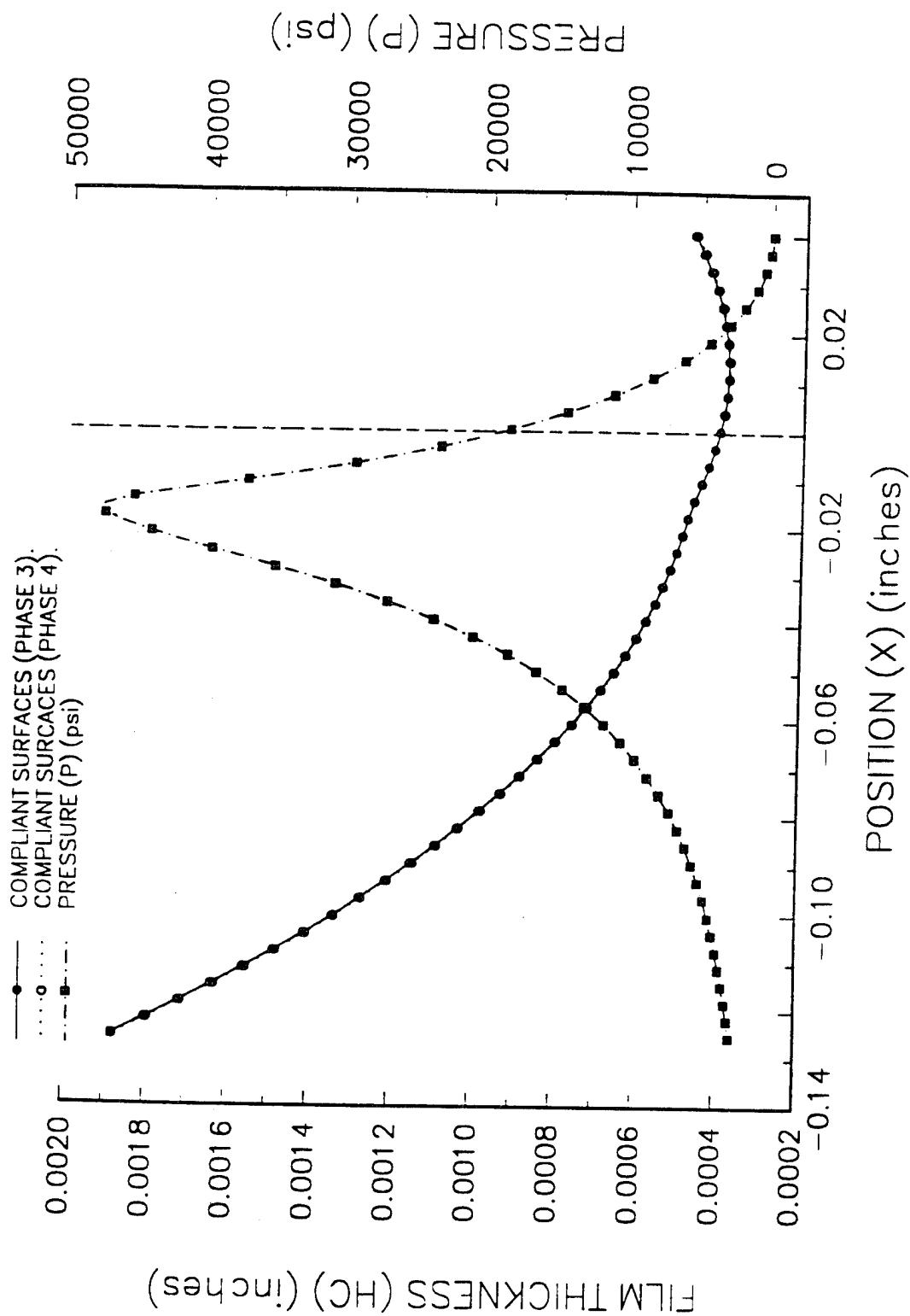
Figure 6.

ELASTO HYDRODYNAMIC RESPONSE.
(pure rolling; N_load = 2432 lb ; Phase 4).

The maximum pressure level of near 50,000 psi is relatively low in comparison with typical values of 400,000 psi in Hertzian contact.

3.1.2 Maxwell Fluids (Viscoelastic Materials)

The above mathematical discussion of EHD films is based on the assumption that the lubricant is Newtonian but has a viscosity which varies with pressure. This approach gives predictions of film thickness that compare favorably with experimental data. However, laboratory measurements of traction gives data that differ somewhat from predicted tractions at high slip velocity ratios. One way to explain this difference is to assume that the Newtonian fluid behaves as a viscoelastic material or a Maxwell (1868) fluid. A Maxwell fluid is one for which the total strain is the sum of viscous strain rate and elastic strain. The relation between shear stress and strain is

$$\frac{du}{dy} = \frac{1}{\mu}\tau + \frac{u}{G}\frac{d\tau}{dx} \qquad (2)$$

where

μ - viscosity

G - shear modulus

u - velocity in x direction

τ - shear stress

This shear stress-shear rate relationship would seem to apply to very viscous fluids and/or fluids that are sheared at a fast rate. Under these conditions Newtonian fluids exhibit a certain amount of elasticity. Since Newtonian fluids become extremely viscous within Hertzian contact regions, the Maxwell model has been used to explain traction measurements of contact surfaces lubricated with Newtonian fluids. The general shear stress-strain behavior of viscoelastic materials is illustrated by Nadai (1963, p 158) (see Figure 7).

Tanner (1960) and Burton (1960) compared the load carrying capacity and friction characteristics of Newtonian fluids verses Maxwell fluids and determined that shear elasticity can affect these parameters by a sizable amount. In general load capacity is lowered and friction is increased by viscoelastic effects.

The analyses were based on rigid cylindrical surfaces having constant tangent velocities due to rotation.

Johnson and Tevaarwerk (1977) developed a method of approximating traction in elastohydrodynamic oil films which is in close agreement with experimental measurements. The authors use a nonlinear Maxwell model,
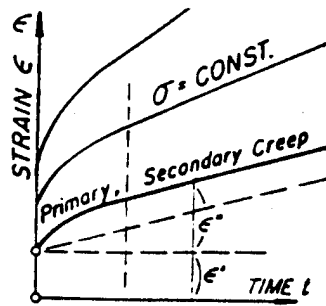
FIG. 7-1. Primary and secondary creep in creep curves.
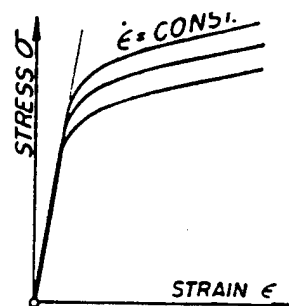
FIG. 7-2. Constant-strain-rate tests.
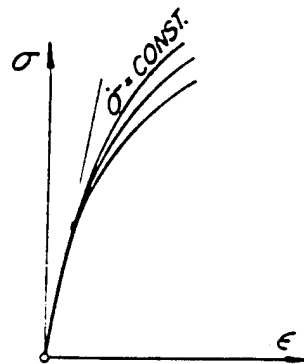
FIG. 7-3. Constant-rate-of-stress tests.
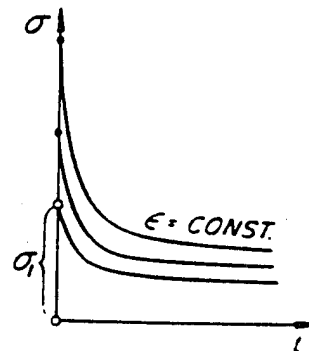
FIG. 7-4. Relaxation of stress.

Figure 7. - Viscoelastic Behavior of a Maxwell Material (Nadai, 1963)

$$\dot{\gamma} = \dot{\gamma}_e + \dot{\gamma}_v = \frac{1}{G} \frac{d\tau}{dt} + F(\tau) \qquad (3)$$

where

    $\dot{\gamma}$ - Shear strain rate

    $F(\gamma)$ - non linear viscous function

    G - shear modulus

to describe the rheological behavior of Newtonian fluids at Hertzian level fluid pressures. The first term accounts for linear elastic strain, while the second term accounts for the nonlinear viscous component of the equation, the Eyring 'sinh law' was taken as the nonlinear viscous function. This constitutive equation is expressed in terms of three independent fluid parameters: the shear modulus G, the zero-rate viscosity η and a reference stress τ_0. These parameters vary with pressure and temperature and are determined experimentally as explained in the paper. The approximation comes from using average pressure and temperature across the film to determine the three independent fluid parameters. Figure 8 illustrates typical traction curves predicted by this method.
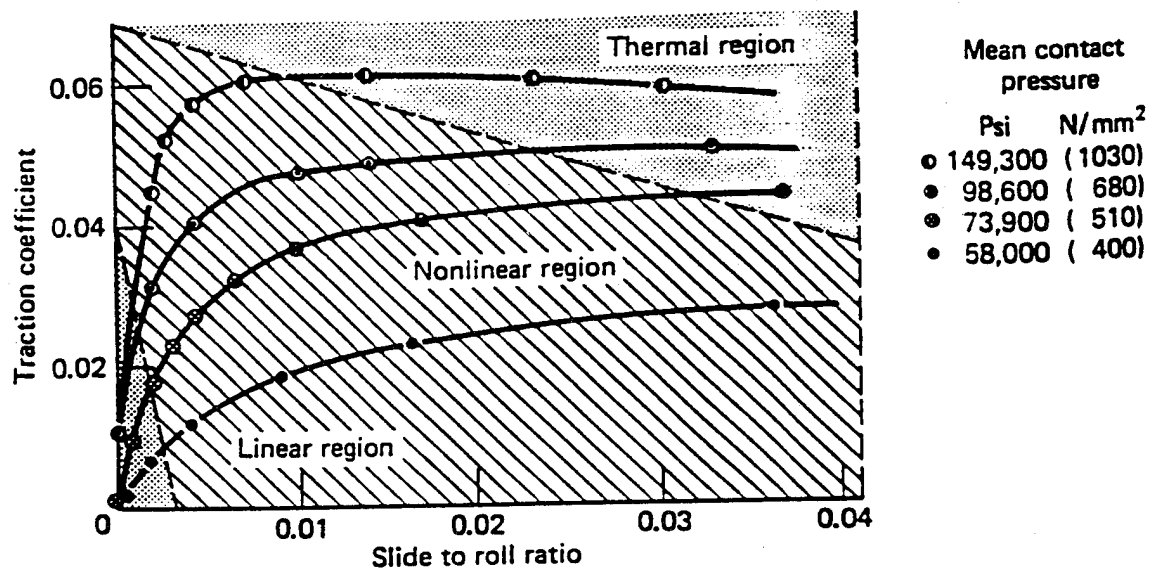
Figure 8. Typical Traction Curves

This method of predicting traction curves for Newtonian fluids is direct and gives predictions that are in good agreement with experimental traction data. This work is expanded further by Tevaarwerk and Johnson (1979).

Bair and Winer (1979) measured the shear stress-shear strain behavior of different liquids under pressure in the amorphous solid state and near the liquid-solid transition. Experimental data show that liquids under Hertzian pressure levels have a limiting shear stress at large shear strains and behave as a plastic solid. This limiting shear stress is a material property which establishes the maximum attainable shear stress in EHD contacts and in traction test rigs. This work supports the speculation for many years that lubricants have a limiting shear strength in EHD contacts. This work explains why traction in EHD contacts seldom exceed one tenth of the average pressure, a phenomena which has not been explained by the assumption of a Newtonian viscous fluid with pressure dependent viscosity.

Bair and Winer (1979 b) use their laboratory measurements of shear stress verses shear rate at Hertzian pressures levels to develop a rheological model defining the behavior of Newtonian fluids between Hertzian contact surfaces. Their model is also a modification of the Maxwell model for visco-plastic materials. The proposed model or relation between shear

stress and shear strain rate is

$$\dot{\gamma} = \frac{1}{G_\infty} \frac{d\tau}{dt} - \frac{\tau_L}{\mu_o} \ln(1 - \frac{\tau}{\tau_L}) \qquad (4)$$

where

μ_o - low shear stress viscosity

G_∞ - limiting elastic shear modulus

τ_L - limiting yield shear stress

Methods for determining these properties are explained in the paper and the paper references. The authors also show how to apply this rheological model to EHD traction predictions. Predicted traction curves compare favorably with traction curves measured by Johnson and Tevaarwerk (1977).

3.2 Non Newtonian Lubricants

3.2.1 Rheological Models

The hyperbolic sine function has been used for many years to express the relation between shear stress and shear rate for ductile metals flowing at high temperatures. This function

29

is expressed as follows

$$\gamma = \gamma_1 \sinh \frac{\tau}{\tau_1} \qquad (5)$$

where γ_1 and τ_1 are material constants at a given temperature.

It was first proposed by Prandtl (1928) as early as 1913 and closely fits experimental data taken on ductile metals loaded at various shear rates and at elevated temperatures. The hyperbolic sine law was independently introduced by Eyring (1936).

Bell (1962) predicted lubrication film thicknesses for Hertzian contacts by modelling the rheology of Newtonian lubricants as a Ree-Eyring (1955) fluid. The shear stress-shear strain relation for a Ree-Eyring fluid is defined by

$$\tau = \frac{X}{\alpha} \sinh^{-1} (\beta\dot{\gamma}) \qquad (6)$$

where X and β depend on fluid pressure as follows:

$$X = X_o e^{\gamma_1 P} \qquad\qquad (7)$$
$$\beta = \beta_o e^{\gamma_2 P}$$

and γ, X_o, β_o, γ_1, γ_2 are constants which depend on temperature.

Predicted film thicknesses using this rheology model are close to those predicted by the Grubin theory if shearing rates are low. At high shearing rates, film thicknesses predicted by the two theories diverge.

Sasaki, Mori and Okino (1962) compared fluid film pressures corresponding to a Bingham plastic lubricant with pressures corresponding to a Newtonian fluid. Film geometry was based on two rotating cylinders in contact; contacting surfaces were assumed to be rigid. Their calculations show that the load capacity and friction for the two types of fluids coincide approximately at high shear rates when the viscosity of the Newtonian fluid is the same as the plastic viscosity of the Bingham fluid.

Dareing and Dayton (1992) measured the rheological behavior of two different powder lubricant slurries and compared the

laboratory with

     a) power law

     b) Bingham plastic

     c) hyperbolic

rheology models. Shear stress verses shear rate plots are given in Figure 9. The two slurries were: 1) graphite/ethylene glycol mixed with a 1:8 ratio by weight and 2) molybdenum disulfide/ethylene glycol mixed with a 1:1 ratio by weight. Rheology constants for each of the fluid models were determined from the laboratory data. Velocity profiles corresponding to each of these fluid models are predicted for pressure induced flow between two parallel surfaces.
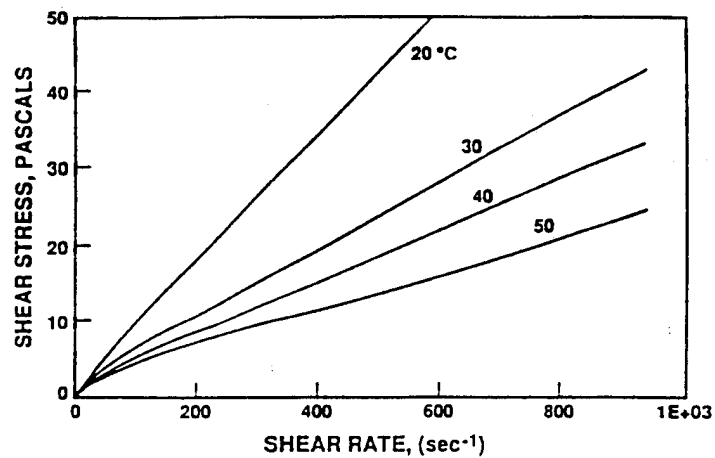
Figure 9-1. Rheology Data for a Molybdenum Disulfide -
Ethylene Glycol Slurry (1:1 mixture)
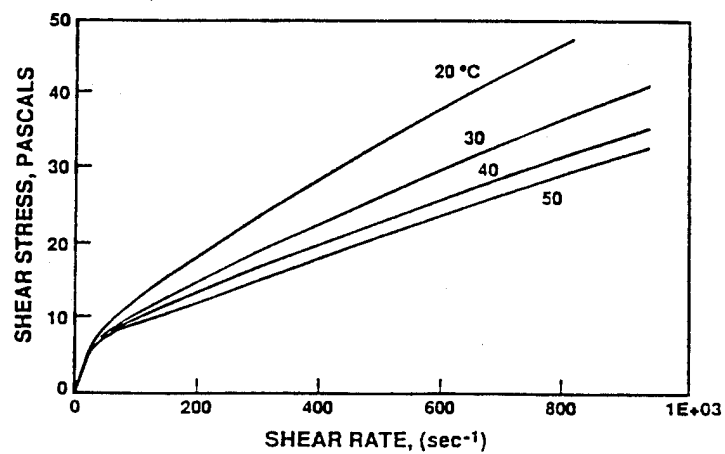
Figure 9- 2. Rheology Data for a Graphite-Ethylene Glycol
Slurry (1:8 mixture)

Figure 9.- Rheology Behavior of Two Powder Lubricant Slurries
(Dareing and Dayton, 1992)

4.0   Non-Newtonian Elastohydrodynamic Lubrication Analysis

4.1   Introduction

The objective of this research was to derive the appropriate governing equations and perform pertinent numerical simulations to predict the performance of the Elastohydrodynamic Lubrication (EHL) line - contact problems with lubricants consisting of a mixture of solid lubricants with a carrier fluid. The behavior of carrier fluid is assumed to be characterized as linearly viscous or what is commonly known as a Newtonian fluid. When mixed with particles mainly consisting of solid lubricants - such as MOS_2 - the lubricant behavior as a whole can no longer be characterized as Newtonian.   A model that can be used for predictive purposes must,   therefore,   properly   describe   the   deformation characteristics of the mixture (cf. Dai & Khonsari, 1991, 1993). It is indeed crucial to point out that this deviation, from what the Newtonian formulation predicts, is known to play an important role on the bearing performance even when the solids content added to the lubricant is small (as low as 1 percent by weight). Research shows that both the friction and the thermal field are altered in the presence of solid par-

ticle (cf. Khonsari & Esfahanian, 1988). These problems are classified as thermohydrodynamic.

The present research is concerned with much higher solids concentrations. Prescribed by experimental work of Dareing & Dayton (1992), the mixture ratio of the solids to carrier fluid can be as high as one to one by weight, although the high solids content used in the experiment was perhaps intended to register a measurable signature of the mixture shear stress as function of the shear strain rate. The measurements of Dareing & Dayton yielded deformation behaviors which they conveniently characterized by three rheological models: the ideal Bingham plastic, the power law, and the so-called hyperbolic law. The experimental results presented were fitted to each of the aforementioned models. Data were presented over a certain temperature range and at relatively low pressures. The implication of these results will be discussed later.

Let us now turn our attention to the three rheological models. The Bingham plastic is commonly used for materials with high solid concentrations. Typical examples are household toothpaste which requires an initial shear stress in order for the flow to commence. Also, recent research dealing with the rheological characteristics of grease recommend a *modified* Bingham plastic formulation as a vital model for the material

deformation (Bair, 1993). Once the flow begins, its behavior is similar to what the Newtonian model predicts so that the shear stress increases linearly with increasing shear rate. The Bingham plastic model predicts the formation of a plug flow where the fluid velocity profile becomes flat in the central region, in a manner that one would expect a solid to move. This is generally referred to as the formation of a central core. The formation of the core makes the analytical derivation much more complicated. In comparison, the power-law model is easier to deal with. In general, a power-law formulation can be used to characterize many non-Newtonian fluids, both shear-thinning and shear-thickening. The hyperbolic law, as introduced by Dareing & Dayton, is less common. However, it appears to yield the best fit to the experimental data compared to either the Bingham plastic and the power-law models under the conditions tested. For the purpose of EHL analysis, it was decided to mainly concentrate on the power-law model. The power-law model is, in fact, what Batra and Dareing used in their recent paper dealing with the flow of mixtures in journal bearings (cf. Batra & Dareing, 1993). However, as described in the following section, the governing equations are derived in a manner that could handle any "simple" non-Newtonian constitutive equation. Therefore, the hyperbolic equation can also be treated using the generalized formulation of the Reynolds equation.

The outline of Section 4.0 is as follows. In Section 4.2, a complete account of the governing equations together with a brief discussion of numerical solution procedure is given. Results of computer simulations and comparison with a number of experimental results are presented in Section 4.3. The summary and concluding remarks with recommendation for future research are discussed in Section 4.4.

4.2. Governing Equations

The most important equation of interest is that of the Reynolds equation which describes the pressure profile in the fluid. The classical Reynolds equation must be modified to take the non-Newtonian behavior of the lubricant into account. In a recent work, sponsored by the Air Force and the University of Pittsburgh, it was shown that it is possible to derive a so-called generalized Reynolds equation that can accept any constitutive equation for a simple fluid (cf. Khonsari, 1992). This formulation appropriately treats the viscosity as a scalar quantity based on the second invariant of the strain-rate tensor. This formulation of a generalized viscosity is frame-indifferent -- a property that many of the existing rheological models tend to violate. Another beauty of the formulation is that the derived generalized Reynolds equation can be extended to include thermal effects. A complete elasto-thermohydrodynamic (ETHD) analysis requires one to

include the viscosity variation as a function of temperature and space. For the problem under consideration, the space variation is bidirectional: both along the film thickness and in the direction of rolling. Since the variation of viscosity with temperature is nonlinear, ETHD computations are considerably more complicated.

4.2.1   Generalized Reynolds Equation

The generalized Reynolds equation reduces to the following equation for an EHL line-contact problem:

$$\frac{d}{dx}\left[\rho h^3 \left(\frac{1}{\mu_{e2}} - \frac{\mu_{eo}}{\mu_{e1}^2}\right) \frac{dp}{dx}\right] = \frac{1}{2}(U_2 + U_1)\frac{d}{dx}(\rho h) + \frac{1}{2}(U_2 - U_1)\frac{d}{dx}\left[\rho h\left(1 - 2\frac{\mu_{eo}}{\mu_{e1}}\right)\right] \qquad (8)$$

where μ_{ei} are the "equivalent" viscosity parameters defined as given below:

$$\frac{1}{\mu_{ei}} = \frac{1}{h^{i+1}}\int_0^h \frac{y^i}{\mu^*}\,dy \qquad (9)$$

where μ^* is what we shall refer to as the apparent viscosity. To simulate the above equation, once the rheological equation is specified, one must first establish a relationship for the apparent viscosity in terms of the shear strain.

38

4.2.2   Power-Law Model

Consider the constitutive equation of power-law given below:

$$\tau = \mu \dot{\gamma}^n \tag{10}$$

In terms of our apparent viscosity formulation, we have:

$$\tau = \mu^* \dot{\gamma} = \mu |\dot{\gamma}|^{n-1} \cdot \dot{\gamma} \tag{11}$$

Therefore, the apparent viscosity for the power-law is:

$$\mu^* = \mu |\dot{\gamma}|^{n-1} \tag{12}$$

It is worthwhile mentioning that by setting the index of the power law to n = 1, one can easily recover the Newtonian results.

4.2.3   Hyperbolic-Law Model

To illustrate the applicability of the formulation to other rheological equations, consider the constitutive equation for the hyperbolic law shown below.

$$\tau = [(\mu\dot{\gamma})^2 + 2\mu\tau_o\dot{\gamma}]^{1/2} \tag{13}$$

which can be written in the form:

$$\tau = \tau_o [\lambda'^2 + 2\lambda']^{1/2} \tag{14}$$

39

where $\lambda' = \mu \gamma / \tau_o$. In terms of the apparent viscosity, the above equation is

$$\mu^* = \mu \left[1 + \frac{2}{\lambda} \right]^{1/2} \tag{15}$$

where $\quad \lambda = \mu \left| \dot{\gamma} \right| / \tau_0$ (16)

The above formulation enables one to numerically solve the same Reynolds equation for both of the models of interest. It is important to point out, however, that the derivation of the elements of the Jacobian matrix requires some further manipulation of the terms.

4.2.4 Mixture Property Variation as a Function of Pressure and Temperature

A very crucial input for the simulations is the variation of properties as a function of pressure and temperature. For most lubricants, the Roelands' relationship is considered to be acceptable. However, the validity of the Roelands' visco-pressure-temperature equation for a mixture must be addressed by proper experimentation. The Roelands' equation used in our

simulations takes on the following form:

$$\mu = \mu_0 \exp\left[[ln\mu_o + 9.67] \left[-1 + (1+ap)^z \left(\frac{T+135}{T_o+135}\right)^{so}\right]\right] \quad (17)$$

where z, so, are constants, (see Tables 4 and 5), *a* is equal
to 5.1x10^9, and *p* is the elastohydrodynamic pressure of the
fluid.

4.2.5   Contribution of the Particle Deformation Under the
        Action of Normal Load

One potentially important aspect of EHL modeling of powder
slurries is the deformation of particles in addition to that
of the bounding surfaces. Clearly, evaluation of deformation
associated with the rolling bodies is a necessary component of
all EHL computations. However, assessment of particle defor-
mation is unique to the study of powder slurries. Let us now
examine the implications of particle deformation in some
depth.

The main reference guiding our theoretical development is the
unique experimental work of Dareing and Dayton (1991). The
experiments were conducted under atmospheric conditions not
necessarily representative of an EHL situation, hence the
uncertainties with the viscosity-pressure coefficients
described earlier.   Another important fact associated with

41

high pressure and high stress situations - typical of EHL problems - is that particles may indeed undergo a significant amount of deformation. The deformation can be either elastic or plastic depending on the operating conditions. The question that arises is whether through this deformation particles could carry a significant amount of load and that whether this additional load could alter the predication of the traction coefficient of the bearing. While the answer to this question is best suited to experimental verification, it is nonetheless, a problem that a careful analyst must take into consideration. To this end, we envision the following situation.

Consider a single spherically-shaped particle placed in the contact region. The particle is bridged across the gap and is assumed to be soft and nonabrasive so that it would deform. The load on a single particle assuming purely *elastic deformation is*:

$$w_{i_{el}} = \frac{1}{3}[d_p - h(x)]^{\frac{3}{2}} d_p^{\frac{1}{2}} \frac{E_{ps}}{2} + p(x) v_p A_{i_{el}} \tag{18}$$

where d_p is the particle diameter, $p(x)$ is the pressure distribution , and v_p is the particle Poisson ratio. The parameter E_{ps} represents the equivalent elastic modules of the particle and the contacting surface defined below:

$$\frac{1}{E_{PS}} = \frac{1}{2}\left[\frac{1 - v_p^2}{E_p} + \frac{1 - v_s^2}{E_s}\right] \tag{19}$$

42

Now the particle mean contact pressure, p_m , is

$$p_m = \frac{w_{i_{\bullet 1}}}{\pi a^2} \qquad (20)$$

where a is the radius of circular contact area determined from the expression:

$$a = \left[\frac{3}{4} \frac{w_{i_{\bullet 1}} d_p}{E} \right]^{\frac{1}{3}} \qquad (21)$$

To recapitulate, equation (18) allows one to determine the load on a *single* particle with a given diameter d_p assuming that the particle deformation is purely elastic. Once this is determined, the average contact pressure P_m can be computed from equation (13), assuming that contact area is perfectly circular. This information can be used if one is willing to perform a more in-depth analysis to account for *plastic deformation*, should the loading condition be such that it would occur. Unfortunately, plastic deformation analyses are by no means trivial. In fact, it could be a worthwhile project in its own right. In what follows, we present a simple and admittedly approximate analytical method for determining the contribution to plastic deformation.

The determination of load carried by particles due to plastic deformation is based on the assumption that there exists a shift load, under which the same value of contact size and

43

average contact pressure would be given either using elastic deformation model or using plastic deformation model (cf. Archard,1980). Consider the situation of plastic deformation in a manner similar to the Brinell hardness test. The radius of circular contact area due to plastic deformation can be approximated by:

$$w_{i_{pl}} = \pi a^2 H_d \qquad (22)$$

where H_d is the hardness of particle. Comparing equation (15) with the expression for the average contact pressure due to elastic deformation given in equation (13), the shift load of an individual deformed particle can be related to the particle hardness in the following fashion:

$$w_{i_{pl}} = \frac{9}{16}\pi^3 H_d{}^3 \left(\frac{d_p}{E_{ps}}\right)^2 \qquad (23)$$

The above expressions were derived for a single deforming particle. The load-carrying capacity due to deformation of all particles that exist in the EHL contact is, therefore, determined by the double summation of:

$$w_p = \sum_1^{N_z} \sum_1^{N_x} w_i \qquad (24)$$

where N_x, N_z are the number of deformed particles in x and z

44

directions, respectively, viz:

$$N_j = l_j \sqrt{\left(\frac{V_f}{l_x l_z}\right) \frac{6\lambda_w}{\pi d_p^3} \frac{(\rho_f/\rho_p)}{[1-\lambda_w(1-\rho_f/\rho_p)]}} \qquad j=1,2 \qquad (25)$$

where, λ_w is the concentration of particles by weight; V_f is the volume of the powder slurry within the region where the contact of particles with bounding surfaces takes place; l_j is the effective length along which the particles deform. The subscript $j=1$ denotes x direction, $j=2$ denotes the z direction where $l_2=1$ (unit width) is assumed.

Finally, the total load composed of load carried by the powder slurry is given by:

$$W_T = W_f + W_p \qquad (26)$$

It is to be emphasized that in the theoretical development heretofore, we have tacitly assumed that particles are uniformly distributed in the contact zone and that they do not pile up at the inlet and that they do not collide with one another. Clearly the consideration of elastic/plastic deformation associated with the particles adds significantly to the complexity of the problem. Nonetheless, realistic evaluation of bearing performance requires paying attention to such details. As a final note in this subject, we must bear in

mind that additional particle parameters such as hardness and the modulus of elasticity are needed. These would present some additional uncertainties since such property data are scarce.

4.2.6 Viscous Dissipation and Shear Heating

To determine the slurry temperature profile, we must turn our attention to the energy equation. In the energy equation, the diffusive heat flux for a mixture is contributed by three individual terms (cf. Rohsenow et al.,1985): (1) heat-conduction as described by the Fourier's law, i.e., $- k \nabla T$, where k denotes the thermal conductivity of the mixture; (2) the contribution due to interdiffusion of species, given by Σ $j_i i_i$, and (3) diffusional conduction term which is of second order and therefore in most situations is negligibly small. The energy equation for a mixture is:

$$\rho \frac{Di}{Dt} = \frac{Dp}{Dt} + \nabla \cdot k \nabla T - \nabla \cdot \left(\sum_i j_i i_i \right) + \Phi + q \qquad (27)$$

where Φ is the viscous dissipation, q is a source term representing the rate of heat generation per unit volume, and i is the enthalpy expressed as:

$$i = \epsilon_i + \frac{p}{\rho} \qquad (28)$$

46

where ϵ_i is the internal energy per unit mass. Assuming that no chemical reaction occurs between the powder and the carrier fluid, i.e., the mixture nonreacting, the term ($\Sigma\ j_i\ i_i$) becomes negligible. We shall next express the energy equation in terms of temperature using the following relationship:

$$\frac{Di}{Dt} = \frac{1}{\rho} (1 - \beta\ T) \frac{Dp}{Dt} + c_p \frac{DT}{Dt} \tag{29}$$

where β is defined as:

$$\beta = -\frac{1}{\rho}\left(\frac{\partial \rho}{\partial T}\right)_p \tag{30}$$

Therefore, for a steady-state, laminar flow, the energy equation reduces to the following equation

$$k\frac{\partial^2 T}{\partial y^2} = \rho\ c_p u \frac{\partial T}{\partial x} + u\frac{T}{\rho}\left(\frac{\partial \rho}{\partial T}\right)_p \frac{dp}{dx} - \mu^* \dot{\gamma}^2 - q \tag{31}$$

As a result, contact with the bounding surfaces in addition to normal stress, the deformed particles may experience slippage between the bounding surfaces. This will give rise to the existence of a shear heating which is represented by the heat source q in the energy equation. The *total* heat generated due to shear heating between the deformed particles and the bounding surfaces is:

$$Q = 2\ f_p w_p \left| U_i - u_p \right| \tag{32}$$

47

where U_i is the velocity of the surfaces $(i=1,2)$ and f_p is the friction coefficient between a particle and the surface. The parameter u_p represents the particle velocity, which is

assumed to be at the average of the surface velocities, viz:

$$u_p = \frac{1}{2}(U_1 + U_2) \qquad (33)$$

The heat source per unit volume is therefore:

$$q = \frac{Q}{V_f} \qquad (34)$$

where V_f was defined in section 2.4.

The boundary conditions for the energy equation are:

$$T_i(x) = T_0 + \frac{1}{\sqrt{\pi \rho_i c_i k_i U_i}} \int_{-\infty}^{x} -k \frac{\partial T}{\partial y} \frac{ds}{\sqrt{x-s}} \qquad i=1,2 \qquad (35)$$

4.2.7 Traction Coefficient

The traction force of the powder slurry is composed of two components: one comes about because of the integrated effect of slurry viscous shear stress over the appropriate length and the other is due to contribution of the shear stress between particles and surfaces. The traction coefficient, f, is simply the ratio of the traction force over the total load, viz.:

48

$$f = \frac{1}{W_T}\left[\int_{-\infty}^{x_b} \mu^*\dot{\gamma}\, dx + f_p w_p\right] \qquad (36)$$

4.2.8   Numerical Solution Procedure

To solve the governing equations, a computer program was developed. The solution scheme utilizes the method of finite difference and is highly iterative. For the case of a pure oil, the program solves the generalized Reynolds equation and the elasticity equations which govern the deformation of the bounding surfaces to determine the pressure distribution and the film thickness profile. The energy equation is also solved simultaneously with the Reynolds equation to accurately characterize the effect of property variation with the temperature rise in the EHL contact. In the case of a mixture, the deformation of the particles (elastic or plastic) are also computed in order to assess the load-carrying capacity of the particles in accordance to the theory described in Section 4.2. The mixture computations are, therefore, considerably more involved.

The output of the program includes a complete prediction of the film thickness (central and minimum), pressure distribution (including the magnitude and location of the pressure spike), temperature distribution along the direction of the sliding and through the film gap (which includes a

49

prediction of the rollers surface temperatures and the mean film temperature at any location in the contact region), and finally the traction results as a function of the slip ratio. The details of the formulations of the Jacobians and the numerical solutions are discussed in a recent paper by Khonsari & Hua (1994) for the case of pure oil which obeys the Bair-Winer Constitutive equation.

4.3. Results and Discussion

4.3.1 Comparison of Theoretical Simulation and Experimental Measurements

Considerable amount of time and effort was invested in validating the numerical simulations by comparing the theoretical predictions with the experimental results conducted by USL using the Air Force traction rig. Before the mixture simulations could be performed, however, a set of "benchmark" results for "clean" oils were needed for the purpose of authenticating the theoretical results by means of comparison with the traction measurements at the University of Southwestern Louisiana (USL). The theoretical development of EHL line contact problem was implemented using the Bair-Winer constitutive equation for oils free of particulate matter. This constitutive equation is based on extensive amount of laboratory experimentation. It correctly characterizes the

50

lubricant behavior with the regard to the limiting shear stress which has been observed in experiments with oils under EHL conditions (cf. Bair & Winer, 1979). It was decided to utilize the Military Oil (MiL-L-7808) for this purpose. Several theoretical and experimental results for MiL-L-7808 were presented in the *quarterly reports*. The general behavior of the solution and the order of magnitude of the measured versus theory were reasonably close. However, the slope of experimental traction curves tended to show a higher gradient at very small slip ratios. This trend persisted at higher loads.

To remove possible source of uncertainty, the following action plan was decided upon and executed:

1. Instrumentation was considerably improved so that measurements at low-slip ratio could be accurately assessed. This required fitting the rig with an accurate tachometer by which the speeds of the master and slave test discs could be measured and checked.

2. To remove uncertainties regarding possible effect of surface roughness, the surfaces were lapped and the surface roughness was measured to insure that it is below the film thickness computed theoretically.

3. To check the theoretical predictions as well of the

experimental results, the tests were repeated under pertinent operating conditions and using a lubricant for which independent published traction data are available.

4.3.2   Comparison to Published Literature

The literature contains experimental results of other researchers that could be used as an additional validation source.   For this purpose Johnson & Cameron's classic experimental paper dealing with EHL line contact was utilized (cf. Johnson and Cameron, 1968). Computer simulations were performed to predict the traction coefficients reported in that paper. The input data used in the simulation is summarized in **Table 4**. Our theoretical predictions were compared to the experimental results of Johnson and Cameron (1968) and the results were found to be in excellent agreement. **Figure 10** shows the comparison.   The following remarks are appropriate:

1. The oil properties play a major role in the simulations. In particular, the pressure-viscosity characteristic has a significant affect on the calculations. In our simulations, we incorporate the Roelands model for the pressure and temperature effects. The Roelands constants were estimated based on the limited data given in Johnson & Cameron's

TABLE 4.   INPUT DATA USED IN COMPUTER SIMULATIONS

	USL experiments	Johnson & Cameron	
Operating conditions			
u_1	7.980	6.604	m/s
u_2	4.788 - 7.980	6.571 - 6.604	m/s
$w \ (=F/B)$	1.45×10^5	$0.96 - 1.89 \times 10^5$	N/m
T_0	296 - 314	303	K
Material properties			
E_1 , E_2	2.0748×10^{11}	2.0748×10^{11}	Pa
ν_1 , ν_2	0.3	0.3	
R_1 , R_2	0.0762	0.0381	m
B	0.00635		m
μ_0	0.084 - 0.039	0.063	Pa · s
Roelands constants			
z	0.6	0.6	
s_0	1.1	1.1	
Bair-Winer Constants			
τ_L	1.14×10^7	1.14×10^7	Pa
β	0.07	0.07	

COMPARISON WITH EXPERIMENT (Johnson & Cameron)
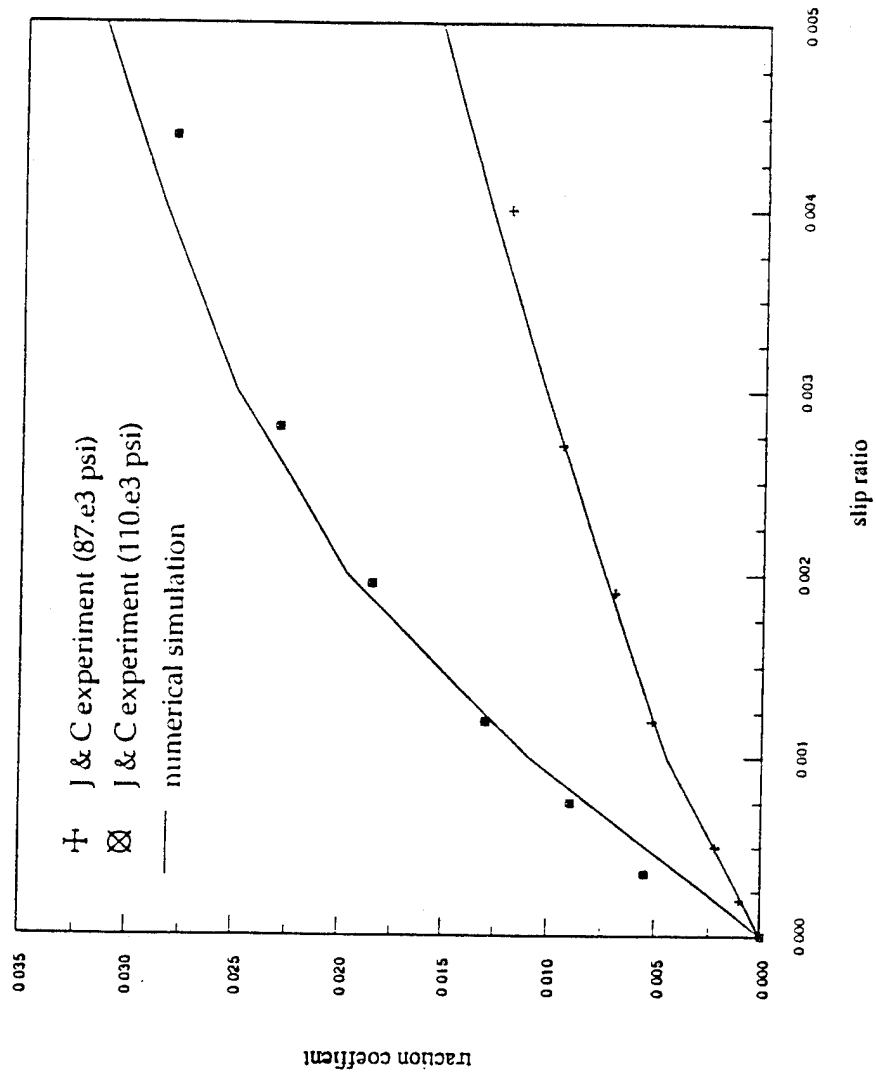
Figure 10. Traction Coefficient prediction and comparison to the experimental results of Johnson & Cameron (1966)

54

report. There is, therefore, some uncertainty with regard to the viscosity data.

2. Johnson & Cameron's paper does not mention any experimental errors. In reality there must be an "error band" on the traction results particularly at low-slip ratios.

3. In addition to the viscosity data, there are other properties pertaining to oil and surfaces that had to be assumed in the simulations. These are, however, of secondary importance.

4. Thermal effects are known to have a major impact on the lubrication characteristics. The computations reported include a realistic solution of the energy equation coupled to the Reynolds equation. The computer code provides a prediction of the temperature profile and updates the viscosity at each finite difference mesh point so that the pressure and shear stresses can be computed accurately. The fact that our computational prediction closely predict the measured results of Johnson & Cameron attest to the accuracy of the temperature predictions. Further-more, the predicted results for traction show a correct nonlinear variation with the slip ratio. The

55

traction rises rapidly with increasing the slip ratio until it reaches a plateau. Depending on the operating conditions, a further rise in the slip ratio causes a drop in the traction coefficient. This trend can only be predicted if the model properly incorporates non-Newtonian effects with thermal consideration. The non-Newtonian formulation used in the analysis is the well-known constitutive equation of Bair & Winer which has been shown to provide realistic results when compared to other, independent experimental traction measurements (cf. Khonsari & Hua , 1994).

4.3.3 Comparison to Experimental Results of USL Utilizing Shell Oil

Experimental measurements were conducted at USL in order to duplicate the results of Johnson & Cameron. For this purpose, the operating conditions had to be carefully set to mimic those of Johnson & Cameron. Experiments were conducted using Shell oil which according to the manufacturer had the identical properties as the European Shell employed by Johnson & Cameron. The initial traction results at USL were consistently greater than our predictions as well as those of Johnson & Cameron (please refer to the quarterly report which contain a complete description of the results and discussion

56

on the comparison between the theory and experiment). Subsequently, a number of improvements were made to the measurements system and also to the surface characteristics of the disks. Perhaps the most important and noteworthy factor was the surface roughness which USL was able to reduce to a significant degree. Please refer to the USL report for a comprehensive discussion.

Figure 11 shows the comparison of the theoretical simulOations and the final set of experimental results by USL. These results pertain to the first attempts at lowering the surface roughness. Two sets of speeds (500 rpm and 1000 rpm) were tested under 200 lb of normal load. The inlet oil temperature was assumed to be 74 °F. The results show that starting from the pure rolling (zero slip ratio) the traction rises rapidly, reaches a plateau and then begins to decline when the slip ratio is increased.

The general trend of the experimental results and, in fact, the magnitude of the traction coefficient are in agreement with the theoretical prediction. Yet, the notable difference remains to be a sharper traction measured experimentally at low slip ratios.

The following items were identified as possible factors which may have contributed to the discrepancy.
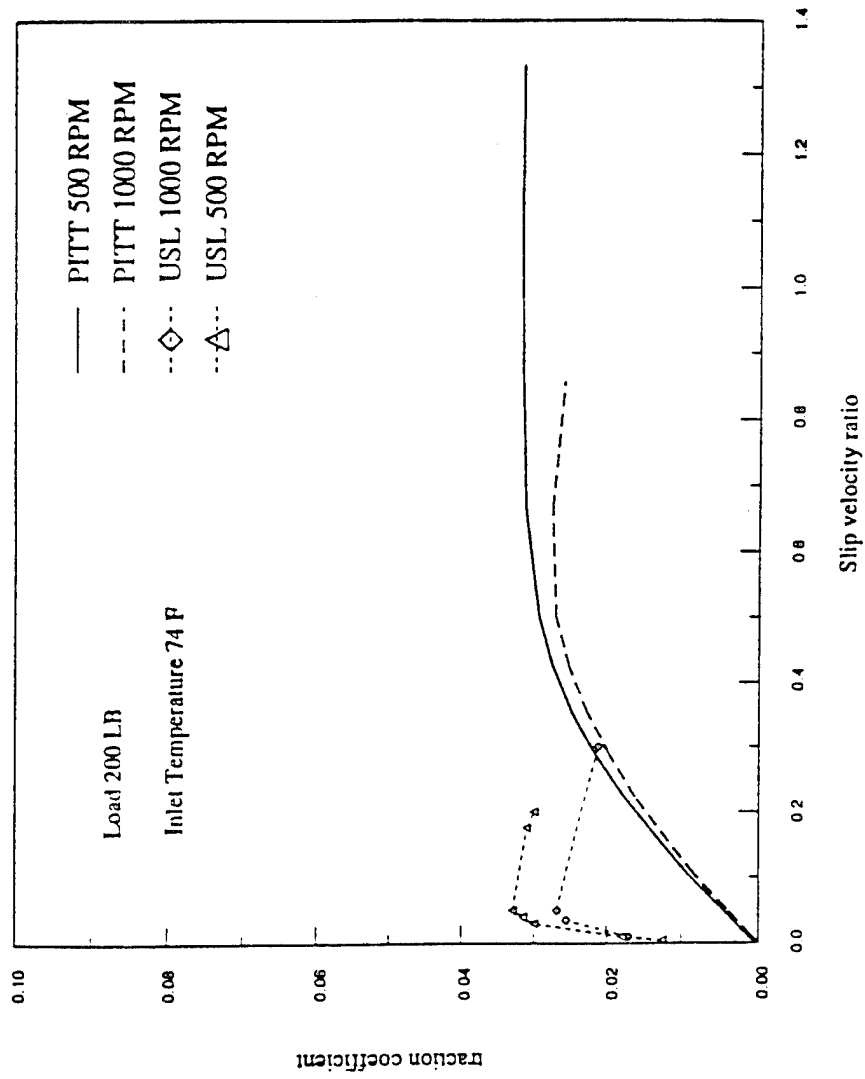
Figure 11. Traction coefficient prediction and comparison to the experimental results of USL.

4.3.3.1   Surface Effects

The most logical source of discrepancy was identified to be related primarily to the surface roughness. This error seems to persist even though the surfaces were lapped to an average roughness value of $R_a = 8 - 10$ μin. The surface roughness described above - i.e., *microroughness* - consists of short wavelength deviation measured using a stylus which converts the vertical motion of a fine diamond tip as the device is traversed along the surface. The average roughness R_a is a relative number which can be used to compare the smoothness of one surface relative to another. It does not give any information regarding the sharpness of the asperities, their frequency of occurrence, or their shape.

Another possible source of error emanating from surface characteristics is the *macroroughness* which is of the long wave length form normally caused by unwanted vibration when manufacturing the surfaces or perhaps during lapping and polishing. The severity of its effect can not be evaluated. Nonetheless, in view of the sharp traction measurement at small slip ratios, it was identified as another parameter which may have played a major role.

4.3.3.2   Operating Effects

It is indeed a difficult task to insure that cylinders are in perfectly aligned position during the entire range of slip ratios.   Even a slight misalignment can severely affect the traction results for all slip ratios.   Clearly, the effect of misalignment is magnified at lower operating speed and small slip ratios, since the film thickness is small.   For calculating the slip ratios, the speed of the cylinders must be accurately measured.   An error in the relative speed of the cylinders directly affects the traction curves. As one moves toward the pure rolling (zero slip ratio) condition, accurate assessment of the speeds becomes exceedingly difficult to maintain.   This fact, therefore, could have contributed to the discrepancy at small slip ratios.

4.3.3.3   Limiting Analysis

In what follows we present an extensive set of simulation results which provide an upper estimate of the traction coefficient at low slips.   This analysis was intended to study the contribution of inlet temperature and the role rheological characteristic of the lubricant on the   predicted traction results   at low-slip values.

4.3.3.4 Temperature Measurements and Simulations

The University of Southwestern Louisiana implemented some oil temperature measurements capability to the system. Thermo-couple readings at the oil inlet and outlet revealed that the oil temperature can rise significantly from the inlet partic-ularly at higher slip ratios. No direct comparison with the theory is intended because these temperatures are merely representative values of a temperature two-dimensional field. In a typical line-contact conjunction, the mean oil tempera-ture experiences a large temperature rise whereas the oil temperature in the vicinity and at the surfaces tend to be relatively small. The results of our prediction is shown in Figures 12 - 14. The important point here is that at a higher value of slip ratio such as 0.3, the inlet temperature of T_1 = 90.9 °F was measured. The temperature at that slip ratio measured at the exit was T_2 = 100.6 °F. Please see the USL quarterly Report for the details.

Figure 12 show the simulations of the 1000 rpm and 200 lb load at inlet temperatures of 74°F and 96°F along with the experi-mental results. As shown, the higher inlet temperature results in a higher traction slope approaching relatively closer to the experiment. However, it is yet significantly below the experiment.
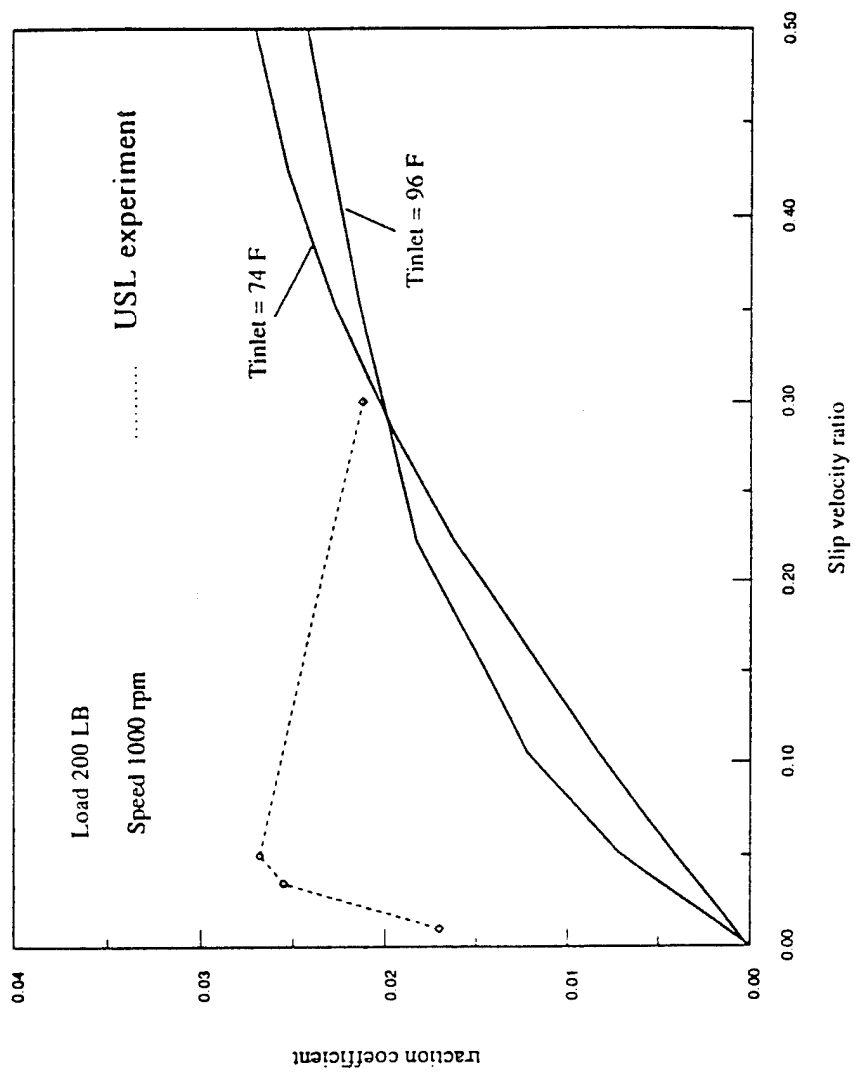
Figure 12. Traction coefficient results with various inlet temperature

Load 200 LB

Speed 1000 rpm

USL experiment

Tmean = 96 F

Tmean = 106 F

Tinlet = 96 F

Slip velocity ratio

traction coefficient
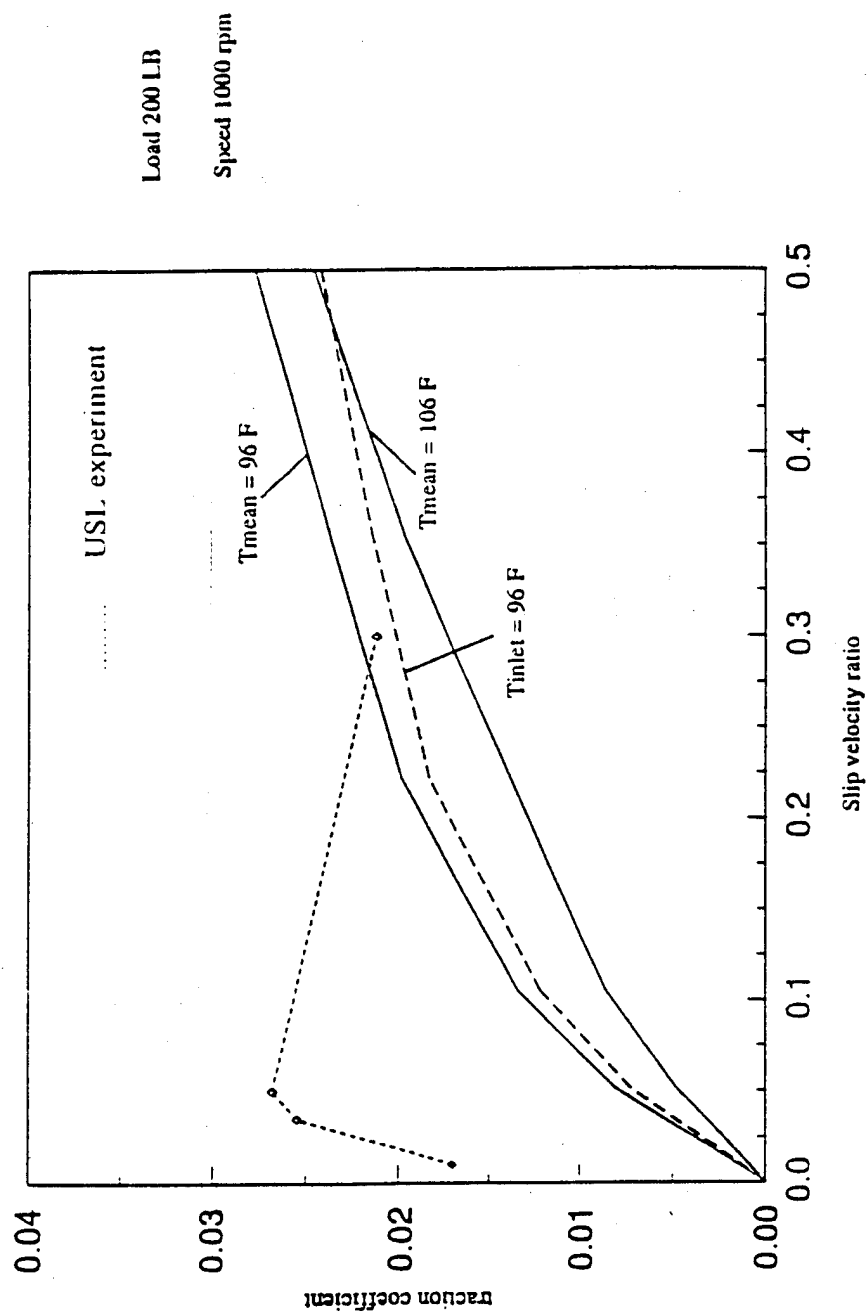
Figure 13 Traction coefficient results at various mean temperature

Load 200 LB

Speed 1000 rpm

USL experiment ....

Newtonian Tmean = 74 F

Newtonian Tmean = 96 F

Newtonian Tmean = 106 F

traction coefficient

0.04

0.03

0.02

0.01

0.00

Slip velocity ratio

0.0   0.1   0.2   0.3   0.4   0.5
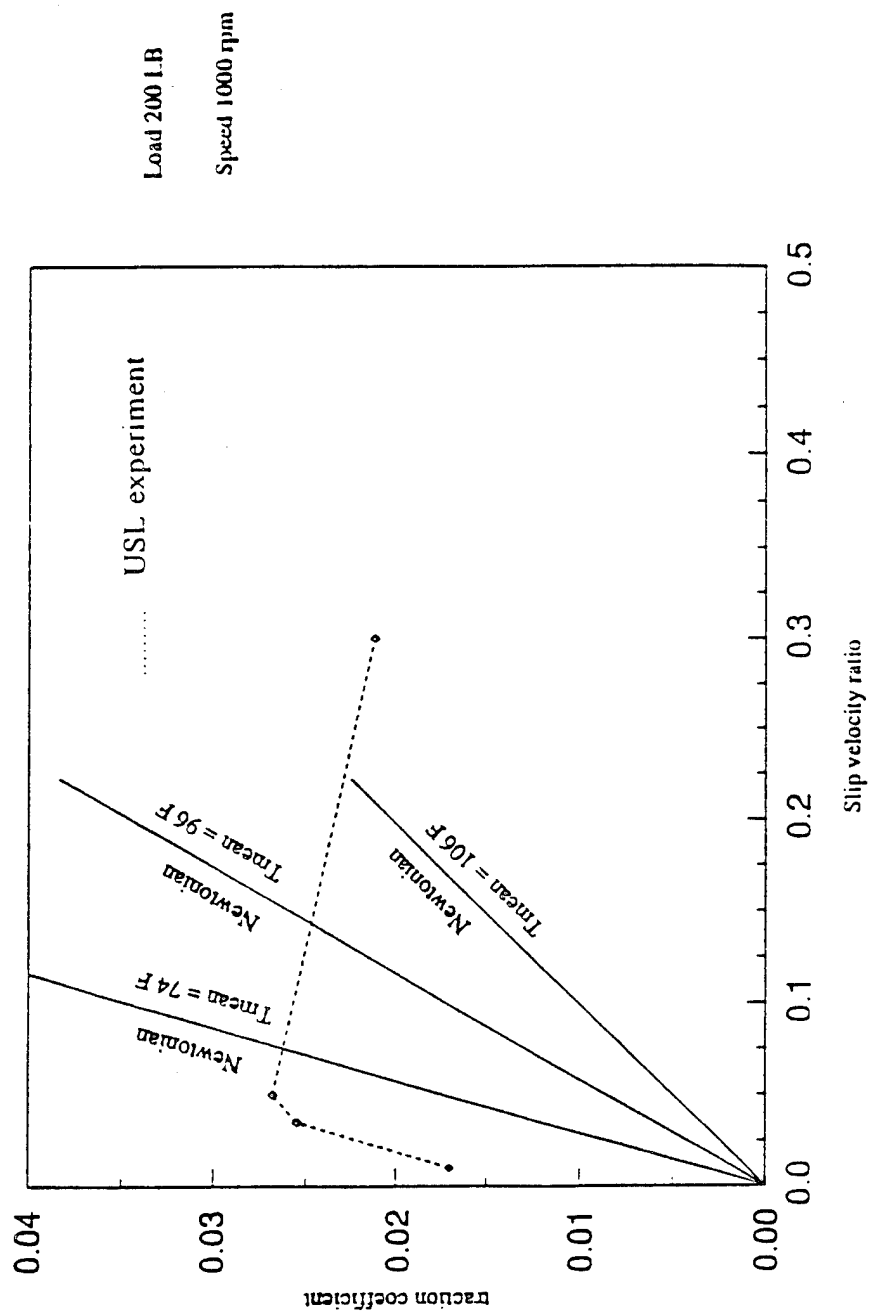
Figure 14. Traction coefficient results with Newtonian rheological model

64

Next a series of simulations was performed where the viscosity were assumed to remain constant with temperature but vary with pressure. In these simulations, a mean temperatures of $T_{mean} = 96$ °F and $T_{mean} = 106$ °F were assumed. The results are shown in Figure 13. While the trend remains similar, the initial slope is smaller than the experiment. From these simulations, we conclude that the temperature effect is not responsible for the large traction slope measured experimentally.

4.3.3.5 Traction Slope and Rheological Formulation (an upper-limit analysis)

Next, it was decided to perform an upper estimate analysis for the traction slope. For this purpose, a Newtonian rheological equation was implemented into the analysis. The rational behind this work is that a Newtonian fluid essentially predicts a *linear* increase in the traction as a function of the slip ratio. The Newtonian formulation fails to show the well-known "saturation" trend of the traction curve. It continues to increase and does not reach a plateau. Figure 14 shows the Newtonian trends predicted for various temperatures. The Newtonian simulation with the lowest mean temperature should result in the maximum slope. As Figure 14 shows, even at a $T_{mean} = 74$ °F, the maximum computed traction slope is still below the experimentally measured values.

It is, therefore, concluded that under the conditions simulated, the temperature predictions or the form of the rheological equation are not responsible for the apparent difference between the theory and experiment. The discrepancy is likely to be caused by microroughness, macroroughness, alignment problems and lack of parallelism of the disks particularly in the axial direction. The last item could, for instance, explain the rise in the torque if there is a point wise contact between the cylinders at low slip ratio, i.e., when the film thickness is not adequate for the separation to occur.

For illustration purposes, the normal trends of traction vs. slip ratio are presented in **Figure 15** which predict how the traction should behave in an EHL line contact configuration upon increasing pressure, speed, and change in the inlet or mean temperature. These theoretical predictions are in agreement with these well-established trends (cf. Gohar, 1988).

4.3.3.6   Final Traction results with Shell Oil: Further lapping of the surfaces

Further experimental measurements were conducted at USL with the Shell oil under 200, 400, and 700 lb. The notable difference in these experiments were that the surfaces were lapped to a higher degree; See USL report, discussion on

66
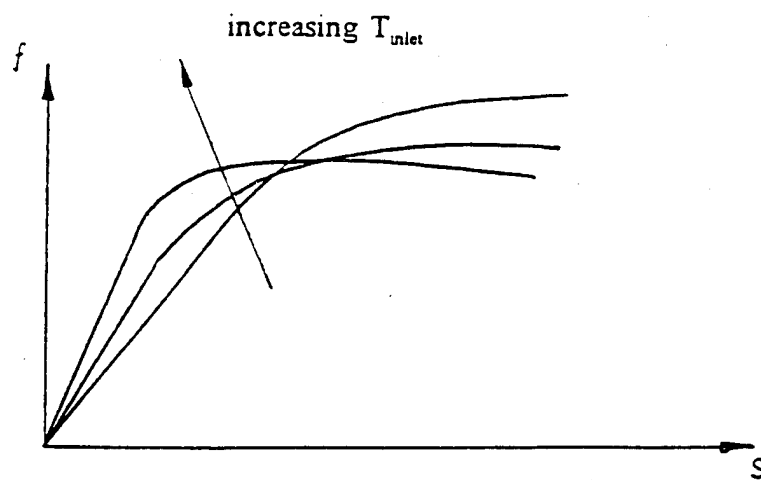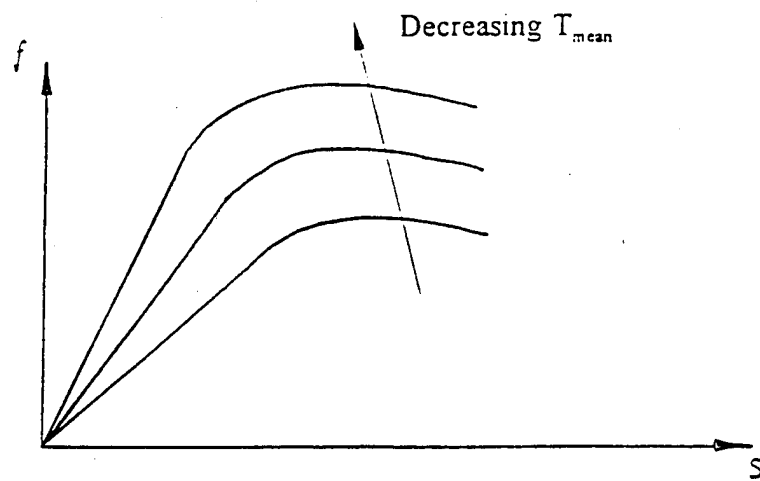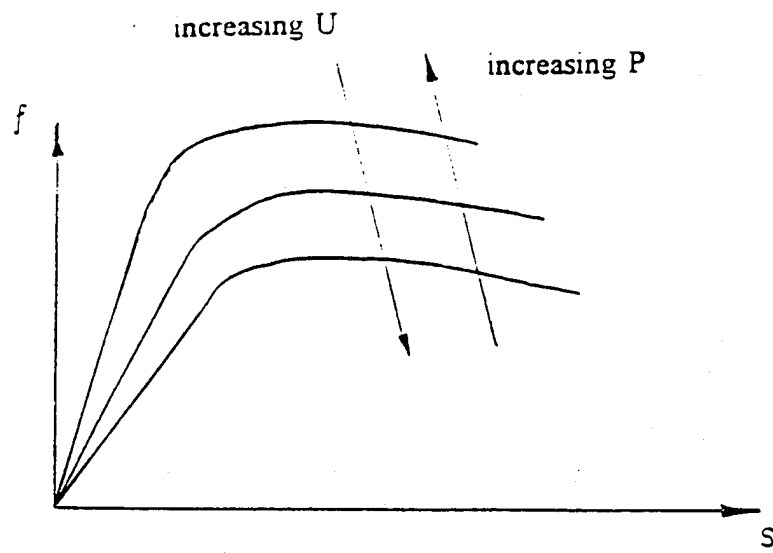
Figure 15. Behavior of Traction curve as a function of slip ratio

lapping and the measured surface roughness. There is a significant reduction in the slope of the measured traction-slip ratio curve. Also, there is a noticeable reduction in the magnitude of the traction where it reaches its plateau. The results of the experiments and the theoretical predictions are shown in Figure 16. As evident, the theoretical predictions are now in excellent agreement with those measured particularly at small slip ratios. These results attest to the importance of the surface roughness and its role on the traction coefficient at low slip ratios. This is an important finding for it points to the need of analytical tools that can incorporate surface roughness into the EHL analysis.

4.4   Slurry Formulation and Simulations

Having established a good comparison base for the theoretical simulations and the experimental traction results, an investigation of the slurry mixture in EHL line-contact was initiated. The experimental measurements were conducted with a graphite mixture in an ethylene glycol carrier fluid at a ratio of 8:1 by weight. The theoretical simulations were confined to this mixture alone. The rheological relation for this mixture was assumed to obey the recommended measurements of Dareing & Dayton (1992). As discussed in Section 2, the elasticity and deformation consideration of the graphite were included in the analysis. The particles were assumed to be

68

SHELL TURBO 68 OIL.

Traction Coefficient

Slip Velocity Ratio

700 lb (simulation)

400 lb (simulation)

200 lb (simulation)

200 lb (experiment)

400 lb (experiment)

200 lb (experiment)
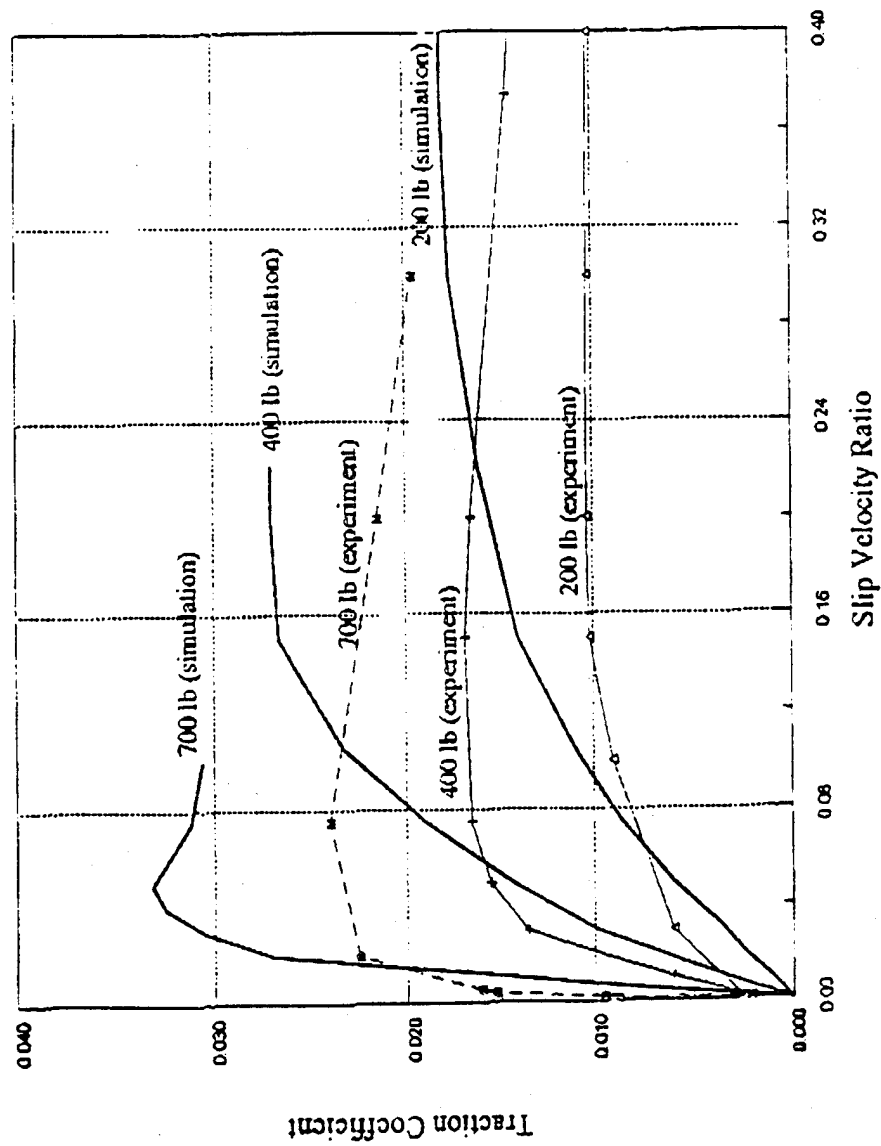
Figure 16. Final traction coefficient results and comparison to USL experiments

69

uniform in size and spherical in shape. The contact is assumed to be fully flooded and there is no pile effect at the entrance. The temperature rise and its concomitant effect on the viscosity is incorporated into the analysis by solving the energy equation.

A series of simulation results was performed to predict the performance of the graphite mixture. The simulations provided the followings information:

1- pressure distribution

2- film thickness

3- temperature

4- traction

Figure 17 shows the results of the traction results predicted using two particle hardness values of 3.8 x 10^8 Pa and 3.0 x 10^9 Pa. These traction values are predicted under the speed of 1000 rpm and 200 lb load. The results show that the hardness value - needed to determine the plastic deformation of the particles- plays an important role on the magnitude of the traction coefficient. As pointed out in the theory section of this report, there is a crucial need for appropriate mechanical property values in predicting the performance of EHL contact. This information must be determined experimentally, though it is not an easy task because of the anisotropy in the mechanical property of lamellar solids. Extensive review of published literature showed that,

Ethylene Glycol - Graphite (8:1)
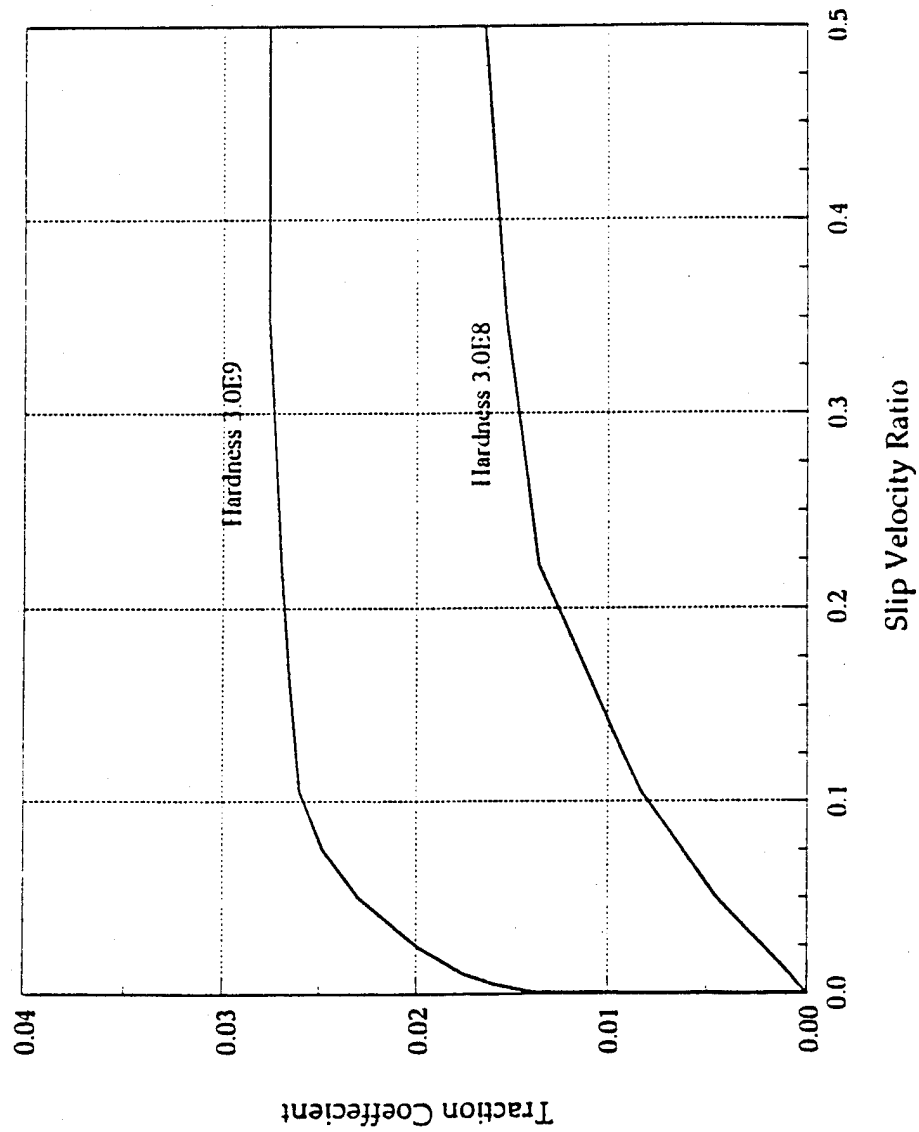
Speed 1000 rpm
Load 2001.B

Figure 17. Traction coefficient of ethylene glycol and graphite slurry with two particle hardness values

71

unfortunately, there is a serious lack of published property values for solid lubricants such as graphite and MoS_2. Furthermore, in most cases the published literature contains a wide range of property values. For the remainder of the simulations, the hardness value of 3 x 10^9 will be used since it thought to be more realistic.

Figure 18 shows the predicted traction results for 700 lb loading at 1000 rpm. Also shown in that Figure are the experimental results of USL with the 8:1 slurry mixture at 700 lb. The hardness value used in these simulations was 3 x 10^9. A list of input used for the simulations is provided in Table 5. The experimental results of the slurry are surprisingly very low. In fact, the order of magnitude of the measured traction coefficient seem to be in the range of what is commonly observed in hydrodynamic lubrication of conformal surfaces such as slider bearings and journal bearings. In conformal surfaces, the surfaces are separated by a thick film of fluid and the projected surface area upon which the load acts is relatively large. Therefore, the stresses are small and the coefficient of friction turns out to be of the order of 0.004. In contrast, in EHL lubrication of rolling element bearings surfaces are non conformal and, therefore, the stresses are exceedingly large. Therefore, the normal range of traction coefficient is much higher. Show in that Figure is the theoretical traction results of "pure" ethylene glycol

72

Ethylene Glycol - Graphite (8:1)
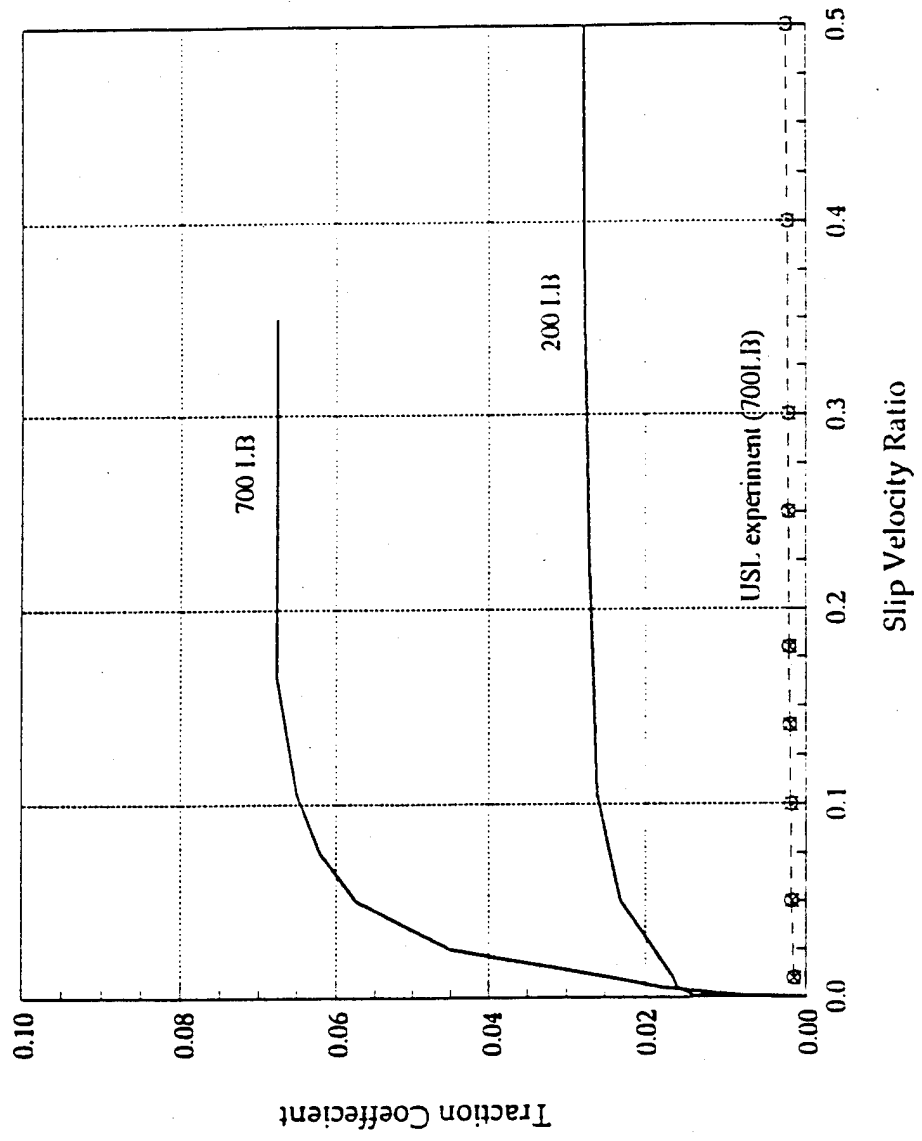
Speed 1000 rpm

Hardness 3.0E09

Figure 18. Comparison of traction coefficient of graphite slurry and USL experiment

TABLE 5. INPUT DATA USED IN COMPUTER SIMULATIONS
[POWDER SLURRY]

Ethylene Glycol + Graphite   8:1

Operating conditions

u_1	7.980	m/s
u_2	7.980 - 13.299	m/s
$w (=F/B)$	$1.451 - 5.077 \times 10^5$	N/m
T_0	308.6	K

Material properties

E_1 , E_2	$2.0748 \cdot 10^{11}$	Pa
v_1 , v_2	0.3	
R_1 , R_2	0.0762	m
B	0.00635	m
μ_0	0.0446	Pa $\cdot$ s

Roelands constants

z	0.6
s_0	0.3883

Power Law Constants

n	0.97

Properties of Particles

D_p	5.0×10^{-6}	m
E_p	8.62×10^{10}	Pa
H_p	$3.0 \times 10^8 - 3.0 \times 10^9$	Pa
v_p	0.25	

74

provided as a benchmark for comparison purposes. These traction results are greater than those of the measured slurry. It is to be noted that ethylene glycol viscosity is low relative to most oils so that this carrier fluid by itself can not adequately protect the surfaces. This was verified by computing the minimum and the central film thickness: h_{min} = 0.5056 micron and $h_{central}$ = 0.55903 micron for the ethylene glycol, In contrast, the computed film thickness values for the slurry are: h_{min} = 1.387 micron and $h_{central}$ = 1.482 micron. The University of Southwestern Louisiana has spent a considerable amount of time and effort to determine any possible source of problem in measuring system. To date, no problem has been found and the data seems to be repeatable. Further research is, therefore, crucially needed to determine the cause of such low traction coefficient. A possible mechanism for this phenomenon could be if the mixture happens to react chemically with the bounding surfaces. If this is found to be the case, the theory would have to be modified since it assumes that no reaction takes place.

Figure 19 shows typical film thickness, pressure distribution for this slurry mixture. The shape of the pressure profile and the film thickness predicted are typical of what one normally encounters in EHL simulations with pure oils. The temperature profile is shown in Figure 20. These results correspond to 700 lb loading at the slip ratio of 0.01. A hardness value of 6.0

Ethylene Glycol - Graphite (8:1)

Film Thickness, H

Pressure, P

X Coordinate
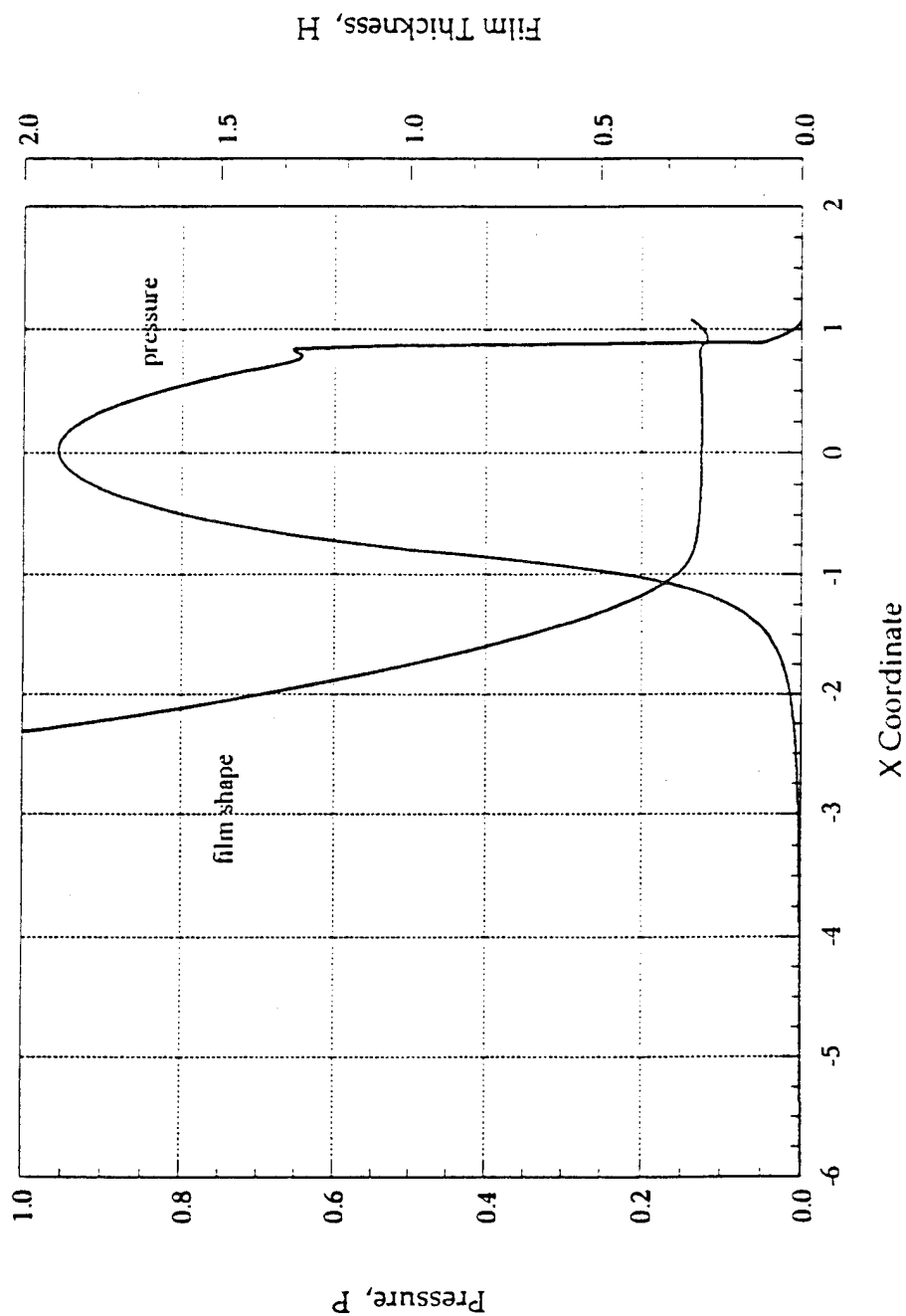
Load 700 LB

Hardness 6.0E9

Slip ratio 0.01

Figure 19. Typical film thickness and pressure profile for graphite slurry

76

Ethylene Glycol - Graphite (8:1)

Figure 20. Predicted temperature profile for the slurry mixture

Load 700 LB

Hardness 6.0E9

Slip ratio 0.01

77

x 10^9 was used in the simulations. The temperature profile shows that there is a considerable rise in the film temperature at the inlet. The temperature of the surfaces, in contrast, tend to be lower. The appreciable rise in the film temperature away from the boundary and in the vicinity of the inlet points to the possibility of a significant viscous dissipation there. Further research is needed to investigate the possibility of particle pile-up at the inlet.

Extensive amount of computer simulation of a slurry mixture containing ethylene glycol and MoS_2 was also undertaken. A complete discussion of the theoretical derivations and results are presented in a paper which has been included in the appendix of this report.

4.5   Summary, Concluding Remarks, and Recommendation for Future Research

The stringent requirements of the Integrated High Performance Turbine Technology (IHPTET) Program calls for a significant rise in engine operating speeds and temperatures.

Specifically, the program requires design modifications that could accommodate doubling the speed and capability of operating in temperatures up to 1500 °F (Dareing and Dayton, 1992). To meet these requirements alternative lubricants must

78

be explored, as conventional lubricants are ineffective beyond roughly 400 °F.

A number of alternative approaches are being considered to combat this problem. One possibility is to utilize a multicomponent lubricant consisting of a mixture of solid lubricant in a carrier fluid. The solid lubricant such as graphite or molybdenum disulfide (MoS_2) could potentially withstand the severe operating temperature environment. The function of the carrier fluid is primarily to deliver the mixture to the bearings. For this reason, the fluid itself does not neces-sarily need to have any positive lubrication capacity. Hence, one may consider ethylene glycol which has a fairly low vis-cosity and burns cleanly without excessive amount of residue.

4.5.1 Elastohydrodynamic Characteristic

The lubrication regime of many vital machine elements, particularly those that are highly loaded, is classified as elastohydrodynamic since the surfaces are nonconformal so that a significant amount of load is carried over a small area. As a result, the stresses are exceedingly large (of the order of 1 GPa) leading to a significant elastic deformation of the surfaces. Although extremely thin, the height of the lubricating film in elastohydrodynamic lubrication (EHL) is

normally larger than the combined surface roughness so that metal-to-metal contact does not occur. Thus, in addition to the elastic deformation of the bounding surfaces, the mechanics of the fluid plays an important role and requires careful consideration.

The key to a successful operation of a rolling element bearing is the lubricant film thickness. An adequate film thickness, if available, can provide a protective layer on the surfaces in relative motion so as to prevent an intimate metal-to-metal contact. In general, the surface and subsurface stress coupled with the fatigue of highly stressed bearings can be all related to the EHL film thickness.

4.5.2 Experiment, Design and Analysis

The design and analysis of multicomponent fluids when used as a lubricant for rolling element bearings is very complex and requires a thorough investigation. There are basically two categories of questions to be addressed:

I.   Can a bi-component lubricant provide an adequate lubrication? and

II.   What are the design and analysis features of the problem?

Category I which is primarily experimental must address the

following questions :

- Is the film thickness adequate?

- Does the temperature rise meet the design requirements?

- Are the frictional characteristics under various

  operating speeds and loading conditions within

  the allowable range?

- Can a bearing be designed to achieve the goals of the

  project?

Under *Category II*, there are   many modeling and scientific

questions:

- What is the appropriate rheological equation of the

  mixture?

- What are the equations that govern the multicomponent

  flow in thin-film lubrication?

- How does the solid-component interact with the bearing

  surfaces?

- What is the deformation characteristic of the solid

  lubricant within the contact region?

- Can the film thickness, temperature rise, and traction

  characteristics be realistically predicted?

- What is the appropriate testing apparatus needed for

  verification of the results?

The experimental investigations primarily dealing with the

friction characteristics of the rolling element bearings were

to be obtained with an Air Force traction rig. The rig was shipped to the USL and was made operational after a considerable amount of time and effort. The EHL analysis of line contact was assigned, under a small subcontract, to Professor Michael Khonsari of the Mechanical Engineering Department of the University of Pittsburgh.

A complete analytical and experimental investigation was initiated. The first phase of experiment included the assembly of an automated data acquisition system for the traction measurement and the theoretical analysis concentrated on developing a general EHL calculation with a single component fluid. The results indicated that surface roughness plays a major role on the traction measurements. The surfaces were lapped to an acceptable roughness level as those used in rolling element bearing and the resulting experimental measurements are found to be in agreement to those of theoretical simulations.

The second phase of the research was to initiate experimentation of a graphite slurry with ethylene glycol at a concentration of 8:1 by weight and simultaneously developing the theoretical analysis. A theory was developed based on the rheological equations of Dareing & Dayton (1991) for graphite slurry flows. All the governing equations and proper boundary conditions were derived and programmed. Prediction of the

82

film thickness, pressure distribution, temperature rise, and traction characteristics were obtained under several operating conditions that could be tested experimentally. At the present time, the experimental traction results are significantly lower than the predicted results.

4.5.3 Future Directions

Several crucial questions must be addressed at this stage of the project which requires modification of the Air Force traction rig. The rig is best suited for elliptical/point contact configuration. However, currently the rig is being used in a line-contact configuration. Also, the traction rig was not intended for operating under near rolling and very small slip ratios. In order to address the questions posed earlier, a testing rig is to be designed and built that could provide us with the needed capability of accurate measurement of the traction in a line-contact configuration. The rig will be instrumented with thermocouple to measure the lubricant temperature so that the temperature rise can be evaluated with confidence. This information is crucially needed in the verification of the theoretical results. It will also help to guide the theoretical modeling, as modification to the existing analysis may be needed. Furthermore, it is imperative that we determine the validity of the extraordinarily small traction measurement with the slurry mixture before such

information is put to use in the field. Finally, the appro-
priateness of the rheological equations for the mixture
behavior at high pressures must be determined. The governing
equations must be revised accordingly if the assumed behavior
happens to be unrealistic.

In résumé, a considerable amount of time and effort has been
spent on this project and we feel that we have made very good
progress. This progress has been possible by very strong
teamwork between the experimentalist at USL and our analytical
team. Continuation of this research will keep this fruitful
collaborative scientific activity alive.

5.0 Laboratory Measurements of Traction Coefficients

5.1 Traction Rig

During the third quarter of 1993, a 400 sq. ft. area was set aside in the Mechanical Engineering Laboratory of Rougeou Hall on the USL campus. This area was provided with a 480v, 100a 3 phase electrical supply and a 90 psi shop air supply in preparation for the installation of the traction rig equipment to be loaned to USL by the USAF Wright Patterson Labs.

The disassembled rig was received mid-August, 1993. Generally the parts were in good condition with the exception of two broken castings on the slave motor. These were repaired by a USL expert in aluminum welding.

The rig parts were placed in the space prepared and arranged in appropriate relationship to each other. The motors and central test stand were bolted to the concrete floor. This was complete by the end of the first week in September. See Fig. 21 for layout of rig installation, Fig. 22 is a photograph of the actual installation.

The diagrams showing the wiring as installed at WPAFB were lost during the transfer to USL. This caused some initial

TRACTION RIG POSITION LAYOUT

20 FT

CONTROLLER

XFORMER

XFORMER

CONTROLLER

LAB WEST WALL

TACH

MASTER MOTOR

CENTRAL TEST STAND

CONTROL CONSOLE

20 FT

OIL PUMP

SLAVE MOTOR

TACH

FIG. 1
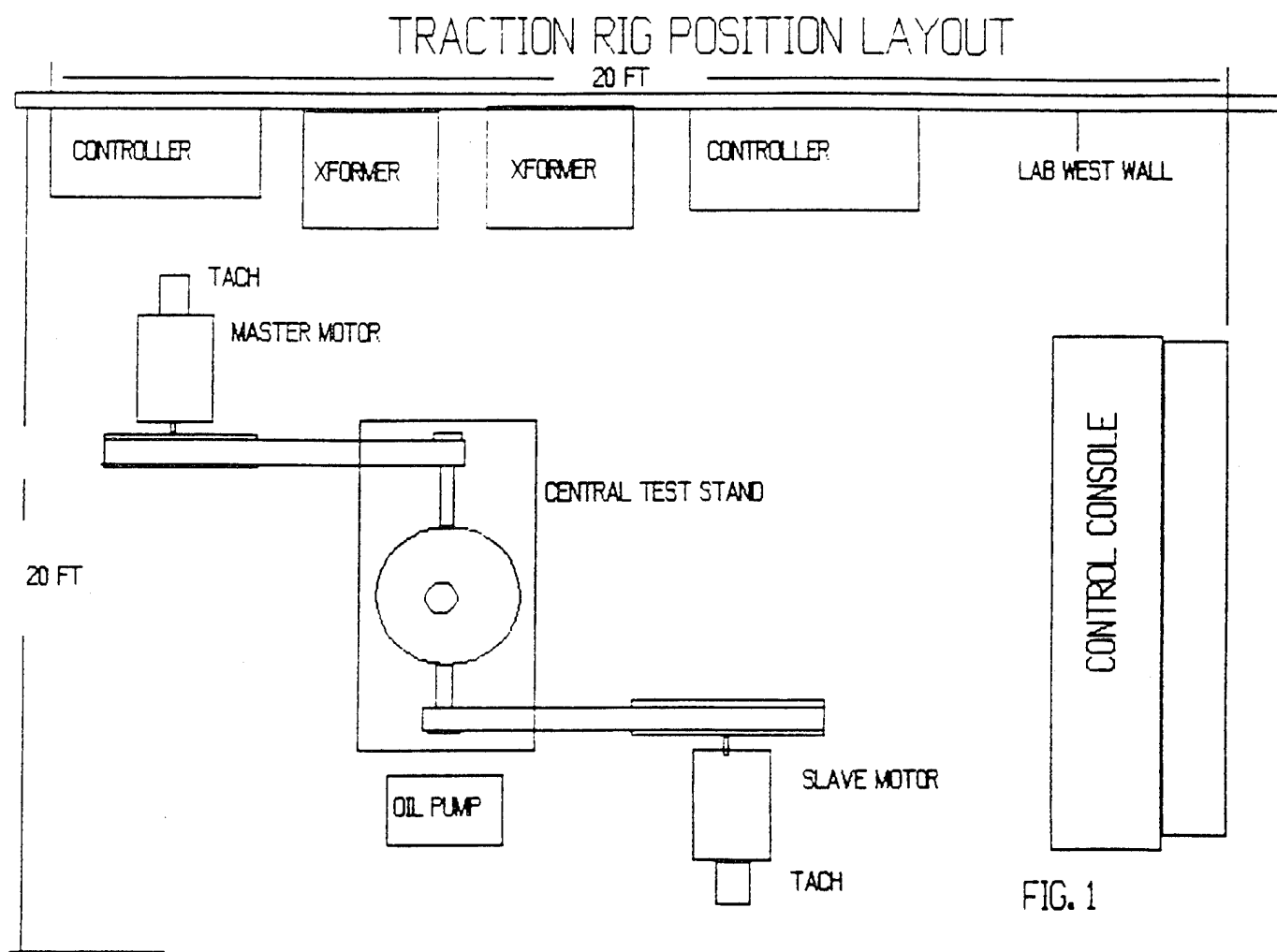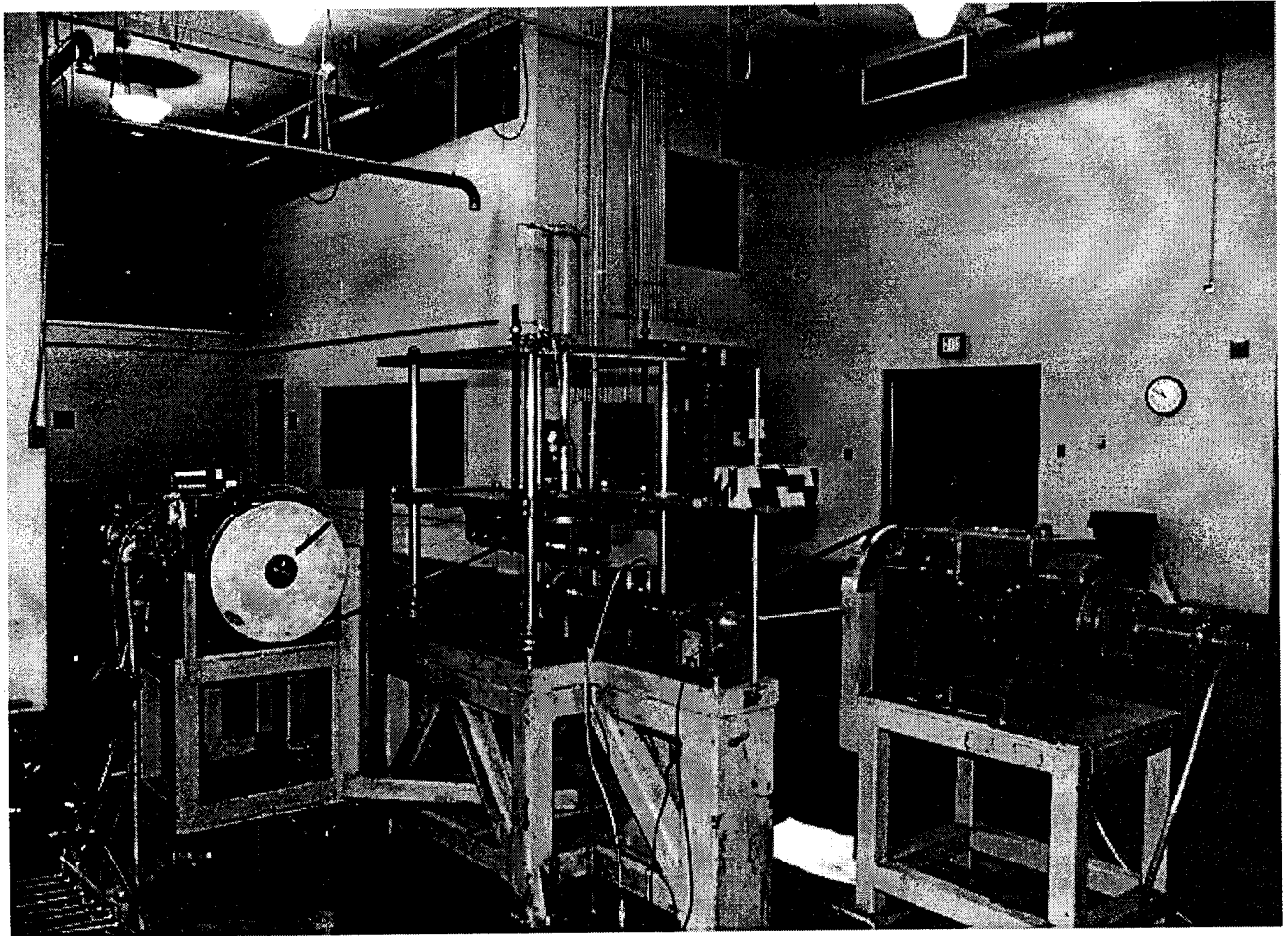
Figure 21.

Figure 22. Traction Rig Installation.

problems in creating a new wiring layout for the Rougeou Hall installation. However, with the help of WPAFB personnel, and by the use of the original diagrams provided by the controller manufacturer, the wiring was adapted to the new location, new conduit was run and the wiring was completed. Mr. Tim Gootee of WPAFB came to Lafayette on Oct. 4, 1993 to assist with final hookup and initial testing. Some start up problems were experienced and close liaison was required between on site personnel, WPAFB personnel and engineers at Eaton Corp (invertor controller manufacturer) before proper operation was achieved. First successful rig operation occurred on Oct. 12, 1993.

The rig was prepared for shakedown testing by reworking the baffles and seals required to contain the supply oil within the central test station compartment. This effort exceeded expectations, and, coupled with an evaluation of the noise generated by rig operation, prompted a decision that a separate room within the laboratory (as had been initially planned) would not be required for the rig. This greatly simplified the installation and reduced the cost associated with the operation of the rig.

The actual equipment included in this installation is listed below.

-    Two 20 HP, 240 V dc   GE Motors equipped with

cooling blowers and tachometer generators - one motor is designated slave (a control related designation - the slave can be operated in a manner that automatically maintains a % speed relative to the other, or master motor), and the other motor is designated master.

- A central test station providing bearings and mountings for two test discs that are positioned so that their peripheries can be placed in contact with each other, and are driven independently through belt drives from the master and slave motors. This station provides means for applying an adjustable (0 to 1000#) load to the test disc interface.

- Two Eaton Corp. invertor controllers rated at 460v, 3 phase, 100 amp, 40kva input, and 250volt, 60 amp, dc output. These controllers each consist of double 3 phase SCR bridges providing variable speed control and regenerative braking to the DC motors.

- 1 Two 40kva transformers, 460v, 3 phase 40kva output, input variable in discreet steps from 208v to 480v, 3 phase.

- A torque transducer (Lowman Corp.) mounted in the drive shaft between the master motor and lower test disc.

- A 1,000# (Omega Corp) load cell mounted between the pneumatic cylinder and the top half of test rig.
- A central operators station. Function of this station is to provide means to control test disc speed and load, and to provide readouts of significant data. Equipment contained includes:
- Pneumatic controls for test load cylinder
- Two Anadex frequency to dc converters to provide analog (dc volts) output as a function of rpm.
- Two Fluke Mfg. Co. counter-timers with digital readout to display test shaft rpm's continuously. Operates from magnetic transducers mounted on test shafts.*
- Load cell digital readout with calibrated dc analog output.
- Torque digital readout with calibrated dc analog output.
- West Inst. Corp temperature readout and limit controller.
- Control potentiometers and appropriate switches.

*The counter timer used in conjunction with the slave motor failed early in the test series and was replaced with an Amatek digital tachometer reading to four places.

5.2 Computer System

5.2.1 Hardware

- Data Translation DT-2801 analog and digital I/O board

- IBM 433DX computer

- Data Translation DT-707 general purpose screw terminal panel

- Anadex model PI-608R frequency to dc converter (2)

- Lebow model 7535 transducer indicator

Speed signals are sent to the computer for A/D conversion by the two Anadex frequency to dc converters. The torque signal is sent via the Lebow transducer indicator. These connections are made to the DT-707 screw terminal which is connected to the DT-2801 board through a 24 pin connector.

5.2.2 Software Development

The first software iteration collected data in the following

manner. The two disk speeds were set, with the slave disk at an RPM of approximately 500 less than the master disk. A signal was then sent to the slave motor to increase speed until the disk speed level is approximately 500 RPM faster than that of the master disk. Data was collected during the speed change and produced both sides of the traction curve. This method worked well for low normal loads. As the loads were increased the torque transmitted at the disk interface tended to affect the speed of the master disk. This occurred when the two disks approached the same speed and produced a "hunting" action as the slave motor attempted to overcome the torque at the interface and continue the speed increase. At its worse this phenomena produced a situation wherein the slave speed was unable to overcome the torque and the two motors remained either in the "hunting mode" or were essentially locked at the same speed level. Although it is felt that this data were accurate it made comparisons of traction coefficients at low slip velocities virtually impossible. For this reason, a move was made to manual control of the disk speeds, with the computer being used for data collection only. In this scenario the speeds of each motor are set by the operator at the desired level. This level is based either on a desired speed difference or a desired torque value. The data acquisition system collects a number of torque and disk speed measurements and calculates average values for each parameter. These measurements can be

used to plot a band of traction coefficient measures or the average can be used as a single point plot. This allowed comparisons of data taken at low slip speeds. It should be pointed out that another area of concern was addressed with the move to this type of measurement scheme. When the data acquisition board is used in the Programmable I/O (PIO) mode each data point that the board receives is sent directly to the computer programming environment for manipulation or storage. Because of the time that this took the data points were not being measured simultaneously. When the move was made to manual control of the speeds there was no reason to remain in the PIO mode of data collection. The alternate mode is termed Direct Memory Access (DMA) and means simply that the data signals are stored directly in the computers memory with a minimum of program control during operation. This mode is obviously much faster and addressed the concern for simultaneous measurements to an acceptable degree.

5.2.3 Capabilities:

The limitations of the data acquisition system are due to instruments that handle the signal directly from the measurement devices; the Lebow transducer indicator and the two Anadex frequency to dc converters. These limitations are due to the update frequency of these instruments. The speed measurements could be made more accurate by receiving signals

directly from a tachogenerator attached to the motor. Another limitation is the fact that slight changes in speed of one disk tend to affect the speed of the other disk especially at higher normal loadings. It is felt that this situation could best be addressed by having one synchronous motor that is able to maintain a set speed despite the torque produced at the disk interface. The second motor speed could then be controlled by the computer and the data collected would be accurate easily interpreted.

5.3 Polishing and Finishing Systems

A crucial part of the total test system is the ability to polish the test wheels to a high finish. Other researchers in the field report having achieved finishes of 6 microinches peak to valley heights (Ry). In order to approach this finish level, a system using lathes, grinders, and special diamond polishing pastes was devised. Please see Fig. 23, which is a photograph of the system as assembled. The following is a description of the procedure used:

- The test wheels were set into a lathe and trued to within 0.0005".

- A very light cut at minimum feed speed was taken with a ceramic tool to provide final trueing and a homogeneous surface.

- A Dumore tool post grinder turning at 22000 rpm was

94

Figure 23. Polishing System.

then used to run a 1" diameter disc against the wheel with various finishing media. The lathe was set at minimum rpm, 45, for this operation.

A typical sequence of finishing media was as follows -

- 400 grit wet paper-remove deep scratches
- 600 grit wet paper-remove all straight scratches
- 6 micron diamond paste - remove all scratches and whorl marks - initiates high polish.
- 1 micron diamond paste - increases polish level.
- 0.05 micron diamond paste - final polish.

The total time elapsed to complete this process was very variable, but approximately 10 hours of actual lathe time was typical. Even at that, we were not able to achieve a 6 microinch level. Approximately 12 microinch was the best we could achieve. Extending the polishing time did not improve results significantly.

5.4 Surface Finish Measurement

A Taylor-Hobson Surftronic roughness gage was used to determine final finish. This gage uses a diamond stylus that is placed upon the surface to be measured and then driven through a preselected travel across that surface. See photos, Fig.24 and 25. The gage calculates roughness, and provides a digital readout of the measurement selected. Our primary
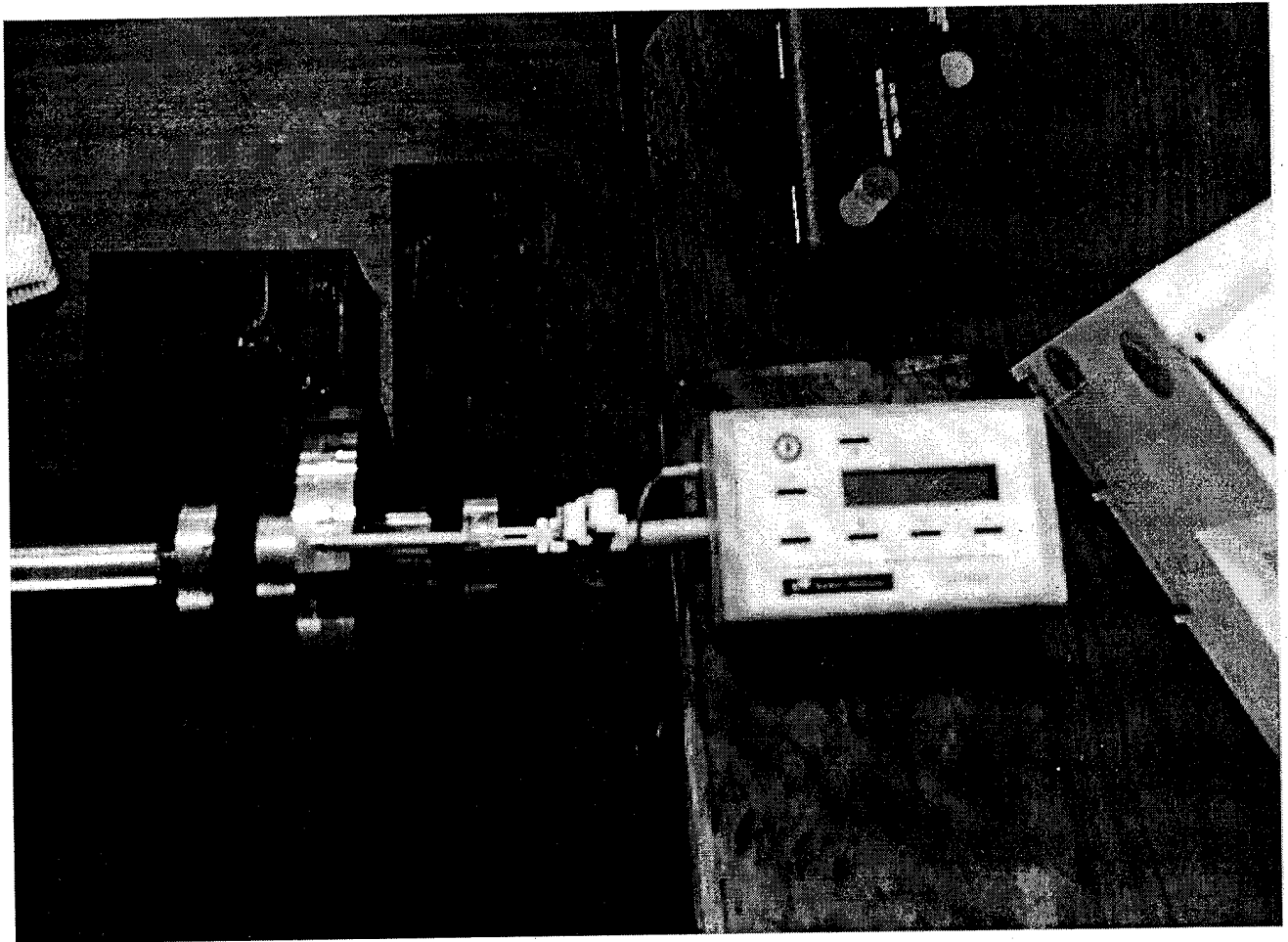
Figure 24. Surftronic Measuring System.
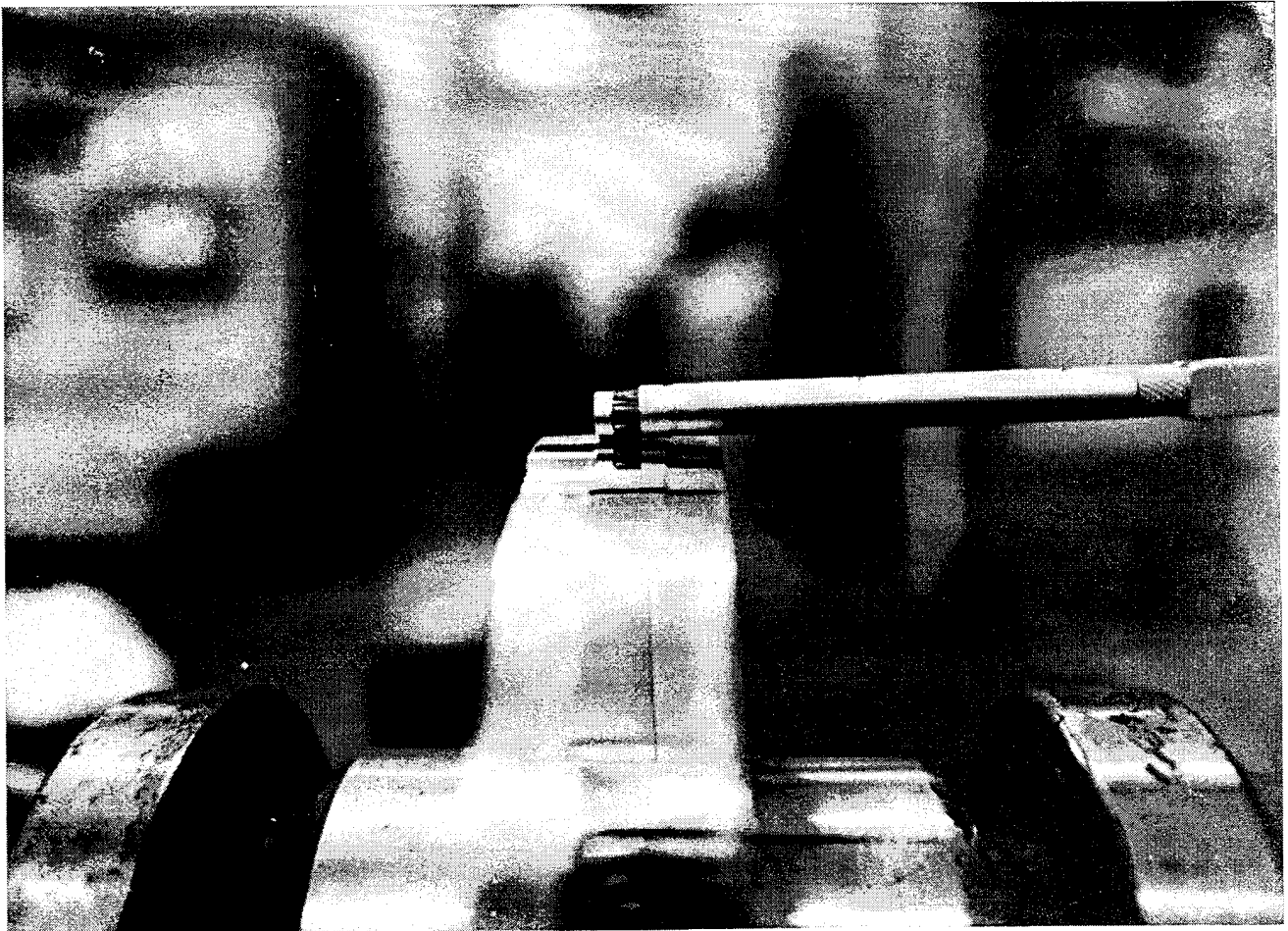
Figure 25. Measurement Stylus on Work Piece.

interest was in the maximum asperities, or measurement of the peak to valley differences on the wheel surfaces. This measurement is designated Ry. Additionally, we used an associated software program that provided a graphical display of surface finish. Ideally, we would have measured the total width of surface (0.25" in our case) and obtained a maximum difference across that total width. In the actual case, we were limited to a maximum measured distance of 0.1" because of gage physical properties and software limitations. Overlapping multiple measurements showed that the 0.1" measurements was quite representative after the final polishing operation, so this limitation was not considered a significant factor. This is significant when macroroughness is considered.

5.5 Rheology

The rheology of the various lubricating medias tested was examined using a Haake system of cup and cylinder specimen holders and associated software and display drivers, see photo, Fig. 26 for a view of the equipment. This system allowed accurate and efficient determination of viscosity and a graphical display showing characteristics of the test media under increasing or decreasing changes in shear rate.
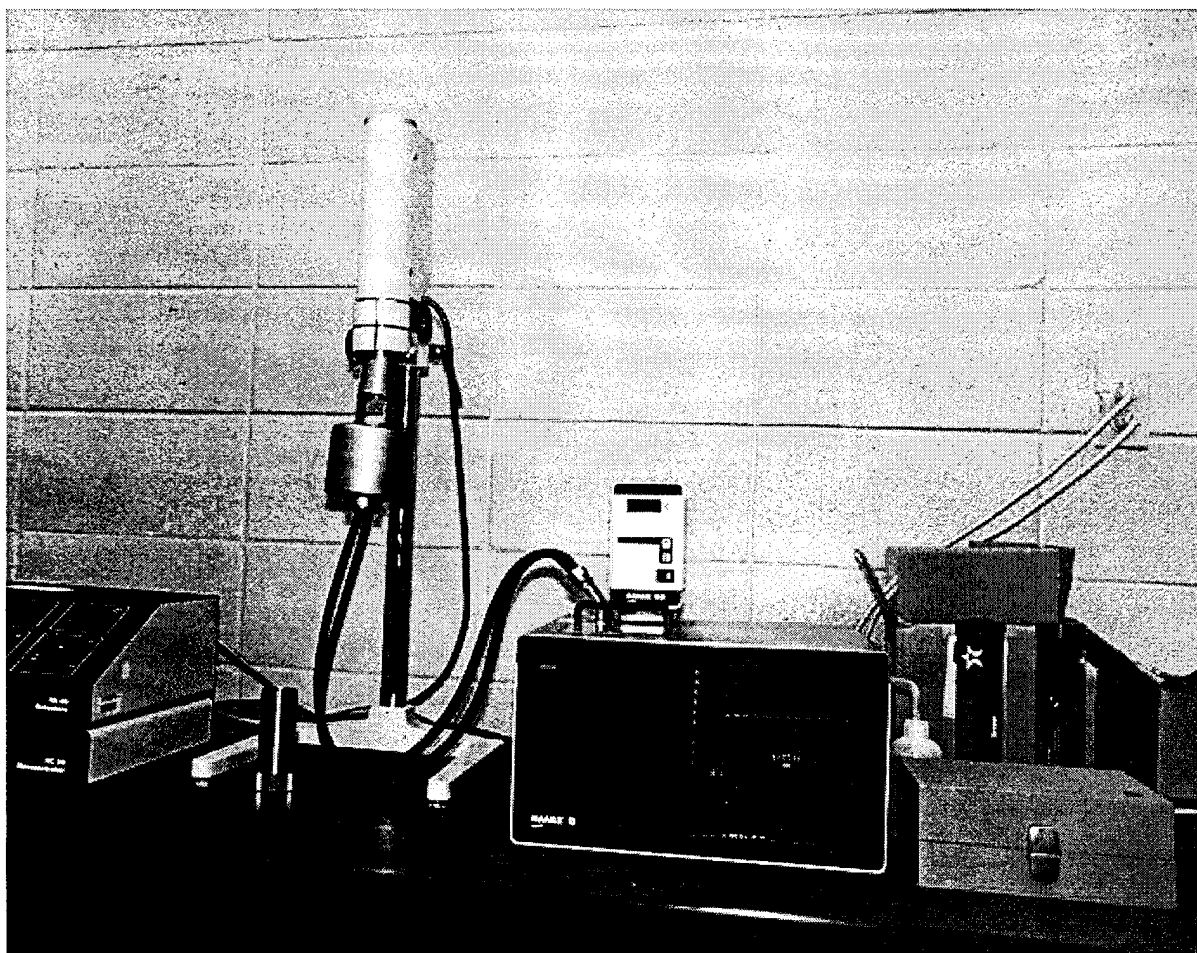
Figure 26. Rheology Equipment.

5.6 Experimental Techniques

5.6.1 Objectives of the Experiment

5.6.1.1 Base Objective

To perform parametric studies of traction characteristics of liquid transported solid lubricants. Parameters to be varied are load, slip velocity, slurry density, and temperature.

5.6.1.2 Related Objectives

To reconcile the test data with the analytical model and to verify analytical model predictions through experimental results.

5.6.2 Initial Testing and Identification of Equipment Issues.

After assembly and initial checkout was completed, the first tests series was run using common automotive lubricating oil, and one 6" flat and one 6" crowned wheel, which gave a point contact between the wheels. The results of that test series is shown in Fig. 27. The shape of the curves was about what was expected, but we had no standard against which to compare our results.

101
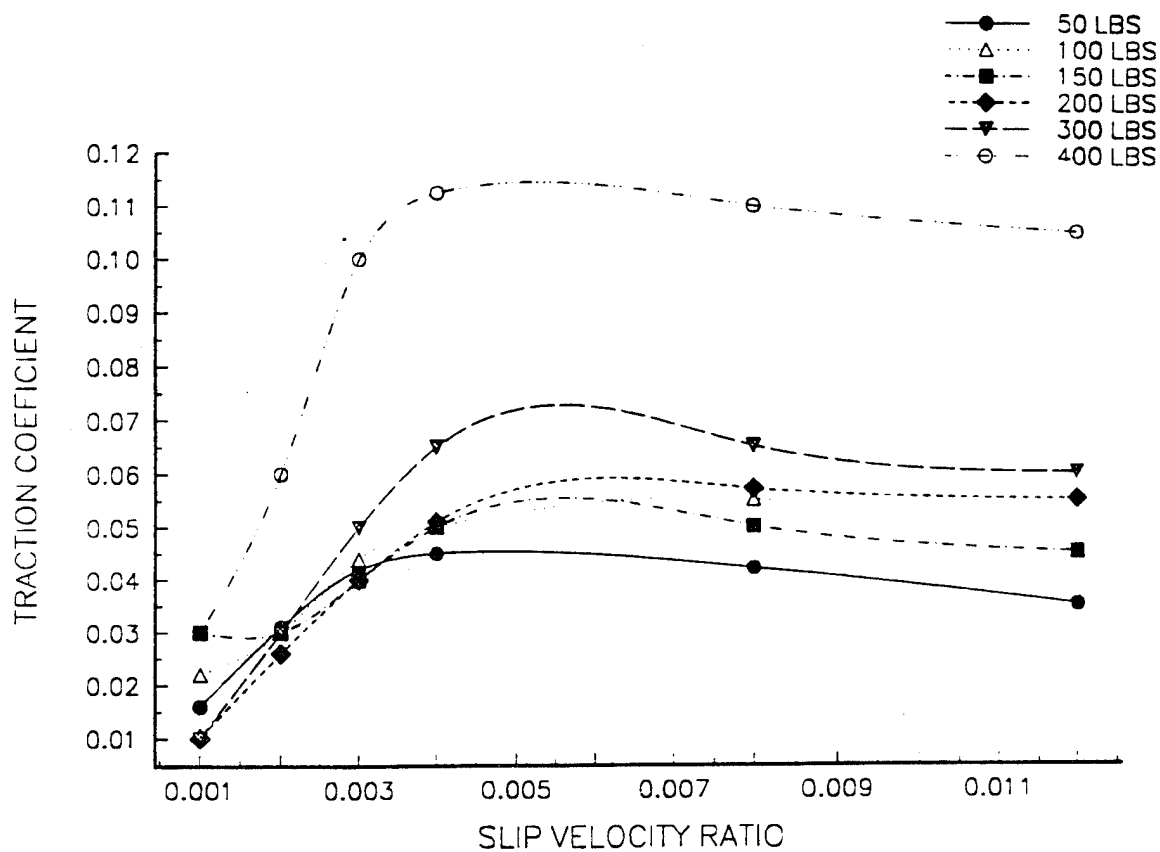
Figure 27.   Initial Traction Rig Data with Automotive Oil.

Figure 28. Wright-Patterson AFB Traction Data – m.1-L-7808J Oil

0-87-2

9549 RPM
6366 RPM
3183 RPM
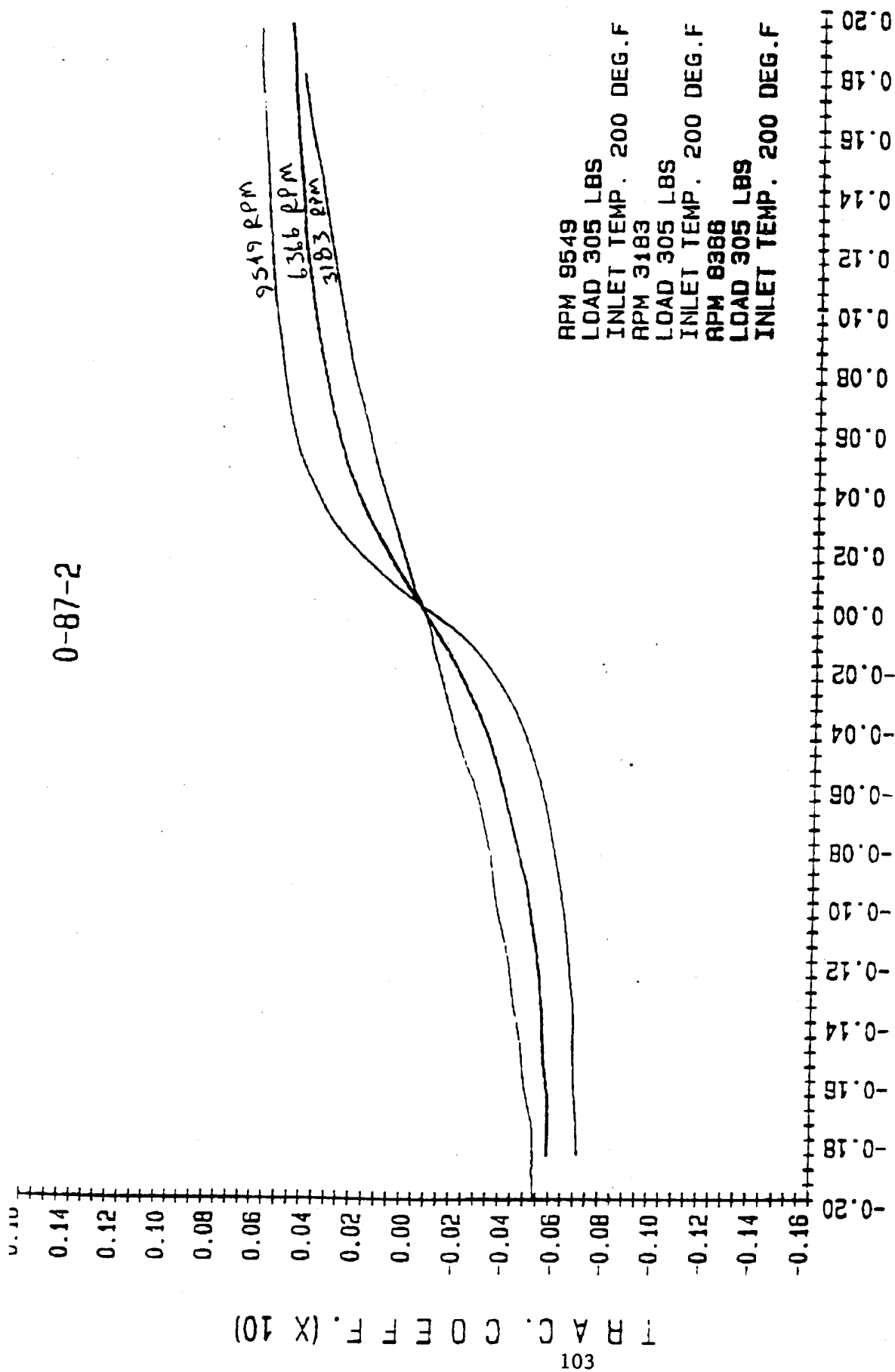
RPM 9549
LOAD 305 LBS
INLET TEMP. 200 DEG.F
RPM 3183
LOAD 305 LBS
INLET TEMP. 200 DEG.F
RPM 6366
LOAD 305 LBS
INLET TEMP. 200 DEG.F

TRAC. COEFF. (X 10)

103

Fig. 28 is a set of curves obtained from WPAFB showing data obtained using a gas turbine lubricant (Air Force Oil, spec MIL-L-7808J) at the conditions shown. Fig. 29 compares the data from Fig. 28 (9435 rpm) to data taken at USL with the same MIL spec oil. The mid part of the curve matches fairly well, but the maximum traction coefficient of the USL test is well below that of the WPAFB data. This was attributed to differences in surface finish (an unknown), and the difference in oil temperature. WPAFB ran the test at 200 deg F oil temperature, the USL test was at 75 deg F. This comparison became somewhat moot because the analytical model that was being used was not set up to use point contact in the calculations. In order to match the experimental and analytical data bases, it was necessary to use two flat wheels, giving a line contact, for all testing. After some experimentation, the width of the contact area was set at 0.25".

As will be seen later in this report, the decision to use line contact had unexpectedly far reaching consequences. The traction rig was not designed to provide precise, adjustable line up between the test wheel surfaces, which is essential for line contact testing, but inconsequential for point contact testing.

Fig. 30 shows the results of the first series of tests using
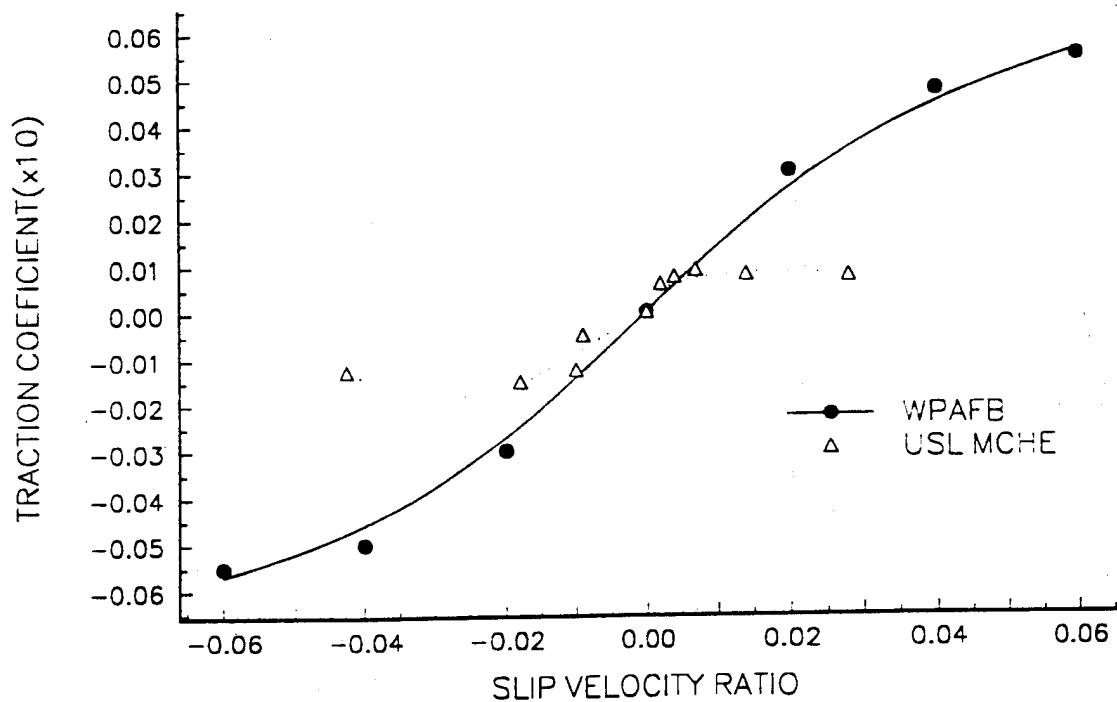
Figure 29. USL Experimental Data vs. Wright Patterson AFB Data.
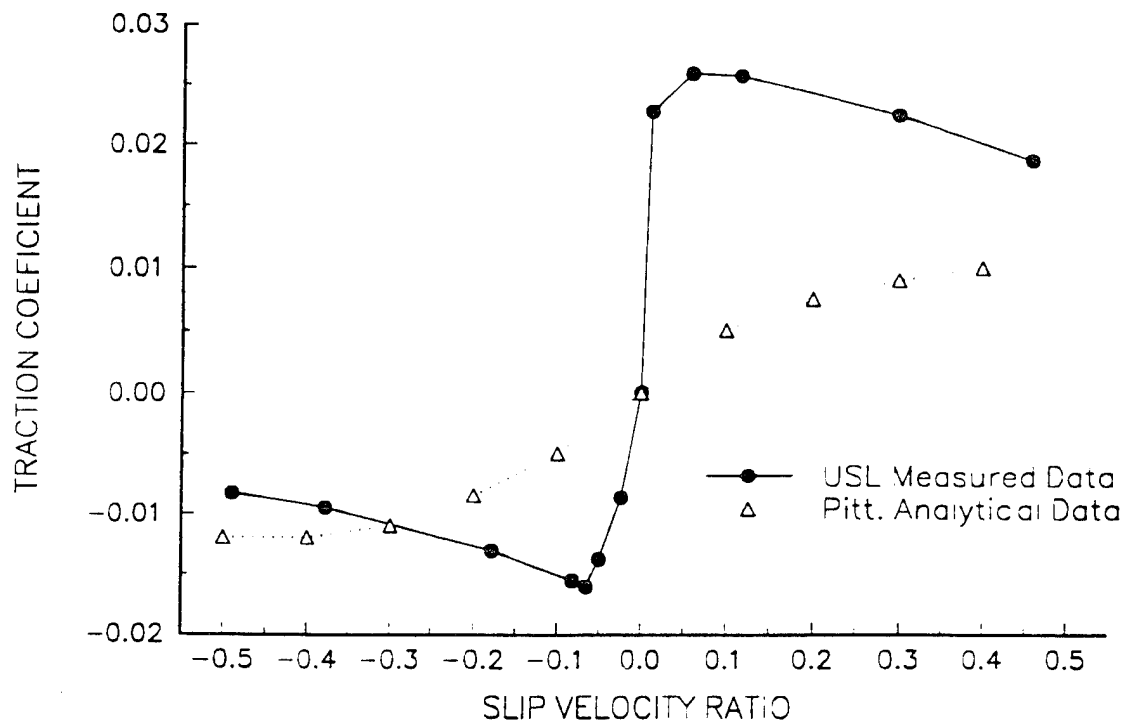
Figure 30.   Initial Measured vs. Analytical Data Comparison.

the 0.25" flat. There was a significant difference between the experimental and analytical prediction. USL (experimentaldata) showed a higher traction coefficient than the analytical data for all values of slip. At this point it was decided to concentrate on the objective of experimental/analytical reconciliation before moving to slurry testing. This decision was implemented through the following actions.

- Literature search had turned up a paper by Johnson and Cameron (1967-68) covering close to the same area of interest. They had used Shell Turbo Oil 33 as their lubricant. Since it appeared that their work could serve as a reference, we decide to use the same oil for our baseline work. Shell Turbo Oil 33 was no longer available, having been superseded by Shell Turbo Oil 68. Shell technical data indicate the two oils have identical temperature, pressure and viscosity characteristics. A quantity of this oil was obtained and was used in all further oil based tests.

- It became apparent that there were a number of assumptions underlying the analytical model that could not be duplicated in the experimental environment. These situations were addressed individually with a goal of reducing their adverse impact to a minimum. Section 5.7 details

107

this work.

5.7 Analytical Assumptions vs Experimental Environment.

ASSUMPTION   ENVIRONMENT

5.7.1 PERFECTLY SMOOTH SURFACES   LESS THAN SMOOTH

The best surfaces obtainable with the techniques and equipment
at hand (see Part I) was a peak to valley height (Ry) of 8 to
12 micro inches. As covered in 5.4, the Surftronic gage does
not allow a continuing measurement over the total 0.25" sur-
face, but is limited to a continuous measurement of 0.1" (this
is not a limitation of the gage, but is caused by the rela-
tionship of the gage probe and test wheel physical dimensions
plus the gage software). There was concern that this might
lead to a macroroughness condition that would be undetected by
the measurement. Evidence suggests that this condition did
exist during early testing when a continuous measurement of
0.03" was being used. Use of the 0.1" measurement
significantly reduced any macroroughness errors. In any
event, the major concern is whether or not asperities on the
test wheel will pierce the film thickness of the lubricant at
the wheel interface. Since the calculated film thickness was
approx-imately 70 μin. at the test conditions used, it would
appear that 12 μin. Ry would provide adequate safety factor.
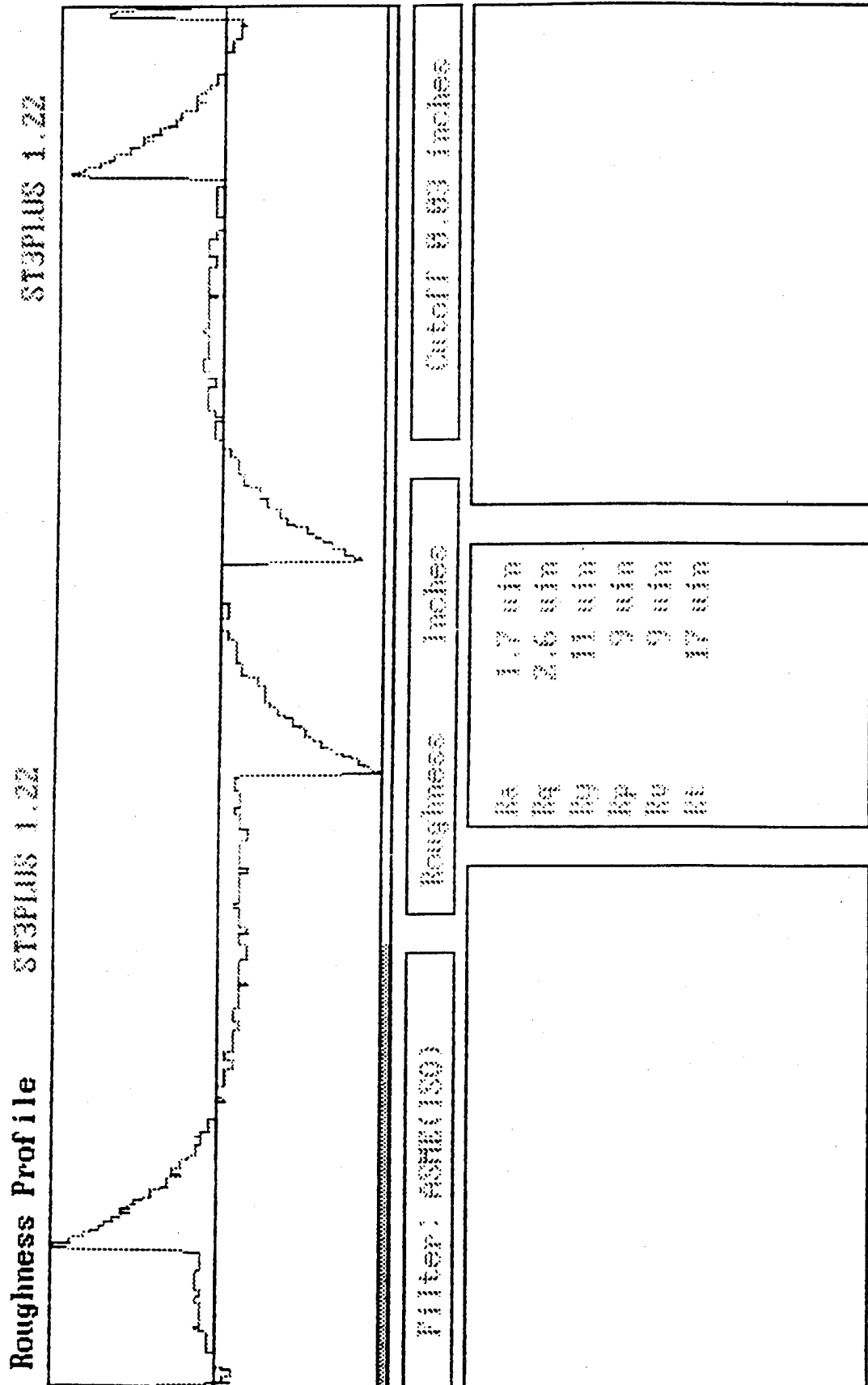
Figure 31.   11 Micro Inch Roughness Profile.

Fig. 31 is a graphic representation of a wheel surface at 11 μin. peak to peak.

Even with the best of polishing techniques, the perfectly smooth surface assumed by the analytical model cannot be achieved. The magnitude of the effect of this difference would be difficult to quantify, but it is a certainty that a rougher surface will tend to increase traction coefficient values especially at low slip speeds.

<table>
<tr><td>ASSUMPTION</td><td>ENVIRONMENT</td></tr>
<tr><td>5.7.2 PRECISELY KNOWN CONTACT AREA</td><td>VARIABLE - ALWAYS
LESS THAN CALCULATED</td></tr>
</table>

Because of flexibility in the rig structure plus some unavoidable crowning of the flat area of the test wheels the faces of the wheels cannot be perfectly parallel during the experiment. Any nonparallelism will reduce the test surface area and effectively increase the stress at the interface area. In order to minimize this effect, the rig was modified so as to include a leveling nut attached to the upper (moveable) platform, see sketch, Fig. 32. Fig. 33 is a close up photo of the test wheel interface. This leveling nut was adjusted to give a minimum torque reading after all other test conditions were set. This technique maximized surface parallelism and contact area. Fig. 34 shows the amount of

110

Figure 32.

111
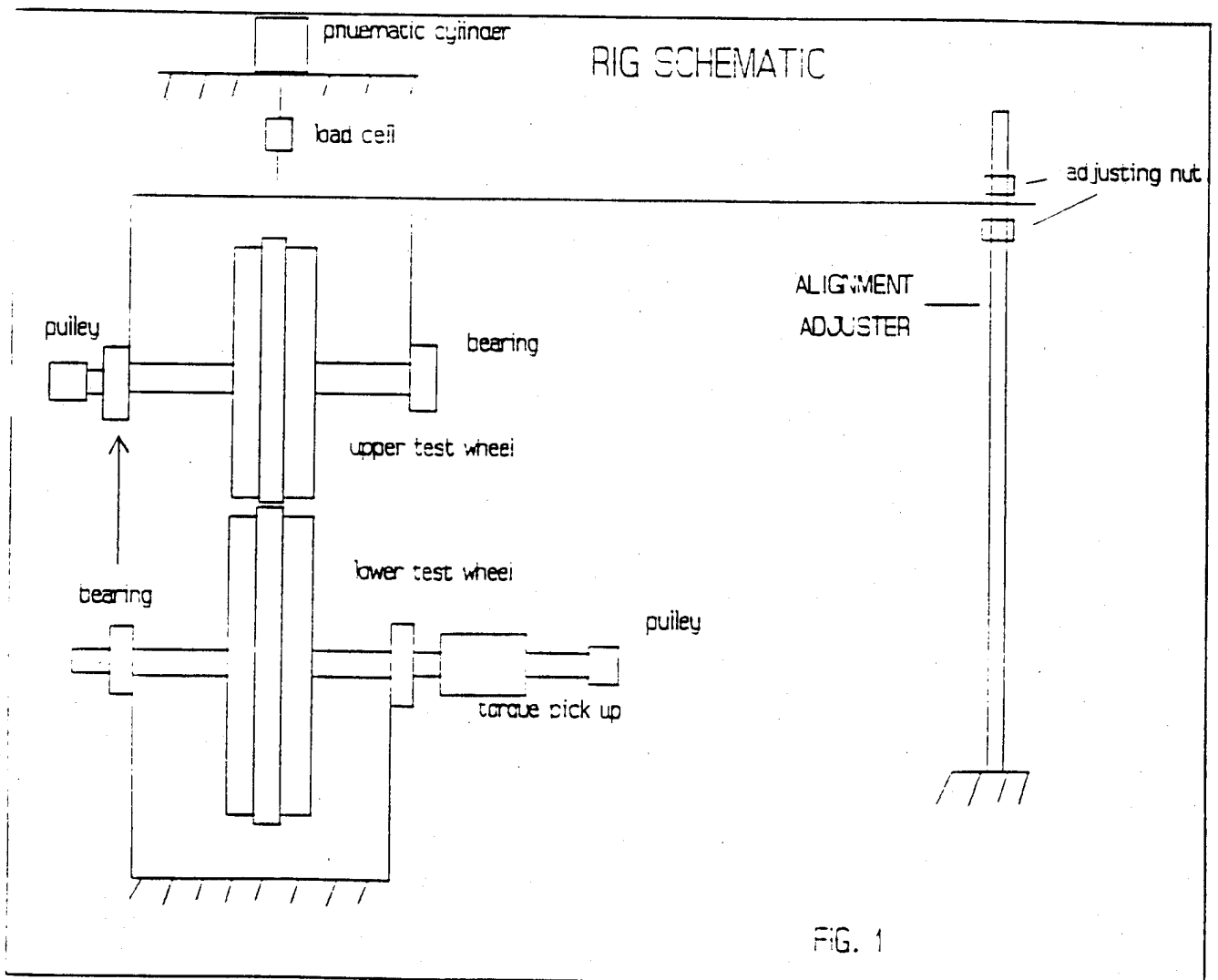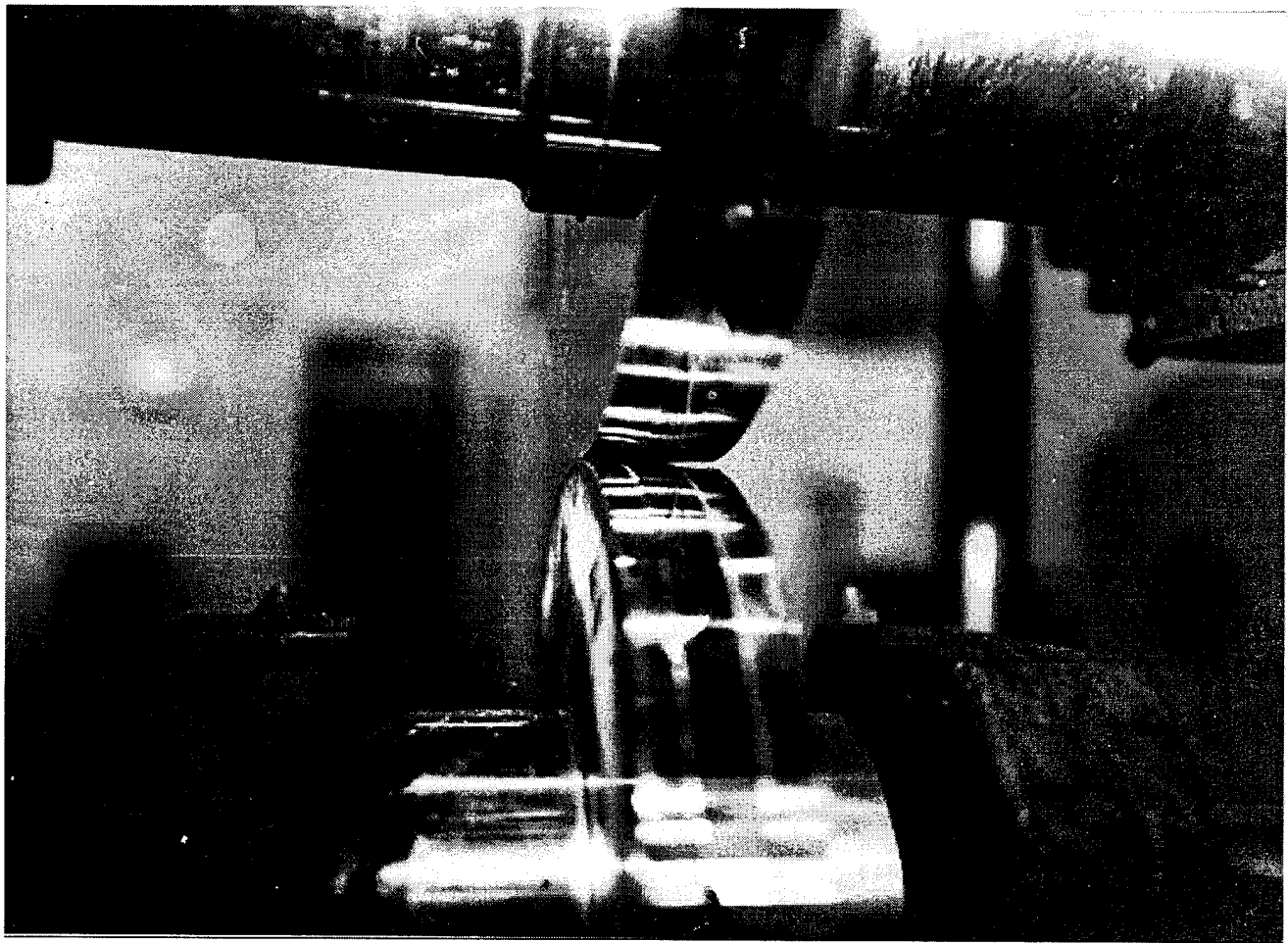
Figure 33.   Test Wheel Interface.
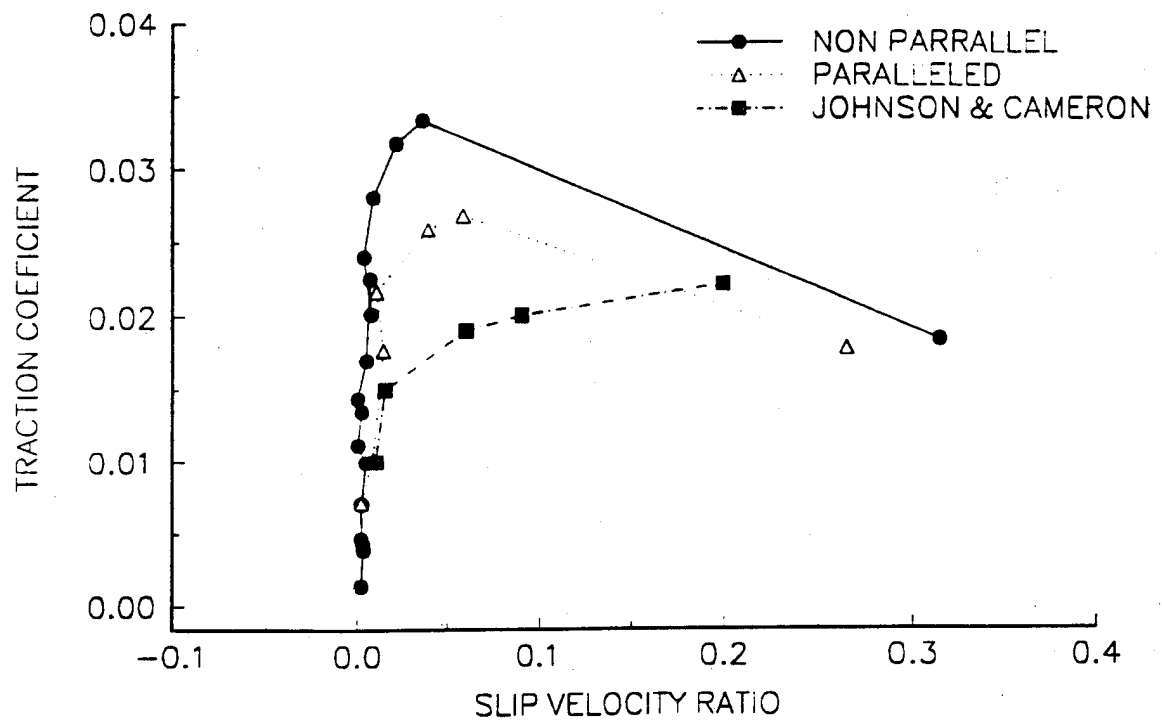
Figure 34.   Effect of Parallel Adjustment

were set. This technique maximized surface parallelism and contact area. Fig. 34 shows the amount of reduction in traction coefficient between the unadjusted and adjusted condition. Another measure of the success of this approach was obtained when scuffing occurred during testing. Generally only about half of the .25" wheel surfaces showed scuff marks. This does not mean the stress is doubled since the lubricant film thickness will tend to even out the pressures. It does mean, however, that the wheels were not perfectly parallel in spite of our best efforts.

It is expected that the result of this reduced contact area would be a higher than calculated traction coefficient for all values of slip.

ASSUMPTION	ENVIRONMENT
5.7.3 PRECISELY KNOWN SURFACE SPEEDS	INHERENT MEASUREMENT ERROR

While the data are plotted in terms of traction coefficient vs slip velocity ratio, the parameter used in analysis is the sliding speed in inches/sec between the wheels. If we assume that the diameters of the two wheels are exactly the same, and that the rpm's of the wheels are taken simultaneously without error, then the surface speed calculation can be made with

114

confidence.   These assumptions create some difficulties as described below.

- The diameters of the two wheels are not exactly the same, but since they can be measured precisely, any error introduced can be corrected.

- The rpm of the wheels is a very difficult parameter to measure precisely at any given instant.   The instruments measure rpm by counting pulses, integrating the result and displaying the answer. With the instruments used for this test, the display updated about once every 1/2 second.   Even after allowing extended stabilization time, the speed of the motors varied by 1/2 rpm or so every second.   The ratio between motor speed and test wheel speed is 1:6, so the test wheel might vary by 3 rpm every second.   Therefore, there is possibly a maximum error of 3 rpm between the rpm readings of the two test wheels if they were taken at the same instant.   If they were taken at two different times the error could be as high as 6 rpm.   This magnitude of error becomes very significant at low slip ratios and low wheel rpms.   For instance, at 1,000 rpm (where most of our data were taken) and a measured slip velocity ratio of 0.006, the actual slip velocity ratio at the instant of measurement could have been anywhere between 0 and 0.012.

This error is reduced by taking a number of measurements and averaging the difference, but the error potential remains. Of course, since the error is the same at all values of slip, its impact on the measurement is reduced as the slip value is increased.

Because of the above, it is felt that the portion of curves with slip values below 0.01 should be treated as a band rather than a single line. If these low slip measurements are critical to analysis, a range of +/- 0.003 should be used at a speed of 1,000 rpm.

It should be noted here that the traction rig is capable of much higher speeds, and that the errors introduced because of the effects outlined above would be significantly less if the speeds were increased. At 10,000 rpm a 0.01 slip ratio would be a 100 rpm difference in wheel speeds and the error introduced by a 1/2 rpm speed change would be insignificant. We had initiated our testing at the higher speeds, but reduced to the 1,000 rpm level because of limitations of the analytical model.

116

| ASSUMPTION | ENVIRONMENT |

5.7.4   SIMULTANEOUS MEASUREMENT OF   INHERENT INSTRUMENT

        SPEED AND TORQUE   DELAY

The data curves are presented as if values of torque (traction
coefficient) and test wheel rpm were measured simultaneously.
Whether the data are read with a computer or manually there is
a slight delay between the readings.   Since the torque
readings tend to be fairly steady at the levels used in these
tests (above 0.04 ft lbs) we do not feel this possible error
to be significant.

| ASSUMPTION | ENVIRONMENT |

5.7.5   PRECISELY KNOWN TEST LOAD   FRICTION IN LOAD

                                           SYSTEM

The load applied during tests is calculated by subtracting the
load reading from the test cell, which is the amount of weight
supported by the test cell, from the tare weight, which is the
total weight of the upper platform of the rig.   The tare
weight was determined to be 720#. Because the upper platform
is held in place laterally by four rods, there is a certain
amount of friction introduced as the platform moves up and
down.   This friction is a variable, but careful attempts at

measurement indicated a level of about 20# maximum. This possible error was noted, but since the vibration of the rig during operation works to reduce it, so we have not included a correction in the calculations.

ASSUMPTION	ENVIRONMENT
5.7.6 NO EXTRANEOUS TORQUE LOSSES	VARIABLE BEARING LOSSES

The analytical model assumes that the torque component of the traction coefficient is made up only of the torque that is created at the interface between the test wheels as the slip velocity is increased. In the test environment there are support bearings between the wheel and the torque transducer. These bearings have a finite rolling resistance that varies as a function of speed and load. Referring again to Fig.32, it is seen that there are three bearings between the wheel interface and the torque transducer that must be accounted for:

- the outboard and inboard wheel support bearings and the inboard bearing of the transducer housing itself.

The following is a description of the methodology used to determine the level of that bearing resistance. The pure turning loss was measured by running the master motor under no load conditions (that is, no contact between the master and slave test wheels) over the range of speeds expected and measuring the torque.

118

The loss due to load on the bearings was measured by then turning the motor at the minimum possible speed (20 rpm) with applied loads of 100, 200, and 300 lbs. This required bringing the slave wheel into contact with the master, so we disconnected the slave motor from the slave test wheel shaft, then only the bearings supporting the test wheels were involved in the measurement. We then took measurements at each load point and divided them by two to obtain the load loss figures. This division was based on the assumption that the master and slave bearing losses are of the same level. We could not run the load test at higher speeds since the necessary introduction of lubricant would have masked the results. We recognize that this method ignores the torque caused by the slight deformation of the wheel at the contact point. The total bearing loss was then calculated in accordance with the following:

Bearing loss = speed loss + load loss + indicator zero reading.

It is interesting to note that the bearing loss changes sign depending upon whether the slave motor is running faster or slower than the master motor. For our test calculations we included a value of .1 lb ft. either added or subtracted from the torque readings depending upon the relative speed. As a result of the above, we feel that our accuracy in obtaining

lbs load and 1000 rpm. This can introduce an error of .0006 to the traction coefficient value, which is not significant except at very low values of friction.

| ASSUMPTION | ENVIRONMENT |

5.7.7 KNOWN LUBRICANT TEMP. AT THE NIP   INLET AND OUTLET
                                           ONLY

The temperature of the oil at the nip (the area between the test wheels operating under the contact pressure) is critical to the calculations. While we applied thermocouples to the inlet between the wheels, and as closely as possible to the outlet, we were not able to measure the nip temperature itself. It may be assumed that the oil supply is great enough that only a slight rise occurs, but we do not have definitive data to this affect.

5.8   Summary of Final Test Results.

After making all of the above described changes in equipment and procedures, a series of tests was run that represented the best possible accuracy. Our purpose was in line with the originally stated objectives of reconciling the test and analytical data, and obtaining data on liquid transported solid lubricant.

120

Fig. 35 shows data taken at 200lb and 400lb load with Shell Turbo 68 oil. It also shows the calculated data for the same conditions at the 200lb load. The experimental results are somewhat lower than the analytical results at slip velocity ratios above .1. It should be noted that the bulk of the preliminary data taken while the equipment and procedures were being developed showed just the opposite, that is, experimental data results above analytical results. Since these later data proved to be very repeatable we conclude that the surface finish and leveling techniques used resulted in lower friction and contact stress.

Fig 36 shows the results of an 8:1 slurry (8 parts by weight ethylene glycol to 1 part graphite) at 400lb and 700lb load. The values of traction coefficient are very low, much lower in fact than what had been predicted. Since this was a surprise, it raised another series of questions that were pursued to insure the accuracy of the data.

- Torque Transducer Accuracy. The torque transducer in use had been in service for an extended time and it was thought that perhaps it might be approaching the end of its useful life. Personnel at WPAFB were able to locate another transducer which was installed on the rig and the slurry test was repeated. Fig. 37 shows the results of that test. There is a slight

121
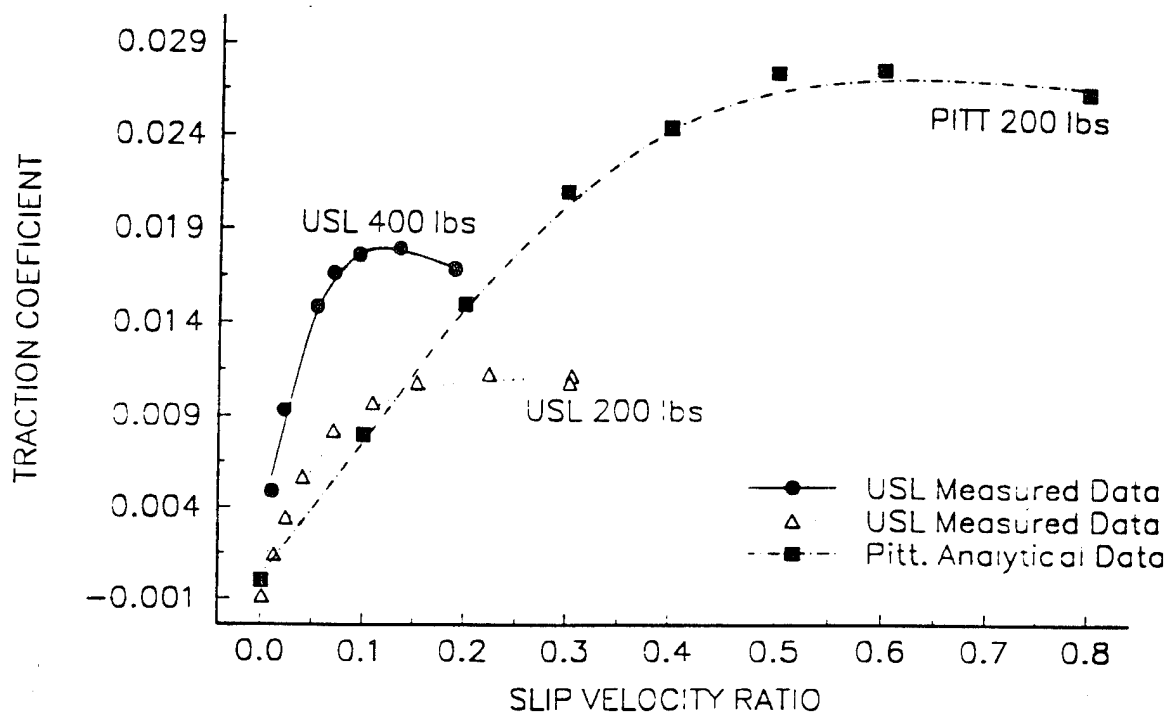
Figure 35.   .25" Flat Experimental vs. Analytical Test
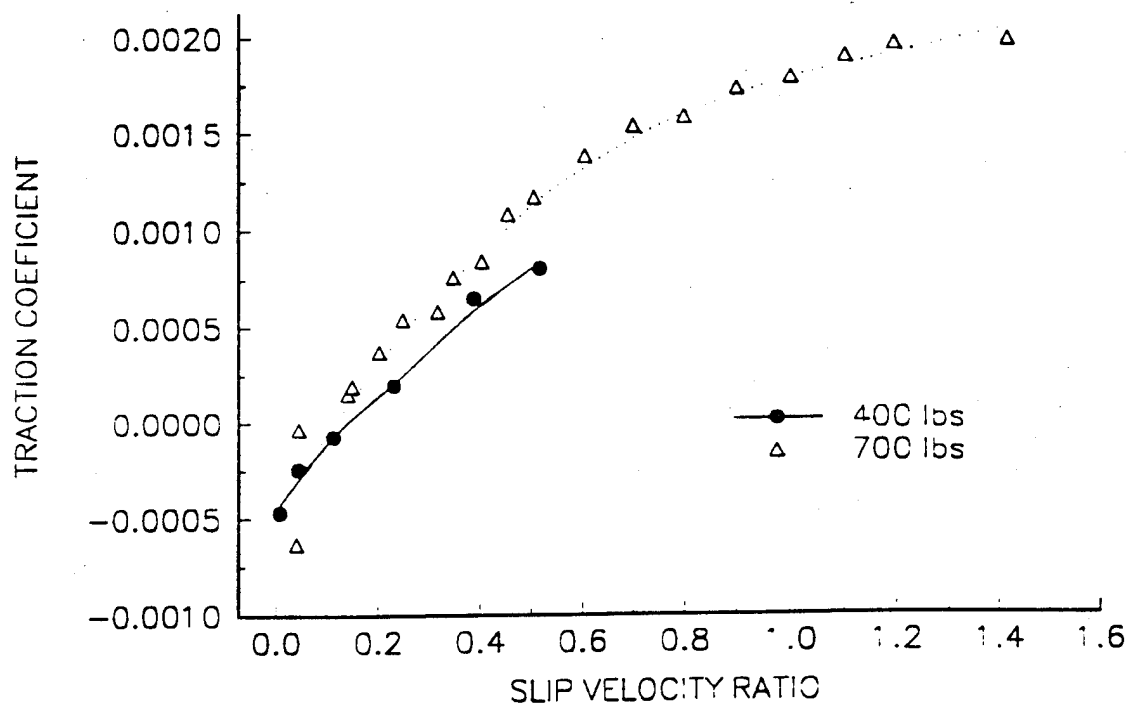
Figure 36.   8:1 Slurry Test

123
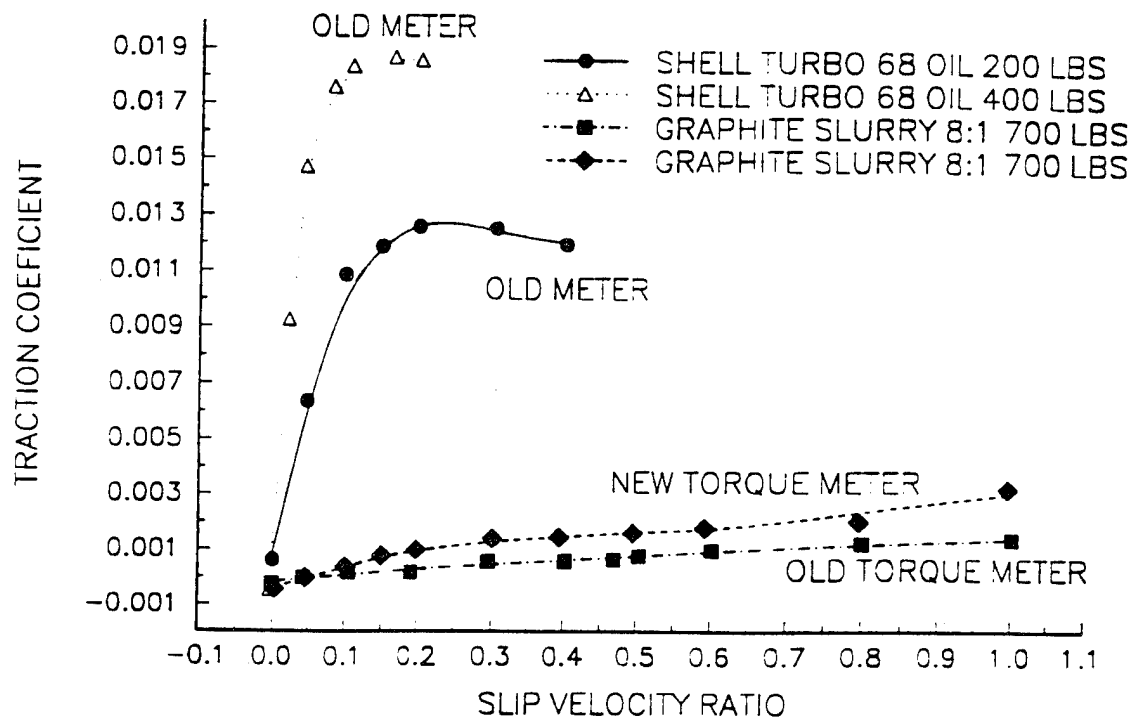
Figure 37.   Old to New Torque Meter Comparison – Slurry Test

124

difference in traction coefficient, but the difference is certainly within the range of expected repeatability.

- Slurry Rheology. The second question addressed the rheology of the slurry. It was anticipated that the viscosity of the slurry would be higher than that of the oil because of the solid particles in suspension. We tested the slurry and the Turbo 68 oil with the results shown on Fig. 38. The slurry viscosity is an order of magnitude below that of the oil.

- Load Measurement Accuracy. 5.7.5 describes an expected error in load measurement of up to 20lbs. The USL Laboratory has obtained a button type pressure transducer that we have used to measure the load directly at the wheel interface. The condition is static, but running vibration was simulated manually. The results confirmed the max. 20lb error.

5.9   Conclusions and Recommendations

Insofar as the test results are concerned, we conclude that the slurry as tested does in fact allow much lower traction coefficients than the Turbo 68 oil under the same conditions. We do not know how this will change with variations in slurry temperature and density. The early test protocol anticipated running at a high enough temperature so that the ethylene

125
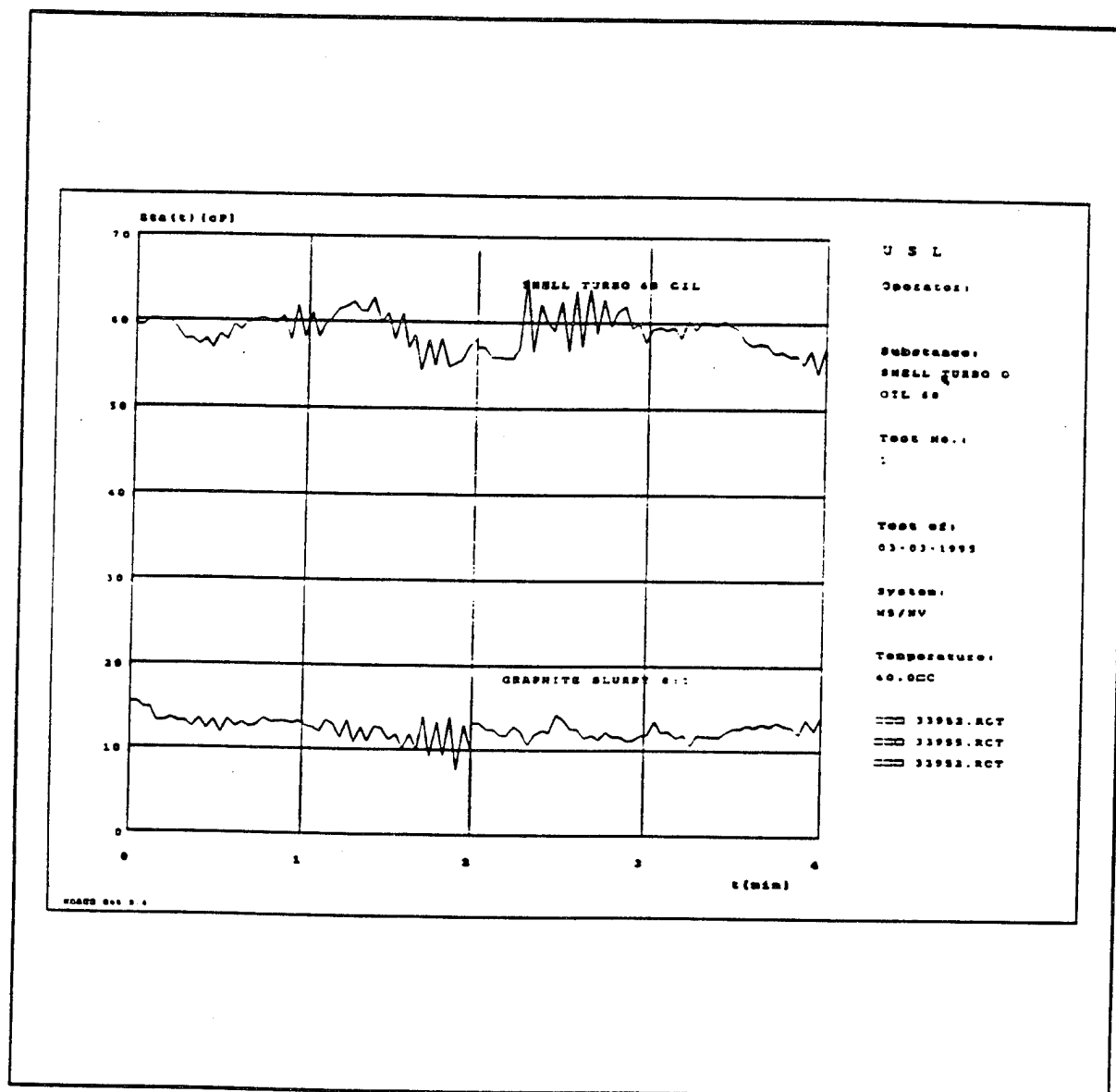
Figure 38. Rheology Results.

126

glycol carrier would evaporate as the slurry is introduced to the nip between the test wheels. The time spent developing the test equipment and techniques precluded running this level of test during the project time allotment.

If further testing is to be authorized, it is recommended that a traction rig be constructed first that better serves the primary objectives of the program. This would include the following features as a minimum:

- Drive motors with absolute speed control (perhaps synchronous motors driven from a well regulated variable frequency supply).

- Speed sensors with instantaneous reading capability. Well filtered tachometer generators should be acceptable.

- Rigid, yet adjustable platforms with optical devices to insure perfect line up of test disc interfaces

- Torque and load transducers using the latest technology to minimize errors and variations.

- A computer control system using parallel input conversion boards with a capability of reading and providing feedback control to at least five channels simultaneously.

- An improved system of trueing and polishing the test wheels.

An estimate on the cost of a system such as the above could be provided after some preliminary design work and an investigation of the equipment available commercially.

6.0 Traction Behavior and Physical Properties of Powder Graphite Lubricants

The section gives a method for predicting traction coefficients of dry graphite powder lubricants. The analysis is based on the assumption that unconsolidated powder lubricants behave as elastic solids when compressed to Hertzian pressures levels in rolling contact regions. This assumption is supported by the classic work of P. W. Bridgman who studied the effects of extreme pressures on physical properties of several chemical substances, including graphite. This section also gives bulk modulus data for graphite powder compressed up to 100,000 psi and shows how this property is used to predict the film thickness of graphite powder in Hertzian contact. Extrapolation of the bulk modulus data developed during this study compares favorably with compressibility data presented by Bridgman.

Our approach, based on Bridgman's classic work, is contrary to Heshmet (1) who postulates that a layered shearing of a compacted power lubricant generates velocity, pressure, density, and temperature profiles akin to those in the liquid lubricant of a fluid film bearing and who further concludes that powder-lubricated disk-on-disk traction versus slip/roll

129

behaves in a manner similar to conventional elastohydrodynamic (EHD) theory.

6.1 INTRODUCTION

The objective of this particular part of the project study was to analytically predict traction coefficients for dry graphite powder lubricants. The basic assumption here is that a thin film of highly compacted graphite powder can be analyzed as a solid film having elastic properties up to the point of yielding. This assumption is consistent with the experimental work of Bridgman (2)(3)(4). Graphite powder lubricants are assumed to be unconsolidated prior to entry to a Hertzian contact region. Once delivered into the contact region, powder lubricants are compacted to Hertzian pressure levels and undergo physical changes.

The analytical prediction of traction coefficients for solid films typically require the following information:

> * thickness of the solid film or coating
>
> * shear strength of the solid film (lubricant)
>
> * coefficient of friction between film and contact surface
>
> * Modulus of elasticity/rigidity
>
> * Poisson's ratio

Film thickness of compacted graphite film is not initially known but can be predicted from calculations based on bulk modulus, which is a function of Hertzian pressure. Film thickness also depends on delivery rate of the powder lubricant, speed of rotation of the disks as well as load. Bulk modulus for a premium graphite powder was determined as part of this study up to a compressive stress of 100,000 psi. This stress level was adequate to cover example traction calculations consistant with the test rig operating conditions. Extrapolation of the data developed during this study is consistent with data reported by Bridgman (5)(6) who conducted compressibility tests at much higher stress levels using smaller specimen volumes.

The shear strength of highly compacted graphite powder is also documented in Bridgman's (2)(3)(4) papers. The coefficient of friction of compacted graphite was established by Boyd and Robertson (7). The modulus of elasticity/rigidity was extracted from bulk modulus. Poisson's ratio was approximated using data given in reference (8).

The sections below describe the experimental steps that were taken to determine bulk modulus and how all the above information was used to determine traction coefficients for graphite films.

The study also gives a direct method for predicting film thickness of dry powder lubricants using bulk modulus data.

6.2 PHYSICAL PROPERTIES OF COMPACTED GRAPHITE POWDER LUBRICANTS

Shear Strength - Bridgman (2)(3)(4) studied the shearing phenomena of a number of chemical substances including carbon (graphite). Test specimens were compressed between flat surfaces having an active pressure diameter of 6.3 mm. Shearing stresses were developed by means of a rotatable transverse arm, containing active pressure surfaces sandwiched between two anvils. Samples of test specimens isolated the rotatable arm from the rest of the test fixture such that torque on the arm was a direct indicator of shear stress level in the test specimen. Tests were conducted by Bridgman up to a maximum compressive stress of 50,000 kg/cm^2 (711,000 psi). Small angular displacements of the arm indicated elastic shear deformation while large angular displacements (60 deg) indicated either slippage at the interface (giving coefficients of friction) or plastic deformation internal to the test specimen (giving shear strength of the test material).

Plots of shearing stress verses normal pressure (corresponding to large angular displacement of 60 deg) typically contained a "knee" separating slippage at the interface and plastic

132

slippage internal to the specimen. This type of data quantifies shearing strength and shows how it increases with applied pressure. While Bridgman does not give this type of curve specifically for graphite, he does state that the shearing strength for graphite at the maximum pressure of 50,000 kg/cm^2 (711,000 psi) was determined to be 10,000 kg/cm^2 (142,200 psi).

Coefficient of Friction - Boyd and Robertson (7) used a test rig patterned after the one by Bridgman (4) to determine the coefficient of friction of liquids, semisolids, and solid materials, including graphite, at applied pressures up to 400,000 psi. Test results indicate that graphite powder lubricant compacted to a pressure level of 400,000 psi has a coefficient of friction between 0.036 and 0.058. Bridgman's discussion of this paper suggested that at the 400,000 psi pressure level slippage probably occurred internally to the test specimen due to plastic flow and not at the interface with the anvil. Peterson and Johnson (9) report coefficients of friction for graphite of 0.06 and 0.11.

Bulk Modulus of Compacted Graphite Powder - Bulk Modulus is defined as the ratio of incremental change in average stress to the corresponding unit volume compression. Bulk modulus (K_m) relates to modulus of elasticity (E) through (see Timoshenko and Goodier (10))

$$K_m = \frac{E}{3(1 - 2v)} \qquad (37)$$

where (v) is Poisson's ratio. Bulk modulus is not a constant for compacted graphite powder but varies with compaction pressure (also see Atluri (11)).

Bulk modulus was determined during this study by compressing graphite powder within a cylinder by means of a solid ram. The compressive force was generated by a materials testing machine which has the capacity to generate up to 200,000 lbs force. Typical applied loads went up to only 50,000 lbs, which generated 100,000 psi compressive stress on the graphite sample. Maximum compressive stress was limited by the strength of the cylinder material, which was high tensile steel (HS420) having a yield strength of 210 ksi.

The axial stress on the graphite plug generated horizontal pressure on the inside wall of the cylinder. The magnitude of this pressure was determined by use of tangential strain measurements at the outside surface of the cylinder. Strain gages were positioned at two locations on the outer surface for this purpose. These strain measurements were also used to determine volume changes of the graphite plug associated with radial expansion.

134

The experiments were conducted at room temperature. Dry graphite powder was placed inside the cylinder barrel in small volume increments until a height of 2 inches of the sample was reached. The graphite powder settled essentially from its own weight. A positive axial load on the graphite powder could not be measured until a certain degree of compaction was reached. i.e, when most of the air in the sample was removed. From that point, the load was applied in steps of 2000 lbs and the corresponding displacement of the ram was measured. Load to the ram reached a maximum level of 50,000 lbs. This load developed an axial compressive stress of 100,000 psi because the cross sectional area of the ram was 0.5 in2. See Figure 39 for displacement vs axial load.

A typical test included measurements of axial force applied to the ram, axial travel of the ram, and circumferential strain measurements at the outside surface of the test cylinder. At the beginning of each test, the ram moved a considerable distance with little required force until the air within the sample was removed. Mathematically, bulk modulus is defined as,

$$K_m = \frac{d\,\sigma_{ave}}{\frac{dv}{v}} \tag{38}$$

where

135

Experimental data at room temperature

(Premium Graphite Grade)

Axial Load (lbs)

Displacement of the ram (inches)

Figure 39.

136
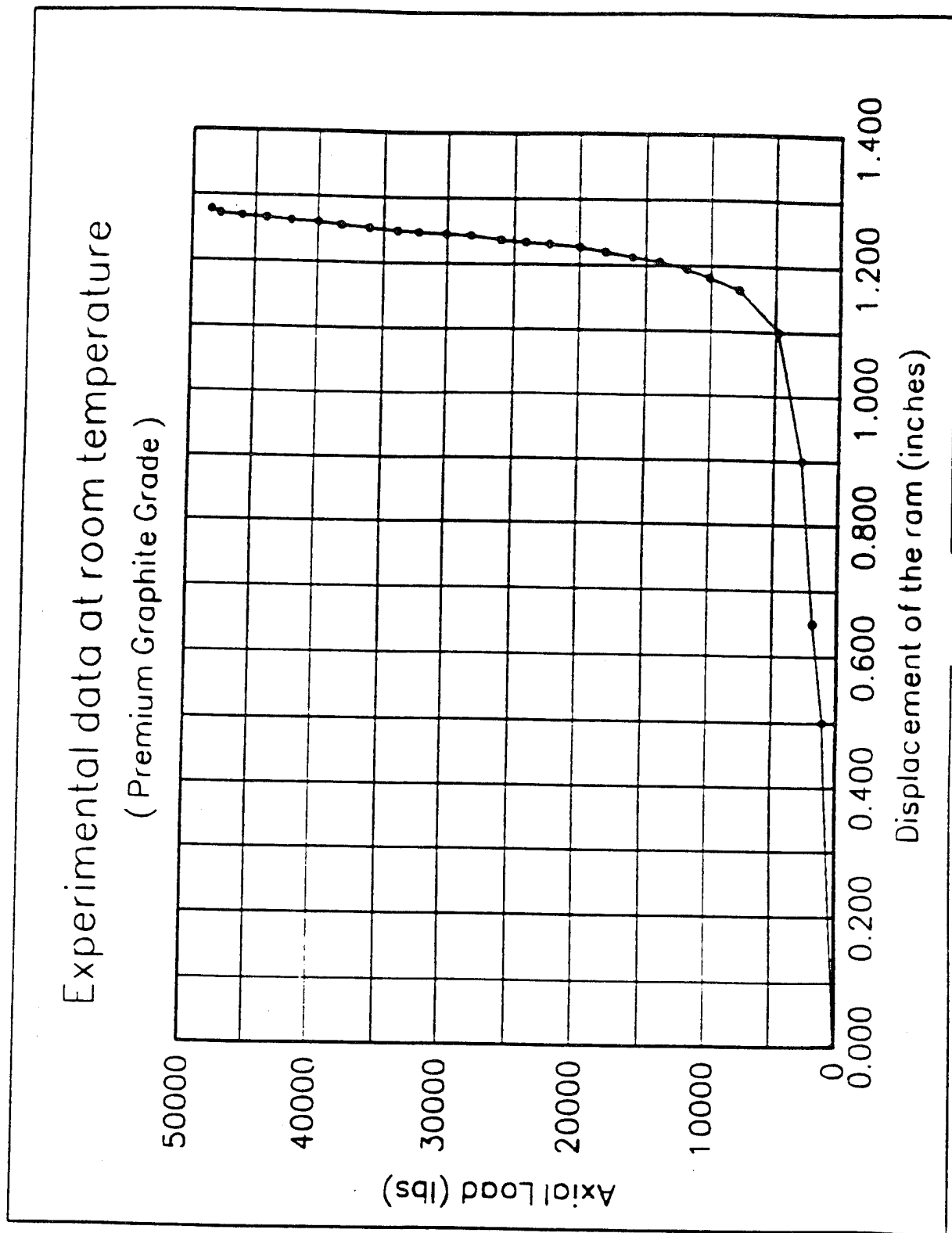
dv — change in volume due to applied $d\sigma_{ave}$

v — volume corresponding to σ_{ave}

$d\sigma_{ave}$ — incremental change in average stress

σ_{ave} — $(\sigma_1 + \sigma_2 + \sigma_3)/3$

In the test procedure described above,

$\sigma_1 = \sigma_a$ (axial compressive stress)

$\sigma_2 = \sigma_r = P_i$

$\sigma_3 = \sigma_\theta = P_i$

$$\sigma_{ave} = \frac{[\sigma_a + 2P_i]}{3} \tag{39}$$

The change in volume, dv, includes the effects of axial displacement of the ram and radial ballooning of the cylinder. Axial displacements of the ram were measured directly. Radial displacements (δr_i) of the inside surface of the cylinder and internal pressure (P_i) were calculated from tangential strain measurements on the outside surface of the cylinder using Lame's thickwall cylinder equations and constitutive equations for elastic materials.

At the outside surface of the test cylinder,

137

$$(\epsilon_\theta)_o = \frac{1}{E} [\sigma_\theta - \nu (\sigma_r + \sigma_z)] \qquad (40)$$

But $\sigma_r = \sigma_z = 0$; so,

$$(\epsilon_\theta)_o = \frac{1}{E} \sigma_\theta \qquad (41)$$

From Lame's equation,

$$\sigma_\theta = \frac{a^2}{(b^2 - a^2)} (1 + \frac{b^2}{r^2}) P_i \qquad (42)$$

which allows internal pressure to be determined from tangential strain measurements.

$$P_i = \sigma_\theta [\frac{(b^2 - a^2)}{a^2} \frac{r^2}{(r^2 + b^2)}] \qquad (43)$$

At outside surface $r = b$. So,

$$P_i = \sigma_\theta [\frac{(b^2 - a^2)}{2a^2}] \qquad (44)$$

The pressure against the inside surface of the cylinder barrel

138

can thus be determined from circumferential strain measurements at the outside surface by combining equations (41) and (44), where $(\varepsilon_\theta)_o$ is determined from strain measurements.

Now consider radial deflections at the inside surface of the cylinder. These deflections directly affect volume calculations.

The hoop strain at the inside surface is,

$$(\epsilon_\theta)_i = \frac{[\sigma_\theta - \nu(\sigma_r + \sigma_z)]}{E} \qquad (45)$$

In the open ended cylinder,

$$\sigma_z = 0 \; ; \quad \sigma_r = -P_i$$

So,

$$(\epsilon_\theta)_i = \frac{[\sigma_\theta + \nu P_i]}{E} \qquad (46)$$

Evaluating Lame's formula at r = a gives

$$\sigma_\theta = [\frac{a^2}{(b^2 - a^2)} (1 + \frac{b^2}{r^2})] P_i \qquad (47)$$

The radial displacement of the inside surface of the cylinder is calculated by combining equations (46), (47), and (48), where (P_i) is determined from equation (44).

Finally,

$$(\epsilon_\theta)_i = \frac{(\delta r)_i}{a} \qquad (48)$$

and

$$(\delta r)_i = (\epsilon_\theta)_i \ a \qquad (49)$$

The volume of graphite inside the cylinder corresponding to a given axial stress condition can now be determined from,

$$v = \pi \ (r_i + \delta r_i)^2 \ l_i \qquad (50)$$

where (l_i) is the length of the graphite powder inside the cylinder. This length is determined by subtracting ram displacement from the initial height of graphite powder in the test cylinder.

140

The above equations can now be used to calculate bulk modulus of compacted graphite powder at the various compaction loads. In finite difference form, the bulk modulus equation becomes,

$$K_m = \frac{\Delta(\frac{\sigma_a + 2P_i}{3})}{(\frac{\Delta v}{v})} \qquad (51)$$

where (σ_a) and (v) are measured directly and (P_i) and (Δv) are calculated from measured data as explained above.

Typical test data generated from the test rig and the above formulations are given in Table 6. One of the first observations from testing was the similarity of magnitudes of the applied axial stress and the radial stress (or pressure) at the inside surface of the test cylinder; notice the last two columns in the table. These data show that the graphite plug, even though consolidated, is very nearly hydrostatic within confined boundaries. This feature was manifested in all of the testing on several different high quality, graphite powder lubricants.

This radial stress on the test cylinder, along with tangential stress, combined to produce high von Mises stress levels and caused failure in early test cylinder designs.

141

Table 6.

Compaction Test Results at Room Temperature
(Premium Graphite Grade)

Volume (cu.in.)	Stress in Theta Dir. (psi)	Average Stress (psi)	Change in Length (inch)	Radial Stress (psi)	Axial Stress (psi)
1.000690	0	0	2.000000	0	0
0.418865	5177	11445	0.836707	9368	15600
0.409823	7067	15291	0.818487	12786	20300
0.403551	8116	17790	0.805873	14685	24000
0.397996	9586	20896	0.794660	17344	28000
0.394974	11230	24279	0.788493	20319	32200
0.391115	13014	27798	0.780645	23548	36300
0.387672	14728	31099	0.773637	26649	40000
0.385636	16513	34785	0.769432	29878	44600
0.384280	17772	37538	0.766629	32157	48300
0.382955	19801	41219	0.763826	35828	52000
0.379496	21201	44393	0.756818	38360	56460
0.378862	22950	47750	0.755417	41525	60200
0.377822	25154	51809	0.753174	45513	64400
0.376895	26623	54714	0.751212	48172	67800
0.375131	28303	58273	0.747568	51210	72400
0.373505	29912	61615	0.744204	54122	76600
0.371456	31521	64689	0.739999	57034	80000
0.370397	33271	68233	0.737757	60199	84300
0.368639	35160	71845	0.734113	63617	88300
0.367451	37259	75677	0.731590	67415	92200
0.366392	39043	79009	0.729348	70644	95740
0.363206	40443	81184	0.722900	73176	97200

NOTE: Initial height of graphite sample = 2.000 inches
        Area of the compression chamber = 0.500 square inch.

142

The total volume (first column, Table 6) of the graphite plug within the test cylinder includes the radial expansion of the inside surface of the test cylinder due to this radial stress (or pressure).

A plot of the average stress on the graphite plug versus volume is given in Figure 40. Bulk modulus can be determined either numerically according to equation (51) or analytically using equation 2 (after curve fitting the data). The data in Figure 41 show how bulk modulus changes with average stress up to 100,000 psi. Extrapolation of this data compares favorably with compressibility data reported by Bridgeman (5)(6).

6.3 GRAPHITE DELIVERY RATE REQUIRED TO MAINTAIN A GIVEN FILM THICKNESS

This section gives a procedure for determining the rate of flow of graphite required to establish and maintain a given film thickness between rolling/sliding discs commonly used in traction test rigs. The procedure is based on simple compaction of dry powder within the Hertzian contact region using bulk modulus data. Compaction pressure is assumed to be constant throughout the film and equal to the average of the Hertzian pressure distribution.

Side leakage from the contact region will affect the
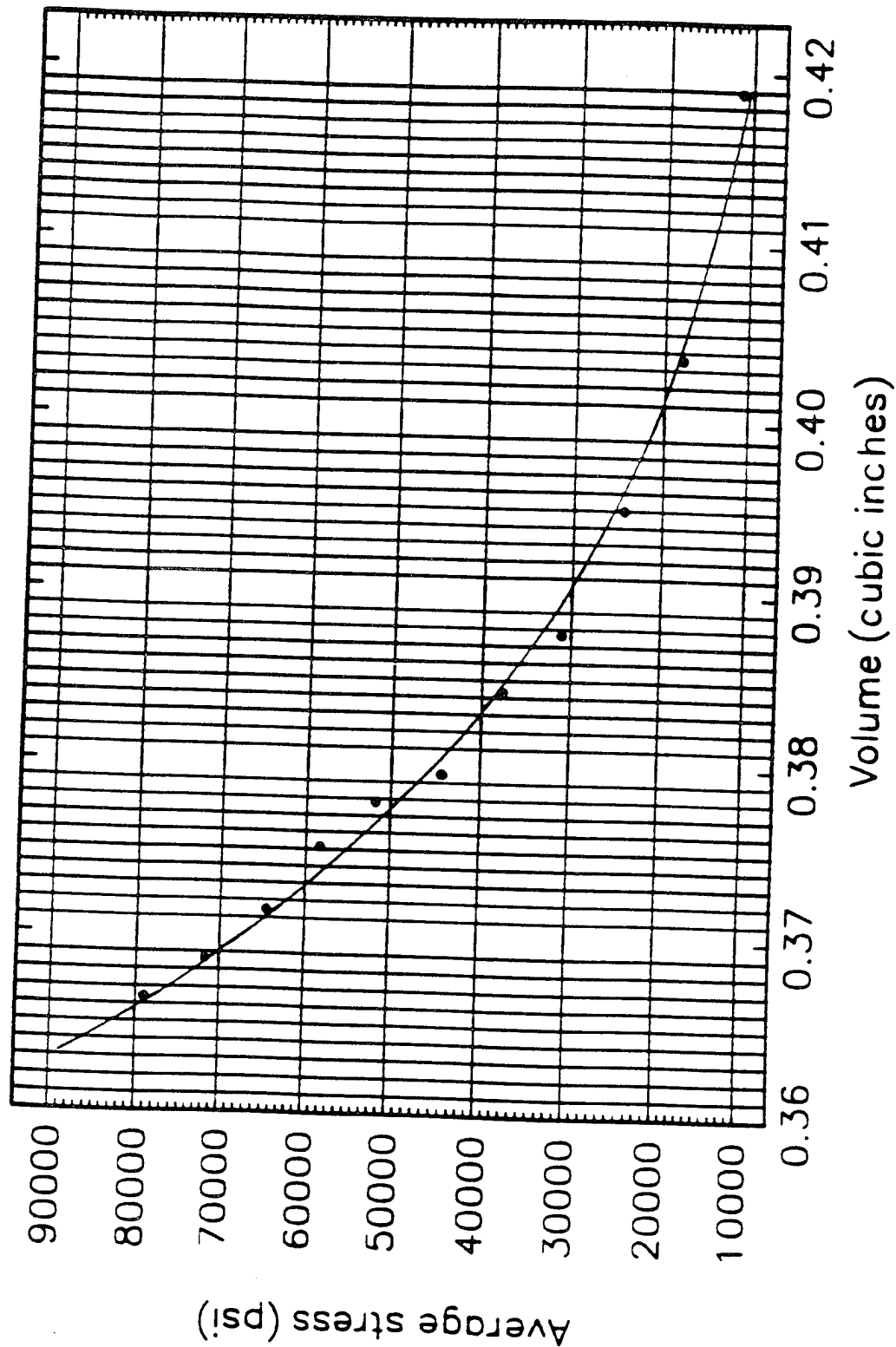
Figure 40.

144

Figure 41.

145
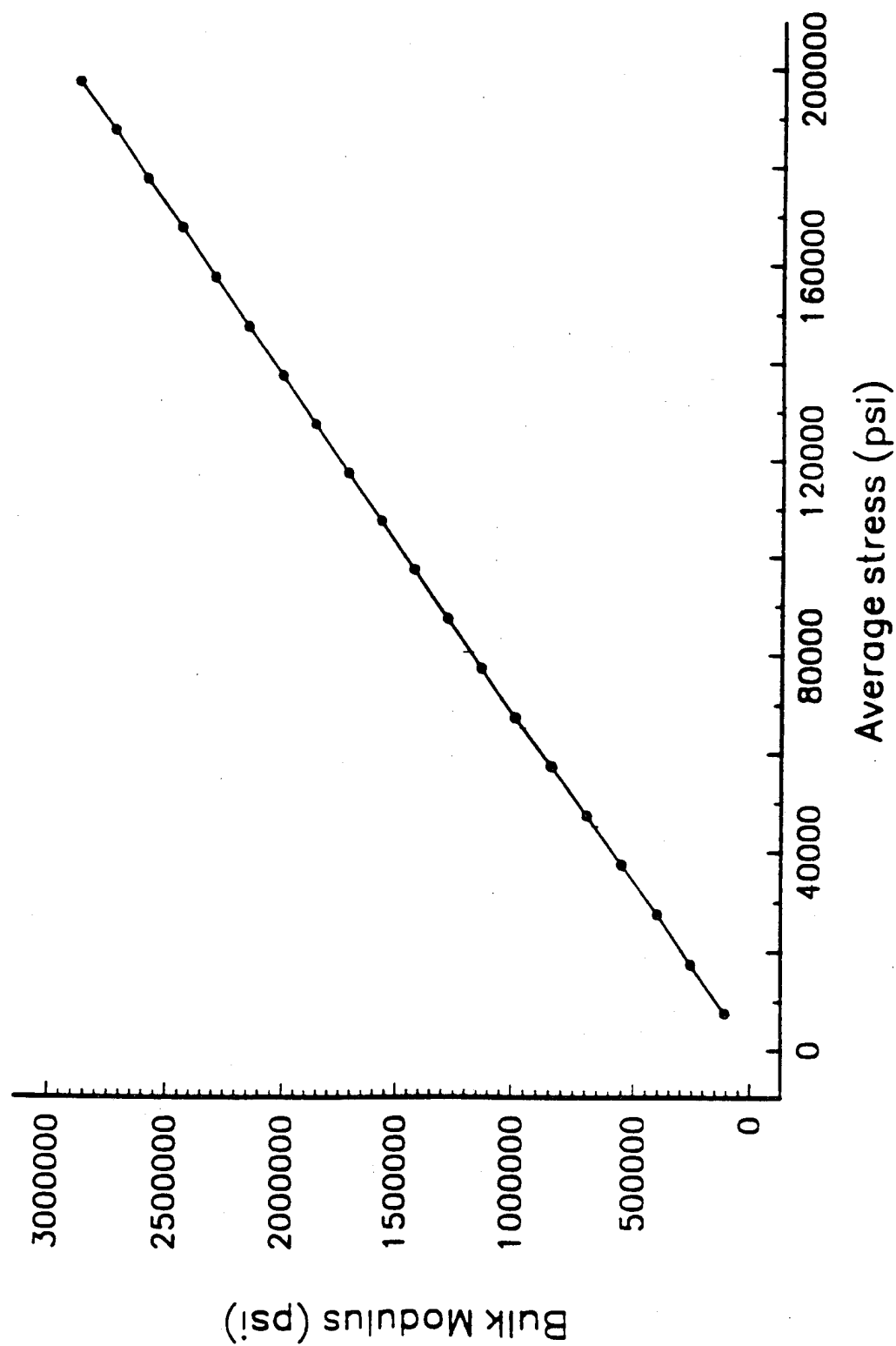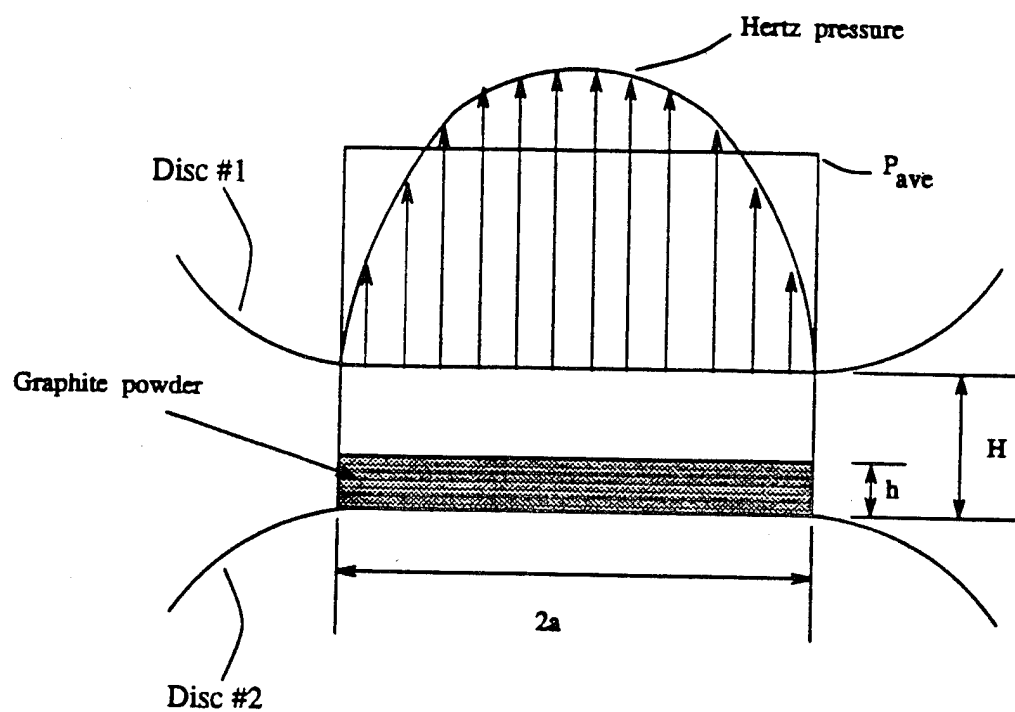
Fig. 42. Compaction of Graphite Powder Lubricant in Hertzian Contact Region

prediction to some extent. Bridgman (5)(6) ignored this effect in his measurements of compressibility by reasoning that friction forces at the interface oppose side leakage. Side leakage was apparently not a concern though film thickness was 0.0025 cm and greater... "the dimensions of the apparatus were such that the film thickness was very seldom reduced below 0.0025 cm (0.000984 inches) and for most substances the thickness was several times as great as this." The thickness of solid films in rolling contact applications is typically smaller than 0.000984 inches; usually in the neighborhood of 0.000100 inches.

Consider an idealized volume between two contacting surfaces defined by height (H), width (2a) and depth (B). Assume that this volume is filled with unconsolidated graphite powder at atmospheric pressure (Figure 42). This assumed condition is much like the compaction tests discussed in the previous section. Next assume that the volume is compacted to a new height of (h) as a result of a uniform pressure defined by the average of the Hertzian pressure distribution. In this scenario, compaction is unconfined in the radial direction; in reality, the time of compaction across the Hertz region is extremely small so lateral flow can be ignored in this discussion. The relation between average pressure and film thickness (h) can be determined through the use of the basic definition of bulk modulus.

The bulk modulus of elasticity (K_m) is defined by,

$$K_m = - \frac{\Delta p}{(\frac{\Delta v}{v})} \qquad (52)$$

where (Δp) is the increment of pressure intensity applied to cause a change in volume of (ΔV). Integration of equation 16 gives

$$\int_1^2 \frac{dp}{K_m} = \ln (\frac{v_1}{v_2}) \qquad (53)$$

The graph of bulk modulus versus average stress (Figure 41) can be approximated by a straight line represented by the following equation:

$$K_m = mp + b \qquad (54)$$

where (m) is the slope of the line, (b) is the offset on the line and (p) is the average stress which is equal to average Hertzian pressure in the contact area.

Substituting the expression for (K_m) as a function of pressure in the above equation, gives

$$\int_1^2 \frac{dp}{(mp + b)} = \ln\left(\frac{v_1}{v_2}\right) \tag{55}$$

from which

$$\frac{mp_2 + b}{mp_1 + b} = \left(\frac{v_1}{v_2}\right)^m \tag{56}$$

where (p_2) is the average Hertzian pressure (p_{avg}) and (p_1) is the average gage pressure. If compression starts at ambient pressure then $p_1 = 0$ psig. Under this condition,

$$\frac{v_1}{v_2} = \left[1 + \frac{m}{b} p_{avg}\right]^{\frac{1}{m}} \tag{57}$$

Here v_2 represents the compacted volume of graphite which results from the average Hertz pressure.

$$v_1 = h(2a)B\left[1 + \frac{m}{b} p_{avg}\right]^{\frac{1}{m}} \tag{58}$$

and (v_1) represents the volume of unconsolidated graphite powder at atmospheric pressure.

The volumetric flow rate of unconsolidated graphite powder (Q_g) is given by,

$$Q_g = v_1/\Delta t \qquad (59)$$

and

$$U = 2a/\Delta t \qquad (60)$$

where (U) is average tangential velocity of the discs.

Therefore,

$$Q_g = (v_1 \, U)/2a \qquad (61)$$

Substituting equation (58) into equation (61), gives the volumetric flow rate of unconsolidated graphite powder required to establish a given film thickness (h) corresponding to an average Hertzian pressure level of (p_{ave}).

$$Q_g = U \, h \, B \, [\, 1 + \frac{m}{b} \, p_{avg} \,]^{\frac{1}{m}} \qquad (62)$$

The corresponding weight rate of flow of unconsolidated graphite powder is determined by,

$$Q_{\gamma g} = Q_g \, \gamma_g \qquad (63)$$

150

The above equation represents the weight rate of flow of unconsolidated graphite powder that has to be supplied to the Hertz contact region to establish a film of thickness (h) for a load level.

Consider now the case where graphite powder is supplied by a liquid carrier. Let (c) be the mixture ratio of weight of unconsolidated graphite powder to the weight of carrier fluid in a given immiscible slurry volume (Figure 43).

$$w_g \, / \, w_t \; = \; c \qquad\qquad (64)$$

The weight rate of flow of a slurry mixture is,

$$Q_{\gamma s} \;\; = \;\; \frac{w_f \, + \, w_g}{\Delta t} \qquad\qquad (65)$$

$$Q_{\gamma s} \;\; = \;\; \frac{w_g}{\Delta t} \; (\frac{w_f}{w_g} + 1) \qquad\qquad (66)$$

$$Q_{\gamma s} = Q_{\gamma g} \; (1/c + 1) \qquad\qquad (67)$$

Recall, the volumetric flow rate of a slurry is,

$$Q_s \;\; = \;\; Q_{\gamma s}/\gamma_s \qquad\qquad (68)$$

but,
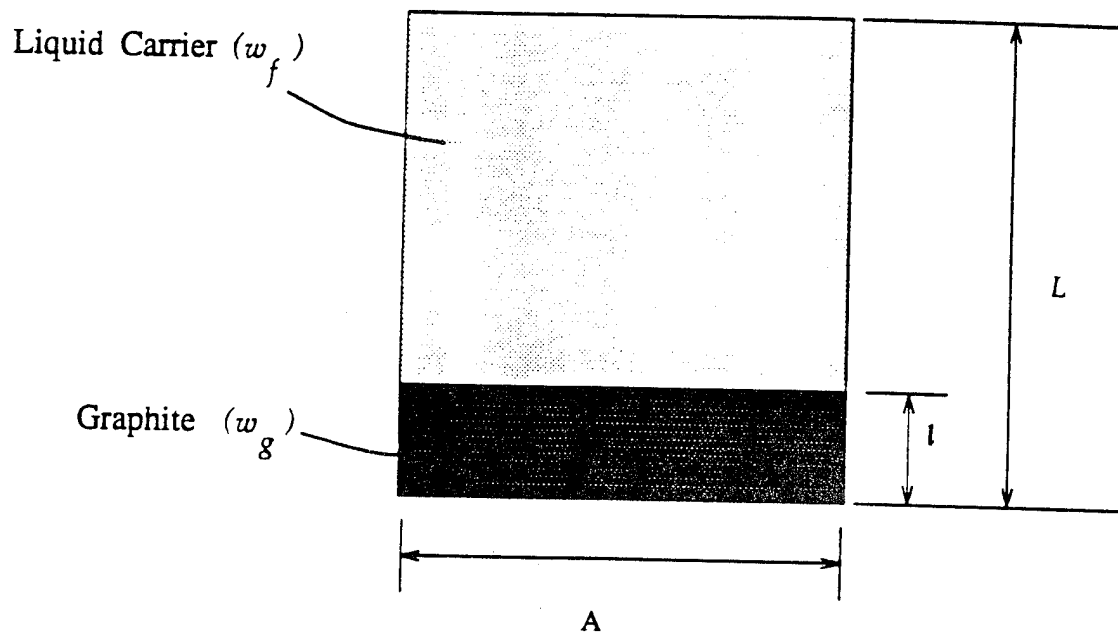
Fig. 43. Slurry Volume having a Mixture ratio of $c = (w_g / w_f)$

$$\gamma_s \ = \ \frac{W_f \ + W_g}{A \ B \ L} \qquad\qquad (69)$$

where (A) is width of the slurry volume, (B) is the thickness and (L) is the length of the slurry volume. Furthermore

$$\gamma_s \ = \ \frac{\gamma_g \ l \ + \ \gamma_f \ (L-l)}{L} \qquad\qquad (70)$$

$$\gamma_s \ = \ \gamma_g \ \left(\frac{l}{L}\right) \ + \ \gamma_f \ \left(1-\frac{l}{L}\right) \qquad\qquad (71)$$

Note from Figure 43,

$$\frac{W_g}{W_f} \ = \ \frac{\gamma_g \ l \ A \ B}{\gamma_f \ (L-l) \ A \ B} \qquad\qquad (72)$$

$$\frac{W_g}{W_f} \ = \ C \ = \ \frac{\gamma_g}{\gamma_f} \ \frac{1}{\left(\frac{L}{l}\right) \ - \ 1} \qquad\qquad (73)$$

which gives,

$$\frac{L}{l} \ = \ \left(\frac{\gamma_g}{\gamma_f}\right)\left(\frac{1}{C}\right) \ + \ 1 \qquad\qquad (74)$$

153

Substituting equation 74 into equation 71, gives,

$$\gamma_s = \frac{\gamma_g}{(\frac{\gamma_g}{\gamma_f})(\frac{1}{C}) + 1} + \gamma_f \left[1 - \frac{1}{(\frac{\gamma_g}{\gamma_f})(\frac{1}{C}) + 1} \right] \qquad (75)$$

The required volumetric flow rate of a given slurry mixture (Q_s) is determined by substituting equation (75) into equation (68).

An example calculation is shown below to illustrate the volumetric flow rate requirements of a given slurry mixture for a given minimum film thickness.

6.3.1 Example Calculation:

The practical question that arises is: What rate of flow of a given slurry mixture is required to establish and maintain a given minimum film of graphite between rotating disks in tractive rolling? The assumption here is that the carrier liquid is burned away just in front of the contact region leaving only the graphite powder to enter the Hertzian contact region. Furthermore it is assumed that the film is rectangular in shape and that film thickness depends only on

154

the compaction of the graphite powder (see **Figure 44**).

The example calculation is based on the following set of numbers:

$$(d_1, d_2) \quad = 6.00 \text{ inches}$$

$$(B) \quad = 1.00 \quad \text{inch}$$

$$(N_1, N_2) \quad = 1,000 \text{ rpm}$$

$$(c) \quad = 1/8$$

$$(\gamma_f) \quad = 3.8097 \text{ lbf/inch}^3$$

$$(\gamma_g) \quad = 0.7859 \text{ lbf/inch}^3$$

Calculations were made to determine slurry flow rate requirements verses desired film thickness for two different applied loads.   Note that the Hertzian width of contact for the two loads are 0.0224 inches for W = 1,000 lbs and 0.0708 inches for W = 10,000 lbs.

The calculated data (**Figure 45**) show that to establish and maintain a minimum film thickness of 0.0001 inches when the applied load is 1,000 lbs, the 1:8 slurry has to be delivered at a flow rate of 0.174 inch^3/sec.   When the load is 10,000 lbs, the required flow rate is 0.19 inch^3/sec.

6.4   PREDICTING TRACTION COEFFICIENTS FOR GRAPHITE FILMS

This section gives a procedure for predicting traction coefficients for dry powder lubricants compressed by Hertzian

155

Diameter = 6.00 "

$N_2 \cong 1000$ rpm

$N_1 = N_2 \cong 1000$ rpm

Diameter = 6.00 "
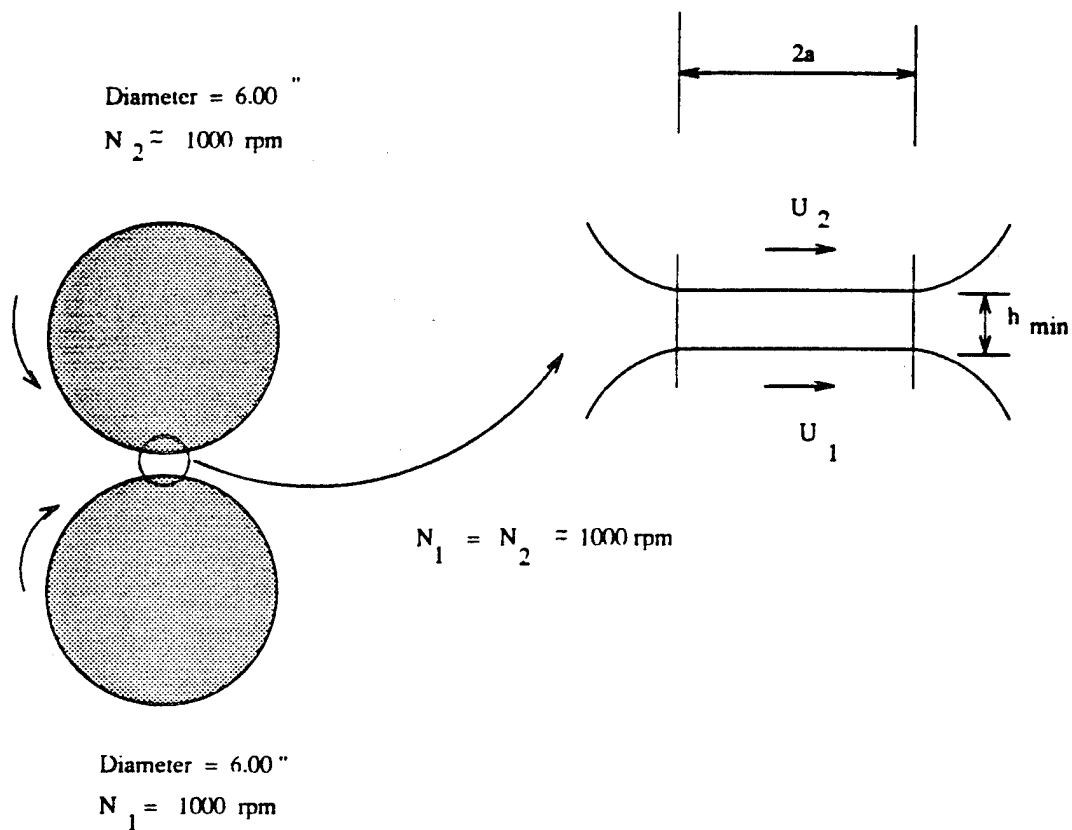
$N_1 = 1000$ rpm

Fig. 44. Two Discs Rotating at approximately 1000 rpm
Seperated by a Graphite Film of Thickness h_min

Comparision of Volumetric flow rate of Slurry Mixture for Loads
(W = 1000 lbs ; W = 10000 lbs) (c = 1 : 8 ; N = 1000 rpm)

Film thickness (h) (inches)

Volumetric flow rate (Qs) (inches³/sec)

0.00002 0.00006 0.00010 0.00014 0.00018 0.00022 0.00026 0.00030

0.600   0.500   0.400   0.300   0.200   0.100   0.000

W = 1000 lbs
W = 10,000 lbs
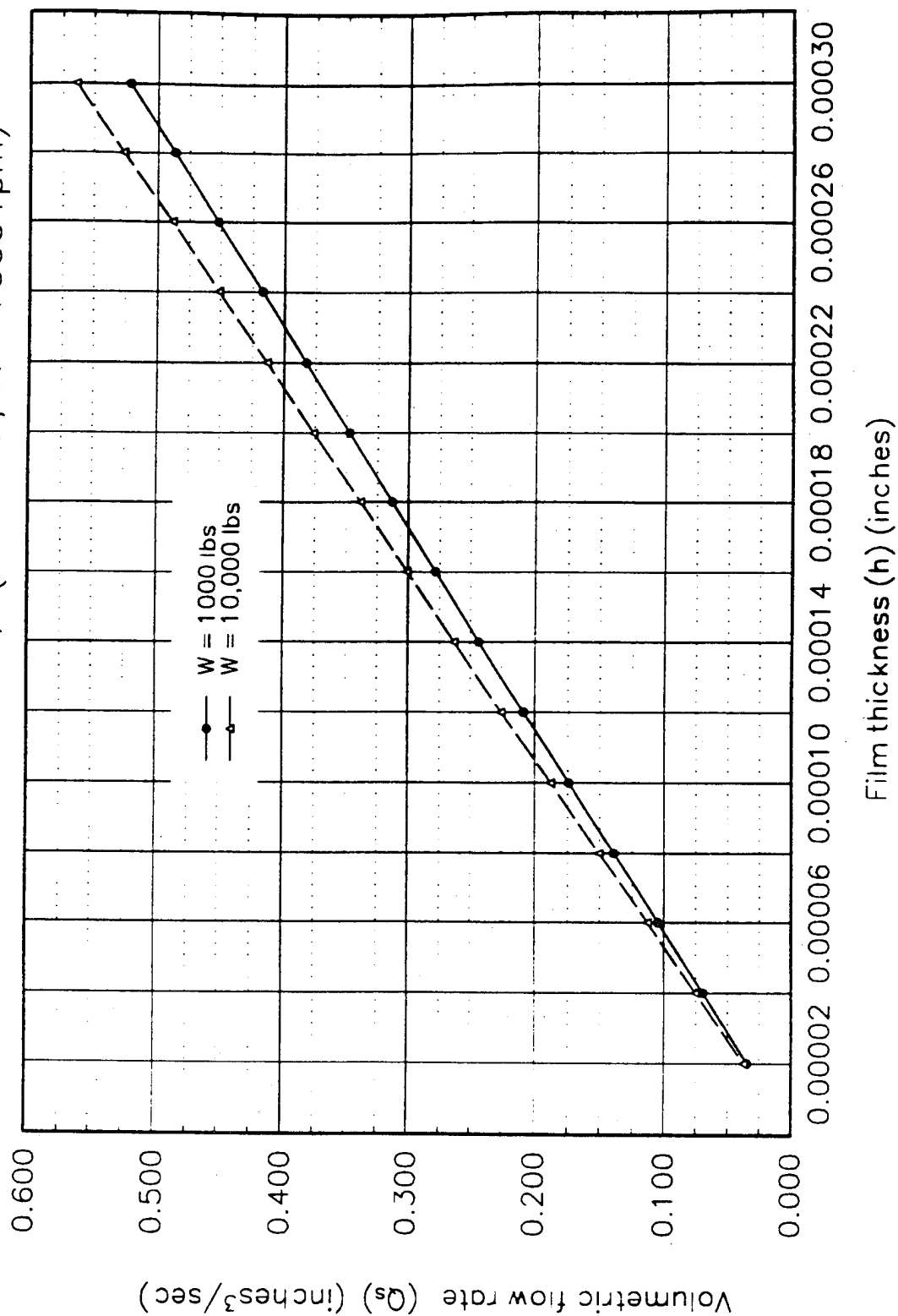
Figure 45.

contact. The method treats the compacted film as a solid having perfectly elastic properties and requires the knowledge physical properties mentioned earlier.

The method of solution for predicting traction coefficients for graphite powder follows the method developed by Dareing (12) for predicting traction coefficients for solid lubricants (teflon) working against soft metal coatings. Other methods of solution are given by Kannel and Dow (13) and Barber and Kannel (14).

In tractive rolling, minute tangential velocities are induced at the contact area of the discs, which is relatively small compared to their average tangential velocities. This difference causes tangential deflections or shear distributions within the solid lubricant film and the substrate. The magnitude of the shear stresses at the interface depends on the magnitude of the relative slip velocity across the solid lubricant film. The shear distributions across the Hertzian contact are determined as follows; consider the movement of two coincident points A and B positioned at the beginning of the Hertz region (see Figure 46). Furthermore, assume that (V_2) is slightly greater than (V_1). As points A and B move to the right, the surfaces are distorted as a result of shear stresses. If the film and coating are stuck together points A and B are supposed to be

158

at the same point. Due to minute differential velocities at the contact region point A is pulled forward and point B is dragged backwards.

The amount of local distortion on the surface of disc #2 at distance (x) is designated by (x_2). The amount of local distortion on the surface of disc #1 at distance (x) is designated by (x_1). The sum of both distortions is given by,

$$x_1 + x_2 = x \ (dv/v) \tag{76}$$

This problem was first addressed by Carter (15) in a study of tractive rolling of dry surfaces. A constant of integration (C) must be included in above equation, where (C) represents the translation of the initial point of contact.

$$x_1 + x_2 = x \ (dv/v) + C \tag{77}$$

This equation applies to each point across the film. Collectively, the set of equations can be put in the following matrix form.

$$\{x_1\} + \{x_2\} = \{x\} \ (dv/v) + \{C\} \tag{78}$$

A second set of equations relates the deflection matrix to the force matrix through the flexibility matrix. The principle of minimum potential energy as applied by Dareing (12) is use here to establish the flexibility matrix for solid films of graphite and substrate.

$$\{x_1\} + \{x_2\} = [[A_1] + [A_2]] \{F\} \qquad (79)$$

The shear force matrix is determined from the simultaneous solution of these two matrix equations. The shear stress distribution follows directly from the shear force distribution.

If the local shear stress is less than the product of the coefficient of friction and local pressure, points A and B (Figure 46) stay stuck together. If the local shear stress is greater than this limiting shear stress, points A and B slide relative to one another. The total friction force is the integral of these shear stresses across the Hertz contact width.

The above procedure can be applied directly to the graphite film problem. What is unknown in this case is the plane at which the graphite will slip or fail. Slippage could occur at the substrate/graphite interface or within the graphite film itself. The total shear force can only be determined after the plane of slippage or failure has been established.
If the shear strength of the compacted graphite is greater than the product of the contact stress and the coefficient of friction at the substrate/graphite interface, slippage will occur at the interface with no failure within the film. On
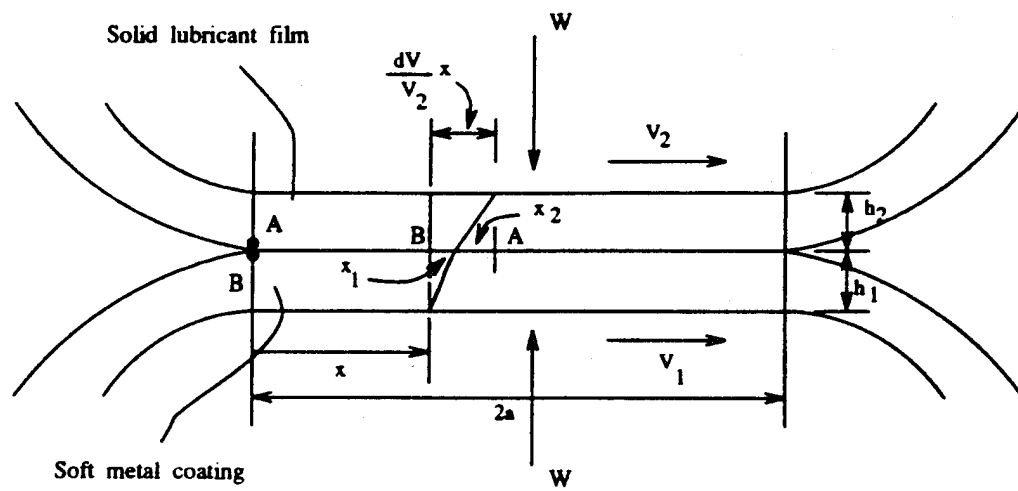
Fig. 46. Surface Displacements Associated with Traction Force (Dareing 1991)

161

the other hand, if the shear strength of the compacted graphite is less than the limiting value (f x p) at the interface, slippage will occur internal to the film. The location of the slippage plane in the latter case can be determined by dividing the film thickness into two films separated by an assumed plane. If the corresponding shear stress along this assumed plane is greater than the shear strength of graphite, failure along this plane is possible. The weakest plane can be determined by repeating this exercise at different planes in the film.

6.4.1 Example Calculation:

Calculation presented here are based on two 6 inch diameter discs pressed together at three different force levels (1,000, 2,000 and 3,000 lbs). Physical Responses within the contact region corresponding to these loads are given in **Table 7**. Because of the low level of Hertzian pressure, slippage is assumed to occur at the graphite/surface interface where the coefficient of friction is assumed to be 0.10. Modulus of rigidity, G, of compacted graphite is calculated at the different load levels assuming a Poisson ratio of 0.25. Film thickness in each case is assumed to be 0.0001 inches.

162

Table 7

Physical Responses Within the Contact Region

Normal Force W lbfs	Contact Width 2a inch	Maximum Pressure pmax psi	Average Pressure pave psi	Bulk Modulus Km x 10-6 psi	Modulus Elast'y Egx10-6 psi
1,000	0.0215	59,200	46,000	0.675	1.012
2,000	0.0304	83,700	65,700	0.975	1.462
3,000	0.0373	102,500	80,500	1.200	1.800

The traction shear stress distribution for this set of numbers and a slip velocity ratio of 0.0005 is calculated according to the preceding theory (see Figure 47). The calculated data show that graphite sticks to the substrate over the initial contact zone from x = 0 to x = 0.01434 inches. Beyond this point the graphite film slides on the substrate surface. The traction coefficient under the slip velocity ratio of 0.0005 is equal to 0.0725. This point is identified in Figure 10 which give the traction curve for all slip velocity ratios. The traction coefficient curve (Figure 48) approaches the assumed value of the coefficient of friction (f = 0.1) for graphite on steel at high slip velocity ratios.

Traction Shear Distribution Inside Hertzian Contact Region
6.00 inch Disks; Slip Velocity Ratio: 0.0005 and Load 2000 lbs.

Position Ratio (x/a)

Traction Shear Stress (psi)

Figure 47.

164
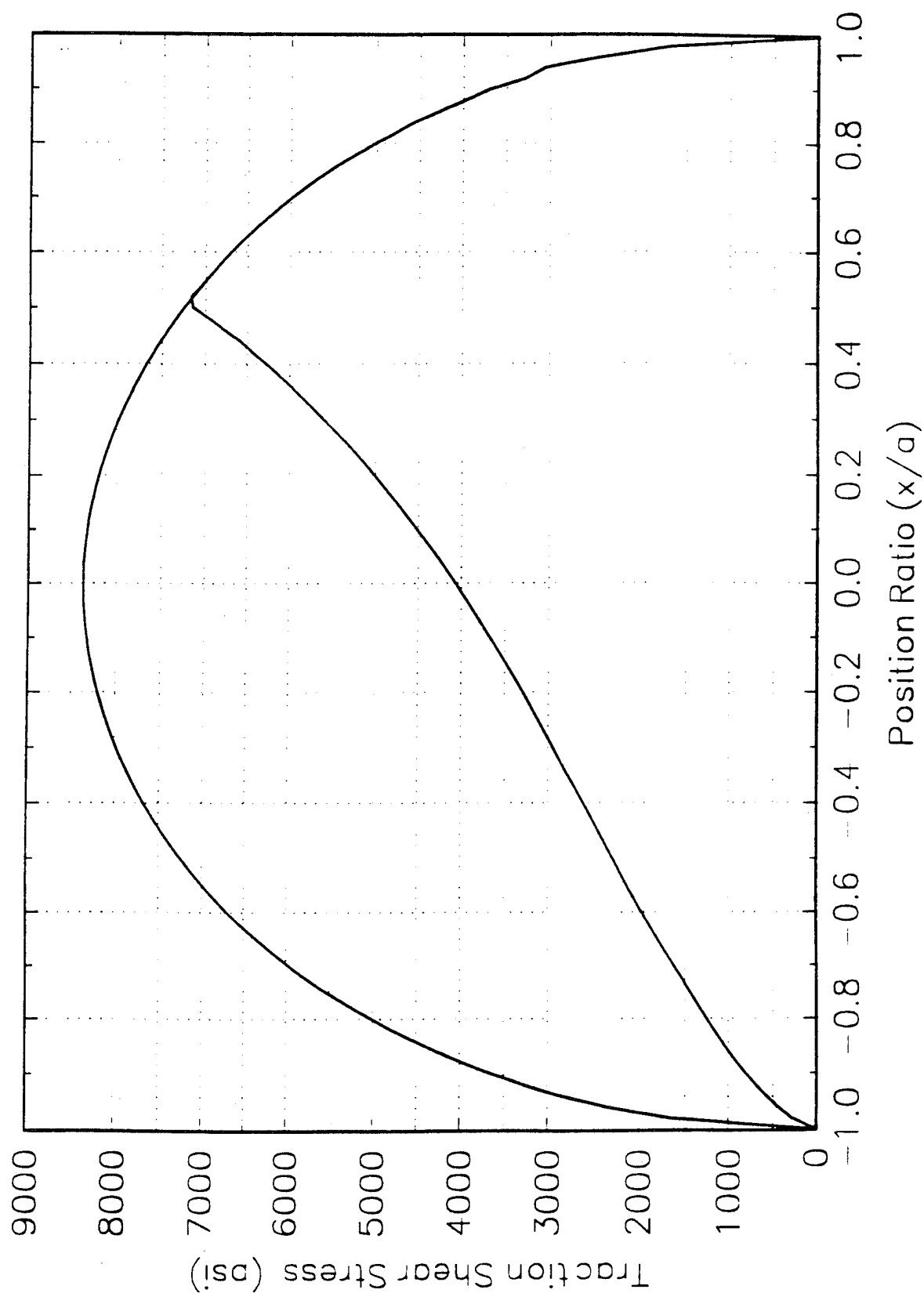
TRACTION COEFFICIENT

6.00 INCH DISKS; 0.0001 INCH GRAPHITE FILM

Figure 48.

165
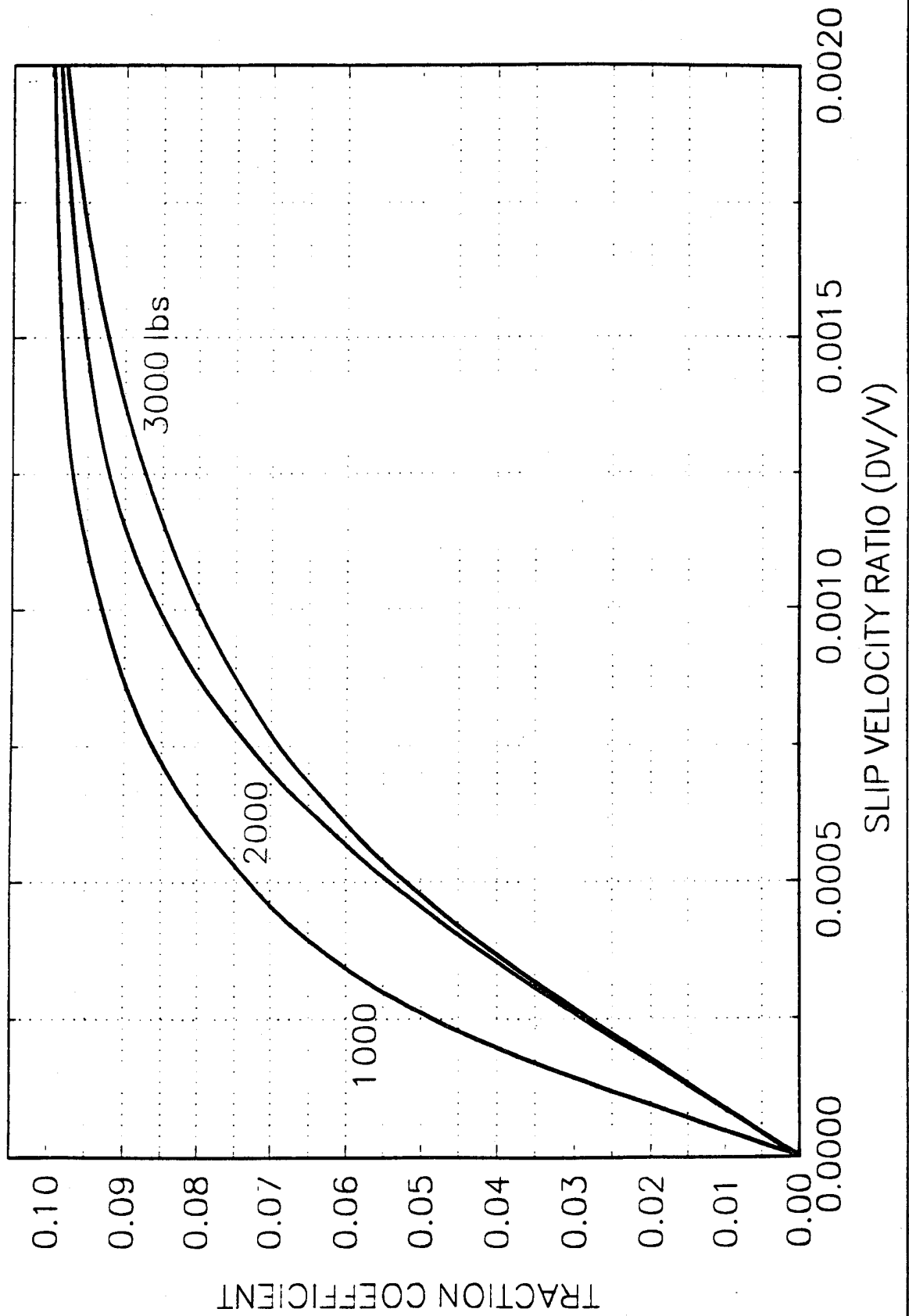
Nomenclature

K_m	Bulk Modulus of Elasticity (psi)
E	Modulus of Elasticity (psi)
v	Poisson's ratio
σ_{ave}	Average Stress (psi)
$\sigma_1, \sigma_2, \sigma_3$	Principal Stresses (psi)
σ_a	Axial Compressive Stress (psi)
σ_r	Radial Stress (psi)
σ_θ	Tangential Stress (psi)
v, v_1, v_2	Volume (inch^3)
$dv, \Delta v$	Change in Volume (inch^3)
$(\varepsilon_\theta)_0$	Hoop Strain at the Outside Surface
a	Inner radius (inch) [also half of Hertz contact width]
b	Outer radius (inch)
P_i	Internal Pressure (psi)
$(\varepsilon_\theta)_i$	Hoop Strain at the inside Surface
$(\delta r)_i$	Radial Strain inside the Cylinder
l_i	Length of Compacted Graphite Powder (inch) [see Figure 1]
$2a$	Hertzian Contact Width (inch)
H	Height of Uncompacted Graphite Powder (inch)
h, h_{min}	Film Thickness (inch)
W	Load (lbf)
$c = w_g/w_f$	Slurry Mixture Ratio (lbf/lbf)

p_{avg}	Average Hertzian Pressure (psi)
Q_g	Volumetric Flow Rate of Unconsolidated Graphite Powder (inch^3/sec)
Q_s	Volumetric Flow Rate of Slurry Mixture (inch^3/sec)
$Q_{\gamma g}$	Weight Flow Rate of Unconsolidated Graphite Powder (lbf/sec)
$Q_{\gamma s}$	Weight Flow Rate of Slurry Mixture (lbf/sec)
γ_g	Specific weight of Unconsolidated Graphite Powder (lbf/inch^3)
γ_s	Specific weight of Slurry mixture (lbf/inch^3)
γ_f	Specific weight of Carrier Fluid (lbf/inch^3)
A	Width of Slurry Volume (inch) [see Figure 5]
B	Depth of the Slurry Volume (inch) [see Figure 5]
L	Height of the Slurry Volume (inch) [see Figure 5]
N_1, N_2	Angular Velocities (rpm)
V, V_1, V_2	Tangential Velocities (inch/sec)
x_1, x_2	Displacements (inch)
x	Position along Hertzian Film (inch)
P	Contact Pressure (psi)
$[A_1]$, $[A_2]$	Influence Coefficients Matrices

{F}   Local Traction Force at Contacting Surface

$\{x_1\}$, $\{x_2\}$ Surface Displacements

S   Shear Strength (psi)

dV/V   Slip Velocity Ratio

7.0 Conclusions and Recommendations

A computer program was developed to solve the governing equations. The solution scheme utilizes the method of finite difference and is highly iterative. For the case of a pure oil, the program solves the generalized Reynolds equation and the elasticity equations which govern the deformation of the bounding surfaces to determine the pressure distribution and the film thickness profile. The energy equation is also solved simultaneously with the Reynolds equation to accurately characterize the effect of property variation with the temperature rise in the EHL contact. In the case of a mixture, the deformation of the particles (elastic or plastic) are also computed in order to assess the load-carrying capacity of the particles in accordance to the theory described in Section 4.2. The mixture computations are, therefore, considerably more involved.

The output of the program includes a complete prediction of the film thickness (central and minimum), pressure distribution (including the magnitude and location of the pressure spike), temperature distribution along the direction of the sliding and through the film gap (which includes a prediction of the rollers surface temperatures and the mean film temperature at any location in the contact region), and

finally the traction results as a function of the slip ratio. The details of the formulations of the Jacobians and the numerical solutions are discussed in a recent paper by Khonsari & Hua (1994) for the case of pure oil which obeys the Bair-Winer Constitutive equation.

The literature contains experimental results of other researchers that could be used as a validation source. For this purpose Johnson & Cameron's classic experimental paper dealing with EHL line contact was utilized (cf. Johnson and Cameron, 1968). Computer simulations were performed to predict the traction coefficients reported in that paper. The input data used in the simulation is summarized in **Table 4**. Our theoretical predictions were compared to the experimental results of Johnson and Cameron(1968) and the results were found to be in excellent agreement.

Experimental measurements were conducted at USL in order to duplicate the results of Johnson & Cameron. For this purpose, the operating conditions had to be carefully set to mimic those of Johnson & Cameron. Experiments were conducted using Shell oil which according to the manufacturer had the identical properties as the European Shell employed by Johnson & Cameron. The initial traction results at USL were consistently greater than our predictions as well as those of Johnson & Cameron (please refer to the quarterly report which

contain a complete description of the results and discussion on the comparison between the theory and experiment.) Subsequently, there were a number of improvements made to the measurements system and also to the surface characteristics of the disks. Perhaps the most important and noteworthy factor was the surface roughness which USL was able to reduce to a significant degree. Please refer to the USL report for a comprehensive discussion.

Figure 11 shows the comparison of the theoretical simulations and the final set of experimental results by USL. These results pertain to the first attempts at lowering the surface roughness. Two sets of speeds (500 rpm and 1000 rpm) were tested under 200 lb of normal load. The inlet oil temperature was assume to be 74 °F. The results show that starting from the pure rolling (zero slip ratio) the traction rise rapidly, reaches a plateau and then begins to decline when the slip ratio is increased.

The general trend of the experimental results and, in fact, the magnitude of the traction coefficient are in agreement with the theoretical prediction.

The results show that the hardness value - needed to determine the plastic deformation of the particles- plays an important role on the magnitude of the traction coefficient. As pointed

171

out in the theory section of this report, there is a crucial need for appropriate mechanical property values in predicting the performance of EHL contact. This information must be determined experimentally, though it is not an easy task because of the anisotropy in the mechanical property of lamellar solids. Extensive review of published literature showed that, unfortunately, there is a serious lack of published property values for solid lubricants such as graphite and MoS_2. Furthermore, in most cases the published literature contains a wide range of property values. For the reminder of the simulations, the hardness value of 3 x 10^9 will be used since it thought to be more realistic.

Figure 18 shows the predicted traction results for 700 lb loading at 1000 rpm. Also shown in that Figure are the experimental results of USL with the 8:1 slurry mixture at 700 lb. The hardness value used in these simulations was 3 x 10^9. A list of input used for the simulations is provided in **Table** 5. The experimental results of the slurry are surprisingly very low. In fact, the order of magnitude of the measured traction coefficient seem to be in the range of what is commonly observed in hydrodynamic lubrication of conformal surfaces such as slider bearings and journal bearings.

The University of Southwestern Louisiana has spent a considerable amount of time and effort to determine any possible

source of problem in measuring system. To date, no problem has been found and the data seem to be repeatable. Further research is, therefore, crucially needed to determine the cause of such low traction coefficient. A possible mechanism for this phenomenon could be if the mixture happens react chemically with the bounding surfaces. If this is found to be the case, the theory would have to be modified since it assumes that the no chemical reaction takes place.

The early test protocol anticipated running at a high enough temperature so that the ethylene glycol carrier would evaporate as the slurry is introduced to the nip between the test wheels. The time spent developing the test equipment and techniques precluded running this level of test during the project time allotment.

If further testing is to be authorized, it is recommended that a traction rig be constructed first that better serves the primary objectives of the program. This would include the following features as a minimum:

- Drive motors with absolute speed control (perhaps synchronous motors driven from a well regulated variable frequency supply).

- Speed sensors with instantaneous reading capability. Well filtered tachometer generators should be acceptable.

173

- Rigid, yet adjustable platforms with optical devices to insure perfect line up of test disc interfaces
- Torque and load transducers using the latest technology to minimize errors and variations.
- A computer control system using parallel input conversion boards with a capability of reading and providing feedback control to at least five channels simultaneously.
- An improved system of trueing and polishing the test wheels.

The paper gives a procedure for predicting traction coefficients for powder lubricants compressed to Hertzian contact pressures. The method of analysis requires prior knowledge of physical properties of the powder lubricant under extreme pressures. Relevant physical properties are: bulk modulus, shear strength, coefficient of friction, modulus of elasticity/rigidity and Poisson's ratio. Each of these physical properties depend on the magnitude of applied compressive stress and the temperature environment. The data given in this paper were obtained at atmospheric temperatures and at compressive stress levels up to 100,000 psi. Powder lubricants being considered for high temperature applications can be analyzed with this method but would require the above physical properties at the specified temperature level.

174

8.0 Acknowledgements

A critical part of this research was the transfer of the traction rig from the Wright Laboratory to the University of Southwestern Louisiana (USL). Once on site, the rig had to be installed, hooked-up, instrumented, calibrated and tested. During the initial baseline testing, the research team realized the importance of developing surface polishing and lapping skills to expedite and maintain proper surface finish on the test disks. Each of these important activities was accomplished through the direct participation and support of

Mr. John Slattery, retired General Electric executive and true friend of the Mechanical Engineering Department at USL.

9.0 List of Referencs

9.1 References for Sections 1.0, 2.0, 3.0

Bair, Scott and Winer, W. O. (1979 a), "Shear Strength Measurements of Lubricants at High Pressure," ASME Jour. of Lubr. Tech., 101, 3, pp 251-257 (1979)

Bair, Scott and Winer, W. O. (1979 b), "A Rheological Model for Elastohydrodynamic Contacts Based on Primary Labaoratory Data," ASME Jour. of Lubr. Tech., 101, 3, pp 258-265

Barber, S. A. and J. W. Kannel (1988), "Evaluation of Slip- Traction Characteristics of Polymeric Transfer Films," ASME Journal of Tribology, Vol. 110, pp 670-673

Bell, J. (1963), "Lubrication of Rolling Surfaces by a Ree- Eyring Fluid," ASLE Trans. 5, 160-171

Bisson, Edmond E., R. L. Johnson and W. J. Anderson (1957), "Friction and Lubrication with Solid Lubricants at   Temperatures to 1000 deg F with Particular Reference to   Graphite," Proc. Conf. on Lubrication and Wear, Inst. Mech. Eng., pp 348-354

Bisson, E. E. and W. J. Anderson (1964 a), **Advanced Bearing Technology**, NASA SP-38, (see Chapter 11, "Extreme-Temperature Bearings" by William J. Anderson; also see references at end of chapter)

Bisson, E. E. and W. J. Anderson (1964 b), **Advanced Bearing Technology**, NASA SP-38, (see chapter 8 "Nonconventional   Lubricants" by Edmond E. Bisson; also see references at end of   chapter)

Booker, J. F. and K. H. Huebner (1972), "Application of Finite   Element Methods to Lubrication: An Engineering Approach", Trans. ASME, Series F: J. Lubr. Technol., Vol. 94, No. 4, p.313

Boyd, J. and B. P. Robertson (1945), "The Friction Properties of Various Lubricants at High Pressures," Trans. Am. Soc. Mech. Engrs., Vol. 67, pp 51-56

Burton, R. A. (1960), " An Analytical Investigation of Viscoelastic Effects in the Lubrication of rolling

Viscoelastic Effects in the Lubrication of rolling Contact," Trans. Amer. Soc. Lub. Engrs. 3, No.1, 1

Cain, B. S. (1950) J. Appl. Mech., 72, 465

Cameron, A. (1966), The Principles of Lubrication, Longmans Green and Company, Ltd, London

Carter, F. W. (1926), "On the Action of a Locomotive Driving Wheel," Proc. Royal Soc., Series A, Vol. 112, pp 151-157

Cattaneo, C. (1938), 'Sul Contatto di du Corpi Elastici: Destribuzione Locale Degli Sfoizi," Rend. Acad. Lincei, Series 6, Vol. 27, pp 342-348, 434-436, 474-478.

Curme, George O. and Franklin Johnston (1952), Glycols, Reinhold Publishing Corp, New York

Dareing, D. W. and R. D. Dayton, (1992), "Non-Newtonian Behavior of Powder Lubricants Mixed With Ethylene Glycol," STLE Tribology Trans, Vol. 35, 1, 114-120

Dareing, D. W. (1991), "Traction Coefficients for Coated Bearing Races Lubricated With Teflon Transfer Films," ASME Jour of Trib, Vol. 113, pp 343-348

Dowson, D. and G. R. Higginson (1966), Elasto-Hydrodynamic Lubrication, Pergamon Press Ltd.

Dowson D. and G. Higginson (1960); "The Effect of Material properties on the Lubrication of Elastic Rollers," J. Mech. Eng. Sci. 2, No.3

Dowson D. and G. Higginson (1959); "A numerical Solution to the ElastoHydrodynamic Problem," J. Mech. Eng. Sci. 1, No. 1.

Eyring, H. (1936), "Viscosity, Plasticity and Diffusion as Examples of Absolute Reaction Rates," J. Chem. Phys., Vol. 4, p 283

Gatcombe, E. K. (1945), "Lubrication Characteristics of Involute Spur Gears - a Theoretical Investigation," Trans. Amer. Soc. Mech. Engrs. 67, 177

Gecim, B. and W. Winer (1980), "A Film Thickness Analysis for Line Contacts under Pure Rolling Conditions with a Non- Newtonian Rheological Model." ASME Paper 80 C2/LUB26

Goyal, K. C. and R. Sinhasan (1991), "Elastohydrodynamic

Studies of Three-Lobe Journal Bearings with non-Newtonian Lubricants," Proc Instn Mech Engrs, Vol 205, pp 379-388

Grubin, A. N. (1949), Central Scientific Research Institute for Technology and Mechanical Egnineering, Book No. 30, Moscow. (D.S.I.R. Translation No. 337)

Gupta, P. K. and J. A. Walowit (1974), "Contact Stresses Between an Elastic Cylinder and a Layered Solid," ASME Journal of Lubrication Technology, pp 250-257

Heathcote, H. L. (1921), Proc. Inst. Automobile Eng. London 15, 569

Heshmat, H. (1990); "High Temperature Solid Lubricated Bearing Development--Dry-Powder-Lubricated Traction Testing," Proc. of the 26th Joint Propulsion Conf., Paper 90-2047 (tested powder and ceramic rollers)

Heshmat, H. (1991), "The Rheology and Hydrodynamics of Dry Powder Lubrication," Trib. Trans., 34, 3, pp 433-439

Heshmat, H. and Walton, J. F. (1991); "The Basics of Powder Lubrication in High-Temperature Powder-Lubricated Dampers," 1991 Intl. Gas Turbine and Aeroengine Cong. and Expo. ASME Paper 91-GT-248

Heshmat, H. (1992), "The Quasi-Hydrodynamic Mechanism of Powder Lubrication: Part II-Lubricant Film Pressure Profile," STLE, Lubrication Engineering, Vol. 48, 5, 373-383

Huebner, Kenneth H. and Earl A. Thornton (1982), The Finite Element Method for Engineers, John Wiley & Sons

Johnson, K. L. (1962), "Tangential Tractions and Micro-slip," Rolling Contact Phenomena, Elsevier, Amsterdam, pp.6-28

Johnson, K. L. and J. L. Tevaarwerk (1977), "Shear Behavior of Elastohydrodynamic Oil Films," Proc. R. Soc. London Ser. A, 356, 215-236

Johnson, K. L. (1985), Contact Mechanics, Cambridge University Press, Chapter 8, p 242

Kalker, J. J. (1971), "Transient Rolling Contact Phenomena," Trans. ASLE, Vol. 14, pp 177-184.

Kannel, S. W. and T. A. Dow (1986), "Analysis of Traction Forces in a Precision Traction Drive." ASME Journal of Tribology, Vol. 108, pp 403-410

Kanumuru, Murali K.R. (1993) "Prediction of Traction and Friction Behaviour of Non-Newtonian Lubricants Using Finite Element Method" M.S. Thesis, University of S.W. Louisiana, Lafayette.

Martin, H. M. (1916) "Lubrication of Gear Teeth," Engineering, Lond., 102, 199

Maxwell, J. Clerk. (1868), "On the Dynamical Theory of Gases," Phil. Mag., vol. 35, pp. 129-145, 185-219; also reviewed by A. Nadai (1963), p 158

Meldahl, A. (1941), "Contribution to the Theory of the Lubrication of Gears and of the Stressing of the Lubricated Flanks of Gear Teeth," Brown Boveri Review, 28, No.11, 374

Milne, A.A. (1957), "A Theory of Rheodynamic Lubrication for a Maxwell Liquid," Instn. Mech. Engrs., Proc. of the Conference on Lubrication and Wear, Paper 41, 66

Mordike, Barry L. (1960) "Lubrication of Solids at High Temperatures," ASLE Trans., Vol 3, No. 1, Apr., pp 110-115

Nadai, A. (1963), Theory of Flow and Fracture of Solids, Vol. II, McGraw-Hill Book Co.

Oh, K. P. and K. H. Huebner (1973); "Solution of the Elastohydrodynamic Finite Journal Bearing Problem," Trans. ASME, Series F: J. Lubr. Technol., Vol. 95, No. 3, p 342

Peterson, Marshall B. and Robert L. Johnson (1954): "Friction of Possible Solid Lubricants with Various Crystal Structures," NACA TN 3334

Peterson, M. B. and R. L. Johnson (1957), "Solid Lubricants for Temperatures to 1000 deg F," Lubrication Eng., Vol 13, No.4, pp 203-207

Poritsky, H. (1950), J. Appl. Mech., 72, 191
Prandtl, L. (1928), "Ein Gedankenmolell zur kinetischen Theorie der festen Korper," A. angew. Math. u. Mech., Vol. 8, pp 85-106; also see Nadai (1963) p 366 and p 521

Reddi, M. M. (1969), "Finite Element Solution of the Incompressible Lubrication Problem," Trans. ASME, Series F.: J. Lubr. Technol., Vol. 91, No. 3, p. 524

Ree, T. and H. Eyring (1955), "Theory of Non-Newtonian Flow, I Solid Plastic System," and "Theory of Non-

Newtonian Flow, II Solution System of High Polymers," J. Appl. Phys. 26 (7), 793-800 (Part I) and 800-809 (Part II)

Reynolds, O. (1875), Philos. Trans. R. Soc. London, 166, 155 Sasaki, T., H. Mori, and N. Okino (1963), "Fluid Lubrication Theory of Roller Bearings, Parts I and II," ASME J. Basic Eng., 166, 175

Skelland, A. H. P. (1967), Non Newtonian Flow and Heat Transfer, John Wiley and Sons

Tanner, R. I. (1960), "Full-film Lubrication Theory for a Maxwell Liquid," Int. J. Mech. Sci., 1, 206

Taylor, C. and J. F. O'Callaghan (1972); "A Numerical Solution of the Elastohydrodynamic Lubrication Problem Using Finite Elements," J. Mech. Eng. Sci., vol. 14, No. 4, p 229

Tevaarwerk, J. L. and Johnson, K. L. (1979), "The Influence of Fluid Rheology on the Performance of Traction Drivers," ASME Jour. of Lubr. Tech., 101, 3, pp 266-274

UNCAR Carbon Company (1970), The Industrial Graphite Engineering Handbook, UCAR Carbon Company Inc., Parma, Ohio

Wedeven, L. D., R. A. Pallini and N. C. Miller (1988), "Tribological Examination of Unlubricated and Graphite-Lubricated Silicon Nitride Under Traction Stress," Wear, Vol 122, No. 2, p 183-206

Wedeven, L. D. and T. A. Harris (1987), " Rolling Element Bearings Operating at the Extremes," Machine Design, V 59, No. 18, Aug, pp 72-76

Zienkiewicz, O. C. (1971), The Finite Element Method in Engineering Science, McGraw-Hill, Londons

9.2 References Section 4.0

Archard, J.F., 1980, "Wear Theory and Mechanism," Wear Control Handbook, Peterson, M. and Winer, W. (editors), ASME publication, N.Y., p.35-80.

Bair, S. (1993) " The High-Pressure Rheology of a Soap-Thickened Grease," to be presented at the STLE/ASME joint lubrication conference in New Orleans October, 1993.

Bair, S. and Winer, W. (1979) " A Rheological Model for

EHL Contacts Based on Primary Laboratory Data," ASME Journal of Lubrication Technology, V. 101, pp. 259-265.

Batra, A. and Dareing, D. " Hydrodynamic Behavior of Graphite Powder Slurries in Journal Bearings," to appear in STLE Tribology Transactions.

Dai, F. and Khonsari, M.M. (1991) " On the Solution of a Lubrication Problem with Particulate Solids," *International Journal of Engineering Science*, V. 29, pp. 1019-1033.

Dai, F. and Khonsari, M.M. (1993)" A Continuum Theory of a Lubrication Problem with Solid Particles," *ASME Journal Of Applied Mechanics*, V. 60, pp. 48-58.

Dareing, D.W. and Dayton, R.D. (1992) "Non-Newtonian Behavior of Powder Lubricants Mixed with Ethylene Glycol," *STLE Tribology Transaction*, V.35, pp. 114-120.

Gohar, R. (1988), *ELASTOHYDRODYNAMICS*, Ellis Harwood Limited.

Johnson, K.L. and Cameron, R. (1967-68) " Shear Behavior of Elastohydrodynamic Oil Films at High Rolling Contact Pressures," Proc. Instn. Mech. Engrs., V.182, Pt.1, No.14, p.307.

Khonsari, M. M. and Esfahanian, V. (1988) " Thermohydrodynamic Analysis of Solid-Liquid Lubricated Journal Bearings," *ASME Journal of Tribology*, V. 110, PP. 367-374.

Khonsari, M. (1992) " High-Temperature Elastohydrodynamic Lubrication," Final report to WPAFB.

Khonsari, M.M. and Hua, D.Y. (1994) " Thermal Elastohydrodynamic Analysis Using a Generalized Non-Newtonian Formulation with Application to Bair-Winer Constitutive Equation", *ASME Journal of Tribology*, V.116, 37-46.

Roelands, C., Vlugier, J., and Waterman, H.(1963) " The Viscosity Temperature Relationship of Lubricating Oils and its Correlation with Chemical Constitution," *ASME Journal of Basic Engineering*, V.11, 601-610.

Rohsenow, W.M., Hartnett, J.P. and Ganic, E.N. (1985) *Handbook of Heat Transfer Fundamentals*, Second Edition, McGraw-Hill Book Company, New York.

9.3 References Section 5

Johnson, K.L. and Cameron, R. (1967-68) " Shear Behavior of Elastohydrodynamic Oil Films at High Rolling Contact Pressures," Proc. Instn. Mech. Engrs., V.182, Pt.1, No.14, p.307.

9.4 references Section 6.0

1) Heshmat, Hooshang; "SOLID-LUBRICATED ROLLER BEARING DEVELOPMENT - statice and dynanmic characterization of high-temperature, powder-lubricated materials, Wright Laboratory Report, WL-TR-92-2050, June 1992

(2) Bridgman, P. W.; "Effects of High Shearing Stress Combined with   High Hydrostatic Pressure," Phys. Rev. 48, 827-847 (1935); also see Collection of Experimental Papers of P. W. Bridgman, Vol. V, paper 112-2929

(3) Bridgman, P. W.; "Shearing Phenomena at High Pressure of Possible Importance for Geology," J. Geol. 44, 653-669; University of Chicago Press (1936);   also see Collection of Experimental Papers of P. W. Bridgman, Vol V, paper 115-3001

(4) Bridgman, P. W.; "Flow Phenomena in Heavily Stressed Metals," J.   Appl. Phys. S, 328-336 (1937); also see Collection of Experimental Papers of P. W. Bridgman, Vol V, paper 116-3018

(5) Bridgman, P. W., "The Compression of Sixty-One Solid Substances to 25,000 kg/cm2, Determined by a New Rapid Method," Proc. Am. Acad. Arts Sci. 76, 9-24 (1945); also see Collection of Experimental Papers of P. W. Bridgman,- Vol V, paper 148-3609

(6) Bridgman, P. W., "The Compression of 39 Substances to 100,000 kg/cm2," Proc. Am. Acad. Arts Sci. 76, 55-70 (1948); also see Collection of Experimental Papers of P. W. Bridgman,Vol V, paper 160-3819

(7)Boyd, J. and B. P. Robertson, " The Friction Properties of Various Lubricants at High Pressures," Trans. Amer. Soc. Mech. Engrs., Vol. 67, pp 51-56

(8) UNCAR Carbon Company, The Industrial Graphite Engineering Handbook, UCAR Carbon Company Inc., Parma, Ohio (1970)

(9) Peterson, Marshall B. and Johnson, Robert L.:

(10) Timoshenko, S. and J. N. Goodier, Theory of Elasticity, Second Edition, McGraw-Hill Book Company, 1951

(11) Atluri, S., "Traction Behavior and Physical Properties of Powder Graphite Lubricants Compacted to Hertzian Pressure Levels", Master's Thesis, University of Southwestern Louisiana, July 1994

(12) Dareing, D. W., "Traction Coefficients for Coated Bearing Races Lubricated With Teflon Transfer Films," ASME Journal of Tribology, Vol. 113 , pp 343-348

(13) Kannel, S. W. and T. A. Dow, "Analysis of Traction Forces in a Precision Traction Drive", ASME Journal of Tribology, Vol. 108, pp 403-410

(14) Barber, S. A. and J. W. Kannel, "A Rheological Model for Elastohydrodynamic Contacts Based on Primary Laboratory Data", ASME Jour. of Lub., 101, 3, pp 258-65

(15) Carter, F.W., "On the Action of a Locomotive Driving Wheel", Proc. Royal Soc., Seroes A, Vol 112, pp 151 -157

Appendix
EHL Analysis By Powder Slurries

ELASTOHYDRODYNAMIC LUBRICATION BY POWDER SLURRIES

D.Y. Hua and M. M. Khonsari *

Department of Mechanical Engineering

University of Pittsburgh

Pittsburgh, PA 15261

NOMENCLATURE

a	radius of circular contact for a deformed particle, m
c_p	specific heat of lubricant, J/(Kg·K)
c_1, c_2	specific heat of upper and lower bodies, J/(Kg·K)
d_p	diameter of particle, m
E	equivalent elastic modulus, N/m²
E_p	elastic modulus of particle, N/m²
E_s	elastic modulus of upper and lower bodies, N/m²
f	traction coefficient
f_p	friction coefficient of particles
h	film thickness, m
H_d	hardness of particle, N/m²
k	thermal conductivity of powder slurry, N/(s·K)
k_1, k_2	thermal conductivity of upper and lower bodies, N/(s·K)
l_1, l_2	effective length of particle contact with bounding surface, m
n	exponential index of power law
N_1, N_2	number of particles within effective length
p	pressure of hydrodynamic lubrication, N/m²
P_m	average contact pressure of deformed particle, N/m²
q	rate of heat generation per unit volume, N/(m²·s)
R	equivalent radius of curvature, m
s	sliding-rolling ratio
S_0	exponent of viscosity-temperature relationship
T	temperature of powder slurry, K
T_0	inlet temperature, K
T_1, T_2	upper and lower surface temperatures, K
u	velocity component in direction of motion, m/s
u_p	velocity of particle, m/s
u_r	rolling velocity, m/s
U_1, U_2	velocity of upper and lower surfaces, m/s
w_t	hydrodynamic load per unit width, N/m

* Please direct all communications on this paper directly to professor Khonsari

186

1. INTRODUCTION

The new generation of advanced turbine engines calls for very stringent requirements for many vital mechanical components such as bearings and seals. For these engines the speed is to be doubled and operating temperatures of the order of 800 °C are thought to be needed (cf. Dareing & Dayton, 1992). Since most conventional lubricants are ineffective at temperatures beyond roughly 200 °C, the need for alternative lubricants is crucial. One possible alternative is classified under so-called powder lubrication which utilizes appropriate lubricating particles such as dry TiO_2 - injected into the clearance space of a bearing. To this end, Heshmat (1992) reports remarkable pressure measurements of a powder lubricated slider bearing, showing a very similar profile as one would expect of a liquid lubricated bearing.

Alternatively, it has been suggested that one could make use of a carrier liquid - instead of air - to deliver embedded solid lubricants into the bearing. The carrier liquid may or may not be a conventional lubricant. For example, Dareing & Dayton(1992) used ethylene glycol to transport a *dense mixture* of graphite or molybdenum disulfide, thus forming what we shall refer to as "powder slurry".

There are two major effects that may take place when a high percentage of particles are added to a carrier liquid: (1) the slurry experiences a significant increase of viscosity as compared to that of the "pure" liquid, free of particles and (2) the slurry may cause a profound change in the rheological behavior of the carrier fluid. To predict the behavior and the performance of bearings lubricated with a powder slurry, one may have to rely heavily on experimental measurements. This is true since unlike most dilute mixtures, Einstein's equation cannot be used to accurately determine the increase of viscosity in terms of particle concentration. Also, the assumption of linearly viscous - commonly referred to as Newtonian - becomes questionable.

Recent archives in tribology contain a number of published papers that deal with relatively low concentrations of solid-liquid mixtures. For example, Khonsari & Esfahanian (1988) performed a thermohydrodynamic analysis of journal bearings lubricated with mixture of MoS_2, oil and teflon-oil at a concentration of 1 percent by weight of solids. The modelling approach suggested there is best suited for concentrations below 5 percent by weight. Khonsari et al. (1990) extended that theory to EHL problems at low solid concentrations. A totally different approach for treating the solid constituent is using the principles of mass transfer theory. This

$w_{i,e}$ load carried by individual particle due to elastic deformation, N
$w_{i,p}$ load carried by individual particle due to plastic deformation, N
w_p load carried by deformed particles, N/m
w_T total load, N/m
z exponent of viscosity-pressure relationship
γ shear strain rate, 1/s
λ concentration of particles by weight
μ viscosity of powder slurry, N·s/m²
μ_o viscosity of powder slurry at ambient pressure and inlet temperature, N·s/m²
μ' apparent viscosity, N·s/m²
v_p Poisson ratio of particles
v_i Poisson ratio of upper and lower bodies
ρ density of powder slurry, Kg/m³
ρ_o density of powder slurry at ambient pressure and inlet temperature, Kg/m³
ρ_1, ρ_2 density of upper and lower bodies, Kg/m³
ρ_f density of carrier fluid, Kg/m³
ρ_p density of particles, Kg/m³
τ shear stress, N/m²

2. THEORY

In the theoretical developments that follow, we have made a number of assumptions in addition to those that are common in TEHL analyses of pure fluids. Some of the assumptions will be described as the development proceeds. At this stage, to simplify the analysis, we assume that (i) particles are spherical in shape, equal in size and homogeneous; (ii) particles are uniformly dispersed in the carrying liquid and that there is no collision between them.

2.1 Generalized Reynolds Equation

In a recent paper, a form of a so-called generalized Reynolds equation was reported that can be used for TEHL analysis of a simple non-Newtonian fluid (cf. Khonsari & Hua, 1994). For a line-contact, the equation takes on the form given below.

$$\frac{d}{dx}[\rho h^3(\frac{1}{\mu_{e0}} - \frac{\mu_{e1}^2}{\mu_{e2}})\frac{\Phi}{\mu_{e0}}]\frac{d}{dx} = \frac{1}{2}(U_2 + U_1)\frac{d}{dx}(\rho h) + \frac{1}{2}(U_2 - U_1)\frac{d}{dx}[\rho h(1 - 2\frac{\mu_{e1}}{\mu_{e0}})] \qquad (1)$$

where μ_e represents what we have termed *equivalent viscosity* defined below:

$$\frac{1}{\mu_{el}} = \frac{1}{h^{l+1}}\int_0^h \frac{y^l}{\mu'(I_2)}dy \qquad l = 0,1,2 \qquad (2)$$

The equivalent viscosity is a function of the *apparent viscosity* of the non-Newtonian fluid, $\mu'(I_2)$, where I_2 represents the second invariant of the strain-rate tensor, i.e., $I_2 = \dot{\gamma}_{ij}\dot{\gamma}_{ij}$. The variation of the apparent viscosity with the shear strain-rate is dictated by the appropriate constitutive equation described next.

2.2 Constitutive Equations for Powder Slurry

Similar to the rheological model of a Newtonian fluid, the relationship between shear stress and shear strain rate can be expressed as,

$$\tau_{ij} = \mu'(I_2)\dot{\gamma}_{ij} \qquad (3)$$

For a non-Newtonian fluid the apparent viscosity is strongly dependant upon the strain rate. According to the experimental work of Dareing & Dayton (1992), the rheological behaviour of

approach is recently reported by Yousif & Nacy (1994) who analyzed a conical journal bearing. Theoretical developments for low and moderate solid concentrations based on the principles of modern continuum mechanics are reported by Dai & Khonsari (1991,1993).

In this paper, we focus our attention to thermoelastohydrodynamic analysis (TEHL) of powder slurries. For the purpose of modeling, we shall use the rheological properties of slurries reported by Dareing & Dayton (1992) who provide experimental results for the viscosity and rheological relations for MoS$_2$ as well as graphite slurries. They show that the power-law model closely fits the experimental data. Batra and Dareing (1993)) recently reported an study of powder slurries in journal bearings using the power law model.

Theoretical development for powder slurries is hindered by a number of complex processes that occur in the contact area. In this paper, we present appropriate governing equations that take into account the deformation of the particles between the bounding surfaces of an EHL line-contact conjunction. Through this deformation, particles are assumed to contribute to the load-carrying capacity. Furthermore, in predicting the lubricant and surface thermal fields, the contribution of the particles as they shear between the surfaces is taken into consideration. Results of extensive numerical simulations are presented for pressure distribution, film thickness, temperature rise, and traction coefficient.

powder slurries can be adequately described by the power law described below.

Power Law Model

The power-law model is one of the most commonly used constitutive equation in engineering for it can be used for a wide class of non-Newtonian fluids including shear thinning fluids (n<1) as well as many dilatant fluids (n>1). The constitutive equation for the power law is given below.

$$\tau = \mu |\dot\gamma|^{n-1} \dot\gamma \qquad (4)$$

where the index of power law, n, depend upon the type and concentration of the powder slurries. The viscosity of the powder slurry, μ, is affected by pressure and temperature. Using equations (3) and (4), the apparent viscosity becomes:

$$\mu'(\dot\gamma) = \mu |\dot\gamma|^{n-1} \qquad (5)$$

2.3 Visco-Pressure-Temperature Relationship

We shall assume that the pressure and temperature affect the viscosity in accordance with the general relation prescribed by Roelands et al. (1963):

$$\mu = \mu_0 \exp\left\{ (\ln\mu_0 + 9.67)\left[-1 + (1 + 5.1\times10^{-9}p)^z \left(\frac{T-138}{T_0-138}\right)^{-S_0} \right] \right\} \qquad (6)$$

where μ_0, which depends on the particle concentration, is the viscosity of the powder slurry at atmospheric pressure and room temperature. the parameters z and S_0 are unique to the lubricant used. This equation has been used extensively by many researchers in modeling EHL problems. Nevertheless, strictly speaking, its validity for powder slurries is yet to be determined experimentally. In the absence of available data, we shall proceed to use this relationship even though the values of z and S_0 for the powder slurries are unknown. Fortunately, the variation of z is relatively small for many fluids. Henceforth, we shall assume that a typical value z for an oil can also be used for a powder slurry. The value of S_0 will be estimated based on the available experimental data of Dareing & Dayton (1992). These authors show the effect of temperature on the slurry shear stress vs. shear strain. There is however no experimental data is

given to assess the effect of pressure on the slurry behavior. The shear stress as function of shear rate of MoS$_2$ ethylene glycol slurry at a concentration of 1:1 are provided in Dareing & Dayton (1992) for a range of temperature to which the interested reader may refer.

2.4 Density-Pressure-Temperature Relationship

The following relationship is used for estimating the density variation as a function of pressure and temperature (Dowson & Higginson, 1966).

$$\rho = \rho_0(1 + \frac{d_1 p}{1 + d_2 p})[1 + d_3(T-T_0)], \qquad (7)$$

where ρ_0 represents the density of the slurry evaluated at the appropriate particle concentration, λ_w, from the following relationship:

$$\rho_0 = \frac{\rho_l}{1 - \lambda_w(1 - \frac{\rho_l}{\rho_p})}$$

Parameters d_i (i=1,3) appearing in equation (7) along with parameters z & S_0 in equation (6) are given in Table 2 and Table 4 in the results section.

2.5 Film Shape

For a line-contact configuration, the film shape is given by

$$h = h_{00} + \frac{x^2}{2R} - \frac{2}{\pi E'}\int_{-\infty}^{\infty} p(\xi)\ln(x-\xi)^2 d\xi \qquad (8)$$

where $h_{ww} = h_0 +$ constant.

2.6 Load Carrying Capacity

The total load carrying capacity of the mixture is composed of two parts: one component results from the deformation of particles, w_p, and the other due to the integrated effect of the pressure in the slurry, w_l, given below

$$w_l = \int_{-\infty}^{\infty} p(x)dx \qquad (9)$$

The contribution of the particles to the load is discussed next.

2.7 Deformation and the Load-Carrying Capacity of Particles

The constitutive equation of Dareing and Dayton (1992) described in section 2.2 was experimentally obtained using a rheometer under the atmospheric conditions. For an EHL application, where the slurry undergoes considerable amount of pressure, it is likely for the particles embedded in the carrier fluid to deform under the application of both the normal load and the local hydrodynamic pressure. Consider a spherically-shaped particle in the contact region, see Figure 1. Under the action of the normal load, the particle may undergo elastic or plastic deformation. The load carried by an individual particle due to *elastic deformation*, $W_{i_{el}}$, is:

$$w_{i_e} = \frac{1}{6}\left[d_p - h(x)\right]^{\frac{3}{2}} d_p^{\frac{1}{2}} E_{pm} + p(x)v_p A_{i_{el}} \tag{10}$$

where the first term results from the elastic deformation of a particle between two roller and the second term is added to *represent* the contribution of the local pressure acting on the particle (cf. Khonsari et al.,1989). Recently the same formulation was adopted by Tudor (1992) in study of influence of additives on traction in EHL. It should be mentioned, however, that accurate consideration of the local hydrodynamic pressure on a particle and its contribution to the load-carrying capacity requires a detailed modeling. For the problem underconsideration, the contribution of the hydrodynamic pressure on the load is relatively small. The term $p(x)v_p A_{i_{el}}$ in equation (10) adequately captures the effect of hydrodynamic pressure. In equation (10) the parameter $A_{i_{el}}$ denotes the contact area of an individual particle; E_{pm} represents the equivalent elastic modulus of the particle and the contacting surface defined below:

$$\frac{1}{E_{pm}} = \frac{1}{2}\left[\frac{1-v_p^2}{E_p} + \frac{1-v_s^2}{E_s}\right] \tag{11}$$

When the particle deformation is elastic, the mean contact pressure, p_m, is

$$p_m = \frac{w_{i_e}}{\pi a^2} \tag{12}$$

where a is the radius of circular contact area given below in terms of the load, particle diameter

and the modulus of elasticity:

$$a = \left[\frac{3}{4}\frac{w_{i_e}d_p}{E_{pm}}\right]^{\frac{1}{3}} \tag{13}$$

In general, when the size of particle happens to be large compared to that of the film thickness, particles may undergo plastic deformation. Consideration of plastic deformation is indeed a difficult task, for there are many uncertainties in the modeling approach. In the absence of experimental data for slurry, in this paper we shall present a simple approach which relates the plastic deformation to the material hardness in a similar manner as the plastic deformation experienced by a spherical indentor in the Brinell hardness test. The relationship between the load and the radius of circular contact area due to plastic deformation is:

$$w_{i_p} = \pi a^2 H_d \tag{14}$$

where H_d is the hardness of particle and a is the radius of circular contact which is assumed to remain approximately the same as given by the elastic deformation evaluated at the so-called critical load. The critical load is the load where both the mean contact pressure and contact size evaluated based on the elastic or plastic deformation yield identical results (cf. Archard, 1980). A spherical particle is, therefore, assumed to deform plastically when the mean contact pressure reaches the hardness of particle, H_d. In other words, in this simplified method, the load carried by particles due to plastic deformation is estimated based on the assumption that there exists a load which yields a mean contact pressure equal to the hardness of particle. Using expressions of equations (13) and (14), the load carried by a plastically deformed particle as a function of particle hardness becomes:

$$w_{i_p} = \frac{9}{16}\pi^3 H_d^3\left(\frac{d_p}{E_{pm}}\right)^2 + p(x)v_p A_{i_p} \tag{15}$$

Where A_{i_p} is contact area of an individual particle due to plastic deformation. The expressions (10) and (15) give the load carrying capacity of a single particle due to elastic and plastic

deformation, respectively. The load-carrying capacity due to deformation of all particles is, therefore, determined by the double summation of

$$w_p = \sum_i^{N_s} \sum_i^{N_t} w_i \qquad (16)$$

where N_s, N_t are the number of particles that come in contact with the bounding surfaces in x and z directions, respectively. Assuming that particles are uniformly dispersed and do not pile up in the contact region, the number of particles is:

$$N_j = l_j \sqrt{\left(\frac{V_t}{l_1 l_2}\right) \frac{6\lambda_w}{\pi d_p^3} \frac{(\rho_t/\rho_p)}{[1-\lambda_w(1-\rho_t/\rho_p)]}} \qquad j=1,2 \qquad (17)$$

where λ_w is the concentration of particles by weight; V_t is the volume of the powder slurry within the region where particles contact the bounding surfaces; l_j is the effective length along which the particles deform. The subscript j=1,2 denote x and z direction, respectively. For a line-contact configuration, $l_2=1$ is used for per-unit-width basis.

Finally, the total load is composed of load carried by the powder slurry and deformed particles defined as:

$$w_T = w_f + w_p \qquad (18)$$

2.8 Viscous Dissipation and Shear Heating

To determine the slurry temperature profile, we must turn our attention to the energy equation. In the energy equation, the diffusive heat flux for a mixture is contributed by three individual terms (cf. Rohsenow et al.,1985): (1) heat-conduction as described by the Fourier's law, i.e. - k ∇T, where k denotes the thermal conductivity of the mixture; (2) the contribution due to interdiffusion of species, given by Σ j i , and (3) diffusional conduction term which is of second order and therefore in most situations is negligibly small. The energy equation for a mixture is:

$$\rho \frac{Di}{Dt} = \frac{Dp}{Dt} - \nabla \cdot q + \nabla T - \nabla \cdot \left(\sum_i j_i i_i\right) + \Phi \cdot q \qquad (19)$$

where Φ is the viscous dissipation, q is a source term representing the rate of heat generation per unit volume, and i is the enthalpy expressed as:

$$i = \epsilon_i + \frac{p}{\rho} \qquad (20)$$

where ϵ_i is the internal energy per unit mass. Assuming that no chemical reaction occurs between the powder and the carrier fluid, i.e. the mixture nonreacting, the term $(\Sigma j_i i_i)$ becomes negligible. We shall next express the energy equation in terms of temperature using the following relationship:

$$\frac{Di}{Dt} = \frac{1}{\rho}(1-\beta T)\frac{Dp}{Dt} + c_p \frac{DT}{Dt} \qquad (21)$$

where β is defined as:

$$\beta = -\frac{1}{\rho}\left(\frac{\partial \rho}{\partial T}\right)_p \qquad (22)$$

Therefore, for a steady-state, laminar flow, the energy equation reduces to the following equation

$$k\frac{\partial^2 T}{\partial y^2} = \rho c_p u \frac{\partial T}{\partial x} + u \frac{T}{\rho}\left(\frac{\partial \rho}{\partial T}\right)_p \frac{\partial p}{\partial x} - \mu \dot{\gamma}^2 - q \qquad (23)$$

As a result, contact with the bounding surfaces in addition to normal stress, the deformed particles may experience slippage between the bounding surfaces. This will give rise to the existence of a shear heating which is represented by the heat source q in the energy equation. The total heat generated due to shear heating between the deformed particles and the bounding surfaces is:

$$Q = 2 f_p w_p |U_1 - u_p| \qquad (24)$$

191

8

9

where U_i is the velocity of the surfaces (i=1,2) and f_i is the friction coefficient between a particle and the surface. The parameter u_p represents the particle velocity, which is assumed to be at the average of the surface velocities, viz:

$$u_p = \frac{1}{2}(U_1 + U_2) \tag{25}$$

The heat source per unit volume is therefore:

$$q = \frac{Q}{V_i} \tag{26}$$

where V_i was defined in section 2.7.

The boundary conditions for the energy equation are:

$$T_i(x) = T_0 + \frac{1}{\sqrt{\pi \rho_i c_i \lambda_i U_i}} \int_{-\infty}^{x} -k \frac{\partial T}{\partial y} \frac{dx}{\sqrt{x-s}} \qquad i=1,2 \tag{27}$$

2.9 Traction Coefficient

The traction force of the powder slurry is composed of two components: one comes about because of the integrated effect of slurry viscous shear stress over the appropriate length and the other is due to contribution of the shear stress between particles and surfaces. The traction coefficient, f, is simply the ratio of the traction force over the total load, viz.:

$$f = \frac{1}{w_T} \left| \int_{-\infty}^{x_b} \mu \cdot \dot{\gamma} \, dx - f_p w_p \right| \tag{28}$$

3.0 RESULTS AND DISCUSSION

A computer program was developed to simulate the governing equations described in Section 2. The numerical solution scheme for the generalized Reynolds equations requires an iterative procedure. The interested reader is referred to Khonsari & Hua (1994) for details. In consideration of the load carried by deformed particles, an additional iteration loop was needed to determine the load carried by powder slurry. This load was obtained by subtracting the load carried by the particles, w_p, from the total load, w_T. The simulations presented in this section

10

correspond to the thermoelastohydrodynamic lubrication of powder slurry composed of a mixture of MoS_2 particles added to ethylene glycol which serves as the carrier fluid. The concentration of particle to fluid is 1:1 by weight. Based on the experiments of Dareing & Dayton (1992), the Newtonian rheological model is adequate for pure ethylene glycol while the power law model can be used for the mixture. The pure ethylene glycol results are generated using the power law model with the index of n=1. The input data used in the simulations is shown in Table 1 - 4.

The property values of MoS_2 particles assumed in the simulations requires some discussion, for particle deformation - elastic or plastic - may play an important role. Molybdenum disulfide is known to have a layered hexagonal structure, thus exhibiting anisotropic behavior in the basal (symmetry) plane and also perpendicular to the basal plane. The elastic modulus in the basal plane is isotropic and can be determined by a tensile test. However, in the direction perpendicular to the basal plane, the elastic modulus is affected by the interaction between layers in compression (cf. Gardos, 1989). For the problem under consideration, it is difficult to ascertain the orientation of the particles in the EHL contact. Most likely as particles go through the contact region, they assume a random orientation. Therefore, for the simulations presented in this paper, we shall assume that elastic modules can be represented by a value between the moduli in the basal plane direction and normal to it.

3.1 Effect of Viscosity Increase for a Powder Slurry

When a high percentage of particles are added to a fluid, the viscosity of the mixture significantly increases. The carrying lubricant, ethylene glycol, is a very thin fluid: at a temperature of 323 K and ambient pressure, it has a viscosity value of $\mu = 0.0049$ Pa·s. In contrast, the viscosity of the powder slurry - MoS_2 + ethylene glycol with ratio as 1:1 by weight is increased to 0.0258 Pa·s, which is in the range of a normal oil (Dareing, et al, 1992). The experimental data also showed that the powder slurry distorts the linearly viscous rheological behavior of ethylene glycol to a shear-thinning type fluid. Since viscosity of a lubricant plays an important role in TEHD lubrication, the simulation results presented show a considerable difference between pure ethylene glycol and its powder slurry.

3.1.1. Pressure and Temperature Profile

The pressure profile and film shape of powder slurry and ethylene glycol are shown in Figures 2A and 2B. Under the load and velocity simulated, the pressure profile using pure

11

192

ethylene glycol is fairly close to that of a dry Hertzian contact. The film thickness is less than 0.5μm which cannot protect the lubricated surfaces, for the surface roughness could be larger than the film thickness. The pure ethylene glycol results are, therefore, presented for discussion purposes, only. The powder slurry, on the other hand, exhibits a typical EHL pressure profile, with a pressure spike near the outlet of contact. A significant increase in the film thickness is seen in the powder slurry, which is indicative of the beneficial effect of adding a large amount of particles into a pure, carrier fluid. Another typical result is that increasing the rolling/sliding ratio tends to increase the pressure spike and shift its location closer to the center of contact. A similar trend for other shear thinning fluids have been reported in the literature (cf. Khonsari & Hua, 1993).

The relatively high viscous dissipation effect resulting from the increase in the viscosity in a powder slurry is the main contributor to the film temperature rise shown in Figures 3A and 3B. In addition to the mid-film temperature profile, Figs. 3A and 3B show the numerical prediction for the temperature rise on the upper surface and on the lower surface for slip ratios of 0.1 and 0.2, respectively. Whereas the powder slurry simulations predict a pronounced temperature rise in both the inlet and the contact region, the temperature profiles for the pure ethylene glycol show a temperature rise at a much lower rate. The powder slurry tends to yield a more profound temperature rise when the slip ratio is increased.

3.1.2. Traction Coefficient

An important consideration in EHL studies is the characterization of the traction behavior. The computed value of traction coefficients for a range of slip ratios are shown in Figure 4. The dashed lines representing pure ethylene glycol, show traction values in the order of 10^3 which are much less than typical EHL traction with normal oil. As pointed out earlier, the pure ethylene glycol results are presented for discussion purposes only since a full consideration of such a thin fluid requires one to include surface roughness effects. Figure 4 also contains two sets of results which are reported for the slurry traction coefficient as a function of the sliding ratios. One case (chain-dot lines) corresponds to the situation where the particle deformation - and therefore the load carrying capacity - is neglected. In other words, the entire load is carried by the powder slurry alone. In this case, the traction behavior is very similar to what is typically observed in traction measurement of shear thinning fluids. Starting from pure rolling, the traction rise from

zero in roughly a linear fashion reaches a plateau followed by a downward trend as the sliding rolling ratio increases. In comparison, the consideration of particle deformation results in noticeably higher traction values. Next we shall examine the effect of particle deformation in greater depth.

3.2 Effect of Particle Deformation

As a particle deforms - elastically or plastically - it will support a portion of the load. Therefore, for a given load w, consideration of particle deformation dictates that a less amount of load is required to be carried by the slurry alone since $w_f = w_t - w_p$. Therefore, the TEHD pressure distribution predicted for the powder slurry within the "contact region" is smaller than that of the ethylene glycol. The occurrence of spike for powder slurry as described earlier is merely due to the increase in the mixture viscosity - see Figure 2.

Another consequence of particle deformation consideration is the shear heating as a result of particle slip at the boundaries. The model predicts that, under the operating conditions simulated, the effects of shear heating due to particle slip at the boundary is of secondary importance compared to the effect of the increase in viscosity. Additional shear between deformed particles and bounding surfaces would further contribute to the rise in the traction coefficient (cf. Fig.4). When the particle deformation is taken into account, the model predicts that the traction coefficient has a finite value even under pure rolling condition (i.e. when S=0). The reason for this phenomenon is that the friction between deformed particles and bounding surfaces would contribute to the traction coefficient, although the rolling friction dominates the shear behavior of powder slurry in pure rolling condition.

3.3 Effect of Particle Hardness

Hardness of particles plays an important role in predicting plastic deformation in our model. A mean hardness value of MoS_2 is generally reported in the range of 1-1.5 Moh's and the maximum hardness in a direction parallel to the basal planes is about 7-8 Moh's (cf Lancaster, 1966). A parametric study of the effects of hardness of MoS_2 on the load carrying capacity is presented in Fig.5. When the hardness is small compared to the elastic modulus, particles tend to undergo a significant amount of plastic deformation under a relatively small load, hence very little load is carried by the particles. The effect of increasing hardness of particles, on the other hand, results in an increase in the predicted load carrying capacity by

deformed particles.

3.4 Effect of Particle Size

Figure 6 illustrates how the particle size affects the load carrying capacity. There is a significant amount of increase in the load that deformed particles carry when the diameter of particles is greater than the film thickness but smaller than $1.5\mu m$. A direct consequence of increasing particles is in the increase of the particle deformation and therefore load carrying capacity. Nevertheless, further increasing of particle size would eventually lead the particles to undergo plastic deformation so that further deformation would not increase the load carried by particles. Consideration must also be given to the number of particles in the contact region. For a given concentration, the number of particles would decrease as particle size is increased. The combination of two factors discussed above will yield a reduction in the load carrying capacity of deformed particles.

4.0 SUMMARY AND CONCLUDING REMARKS

A general procedure for performing thermoelastohydrodynamic analysis of powder slurries is presented. The appropriate governing equations include a generalized non-Newtonian TEHL formulation that can accept any simple constitutive rheological equation. Consideration are given to the particle deformation (elastic or plastic) and shearing effects thereof. In computing the elastic deformation, in addition to the normal load, the effect of local hydrodynamic pressure was taken into consideration in an approximate fashion. The plastic deformation model was based on a simple relationship between the mean contact pressure and the particle hardness. Experimental tests are needed to better assess the property values assumed in this paper, to verify and perhaps to make improvement in the model particularly for the assessment of the particle deformation. A computer program was developed to simulate the governing equations. Results are presented for a slurry made of MoS_2, particles mixed with ethylene glycol, as a carrier fluid, at a concentration level of 1:1 by weight. This slurry is known to exhibit behavior than can be effectively characterized using the power-law model. The viscosity of this mixture is considerably higher when compared to that of the carrier fluid alone. Whereas the ethylene glycol may not adequately protect the surfaces, the mixture is found to provide the necessary film thickness to prevent surface to surface contact. Extensive numerical simulations were performed to predict

the performance of this mixture in an EHL line-contact configuration. The results show that the behavior of MoS_2 slurry, particularly the pressure profile, is similar in trend to what one encounters in a typical EHL solution with conventional lubricants. However, depending on the operating conditions, it is found that the lubricating particles inserted in the slurry, themselves, tend to carry a portion of the load through which they tend to undergo significant amount of deformation. Furthermore, as a result of the slippage of the particles at the bounding surfaces, there is an increase in the temperature field. Most importantly, the deformation consideration gives rise to traction coefficients higher than that of typical shear-thinning lubricants.

ACKNOWLEDGEMENTS

14

15

REFERENCES

Archard, J.F., 1980, "Wear Theory and Mechanism," *Wear Control Handbook*, Peterson, M. and Winer, W. (editors), ASME publication, N.Y., p.35-80.

Baira, A. and Dareing, D. W., 1993, " Hydrodynamic Behavior of Graphite Powder Slurries in Journal Bearings," to appear in *STLE Tribology Transactions*.

Dai, F. and Khonsari, M.M., 1991," On the Solution of a Lubrication Problem with Particulate Solids," *International Journal of Engineering Science*, V. 29, pp. 1019-1033.

Dai, F. and Khonsari, M.M., 1993," A Continuum Theory of a Lubrication Problem with Solid Particles," *ASME Journal Of Applied Mechanics*, V. 60, pp. 48-58.

Dareing, D.W. and Dayton, R.D., 1992, "Non-Newtonian Behavior of Powder Lubricants Mixed with Ethylene Glycol," *STLE Tribology Transaction*, V.35, pp. 114-120.

Dowson, D. and Higginson, G.R., *Elastohydrodynamic Lubrication*, Pergamon Press, 1977.

Gardos, M.N., 1989, "On the Elastic Constants of Thin Solid Lubricant Films," Proceedings of the 16th Leeds-Lyon Symposium on Tribology, Lyon, 3-13.

Heshmat, H., 1992 , " The Quasi-Hydrodynamic Mechanism of Powder Lubrication: Part II - Lubricant Film Pressure Profile," *STLE Lubrication Engineering*, V. 48, pp. 373- 383.

Roelands, C., Vlugter, J., and Waterman, H., 1963, " The Viscosity Temperature Relationship of Lubricating Oils and its Correlation with Chemical Constitution," *ASME Journal of Basic Engineering*, V.11, 601-610.

Rohsenow, W.M., Hartnett, J.P. and Ganic, E.N., 1985, *Handbook of Heat Transfer Fundamentals*, Second Edition, McGraw-Hill Book Company, New York.

Khonsari, M. M. and Esfahanian, V. , 1988, " Thermohydrodynamic Analysis of Solid-Liquid Lubricated Journal Bearings," *ASME Journal of Tribology*, V. 110, PP. 367-374.

Khonsari, M.M., Wang, S.H. and Qi, Y.L., 1989, "A Theory of Liquid-Solid Lubrication in Elastohydrodynamic Regime", *ASME Journal of Tribology*. V.111, 440-444.

Khonsari, M.M., Wang, S.H. and Qi, Y.L., 1990, "A Theory of Thermo-Elastohydrodynamic Lubrication of Liquid-Solid Lubricated Cylinders", *ASME Journal of Tribology*, V.112, 259-265.

Khonsari, M.M. and Hua, D.Y., 1994, " Thermal Elastohydrodynamic Analysis Using a Generalized Non-Newtonian Formulation with Application to Bair-Winer Constitutive Equation", *ASME Journal of Tribology*, V.116, 37-46.

Lancaster, J.K., 1966, "Anisotropy in the Mechanical Properties of Lamellar Solids," *Wear*, V. 9, 169-188.

Tudor, A., 1992, "Some Aspects of Influence Additivated Oils About Traction Force in Elastohydrodynamic Regime," Proceedings of 6th Conference on EHD Lubrication and Traction, University of Suceava, Romania.

Yousif, A., and Nacy, S. , 1994, " The Lubrication of Conical Journal Bearings with Bi-Phase (Liquid-Solid) Lubricants," *Wear*, V.172, 23-28.

Table 1 physical properties of cylinders

E_i	2.075×10^{11}	Pa
υ_i	0.3	
ρ_i, ρ_i	8000.0	kg/m³
k_1, k_2	38.0	N/(s·K)
c_1, c_2	470.0	J/(kg·K)

Table 2 physical properties of lubricant

	powder slurry	ethylene glycol	
μ_o	0.0258	0.0049	Pa·s
ρ_o	1781.0	1093.2	kg/m³
k	0.2668	0.2668	N/(s·K)
c_p	2488.6	2488.6	J/(kg·K)
n	0.991	1.0	

Table 3 physical properties of particle

E_p	3.4×10^{10}	Pa
υ_p	0.13	
H_d	3.136×10^{9}	Pa
ρ_p	4800.0	kg/m³
d_p	2.0×10^{-6}	m
f_p	0.1	

196

LIST OF FIGURES

Table 4 typical operating condition

w_i	5.7×10^3	N/m
u_i	8.0	m/s
s	0.1	
R	0.05	m
T_0	323	K
z	0.6	
S_0	0.9499 (powder slurry)	
d_1	1.2 (ethylene glycol)	
d_2	0.583×10^9	m²/N
d_3	1.684×10^9	m²/N
d_3	-6.5×10^4	1/ K
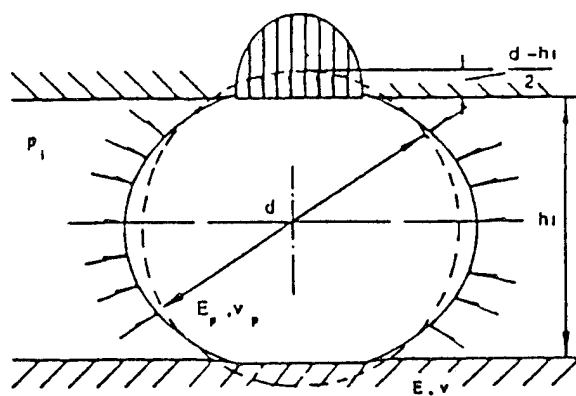
Figure 1   Illustration of a deformed particle in the contact region
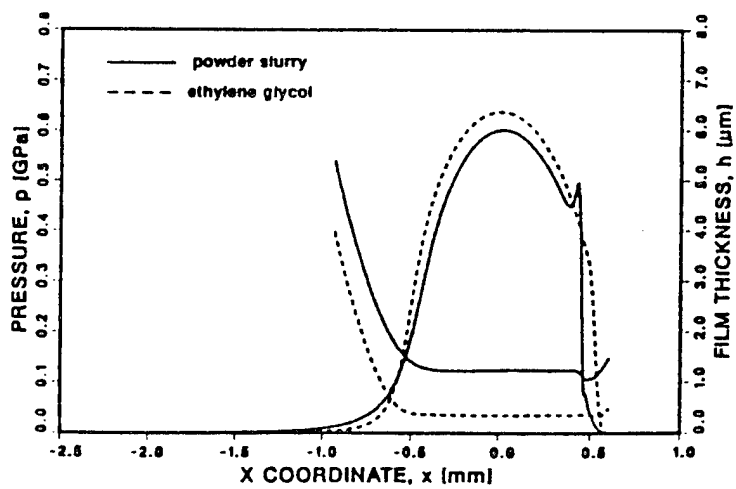
Figure 2A   Pressure profile and film thickness
(w= 0.57×10⁶ N/m, u,= 8.0 m/s, d,= 2.0μm, s=0.1)
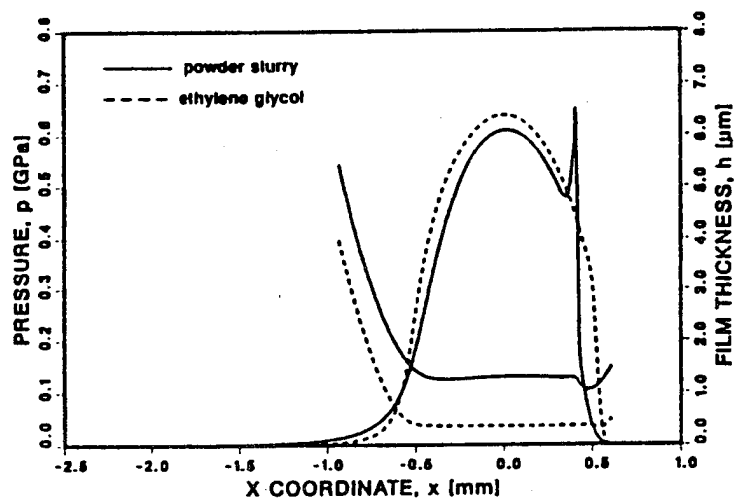
Figure 2B   Pressure profile and film thickness
(w= 0.57×10⁶ N/m, u,= 8.0 m/s, d,= 2.0μm, s=0.2)
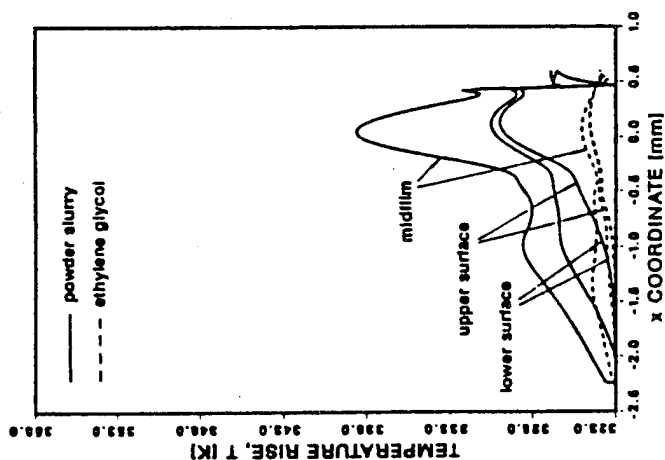
Figure 3A   Temperature rise
(w= 0.57×10⁶ N/m, u,= 8.0 m/s, d,= 2.0μm, s=0.1)
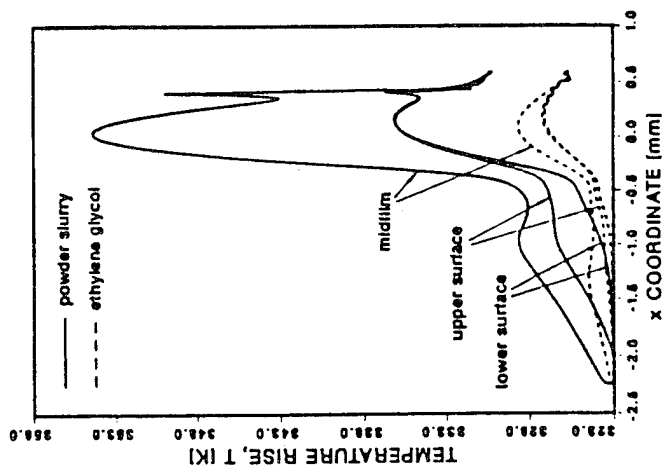
Figure 3B   Temperature rise
(w= 0.57×10⁶ N/m, u, = 8.0 m/s, d, = 2.0μm, s=0.2)
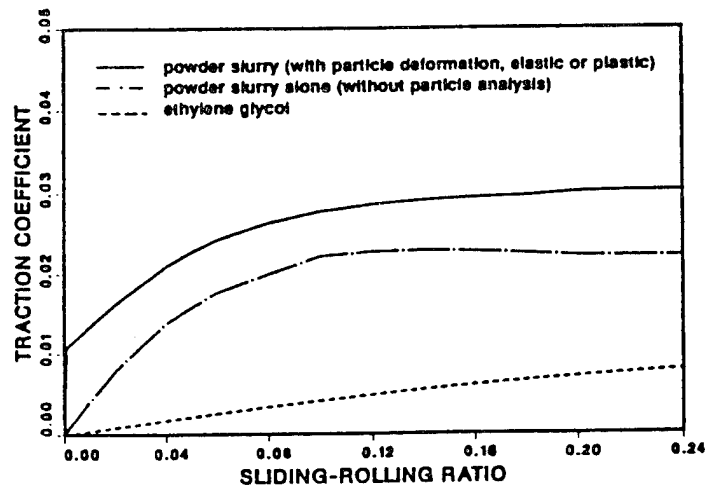
Figure 4   Traction coefficient
(w= 0.57×10⁶ N/m, u,= 8.0 m/s, d,= 2.0μm)

200
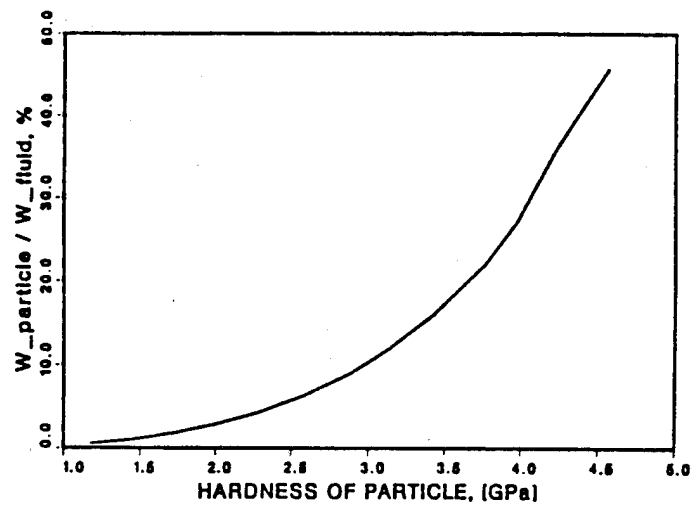
Figure 5   Load carrying capacity of deformed particles vs. hardness of particle
(w= 0.57x10⁴ N/m, u,= 8.0 m/s, d,= 2.0μm, s=0.1)
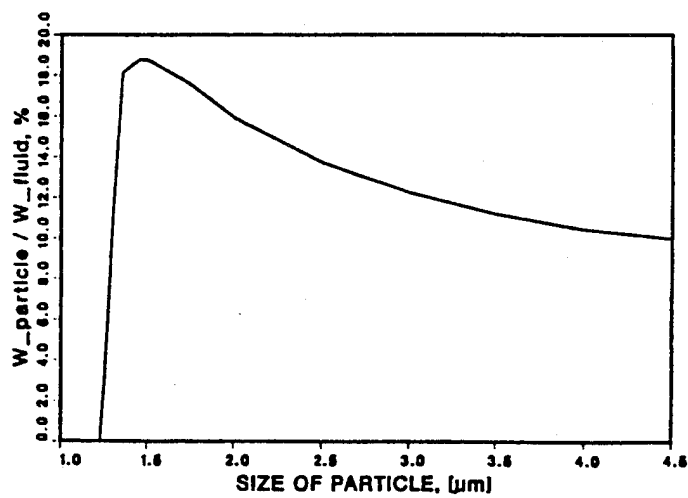
Figure 6   Load carrying capacity of deformed particles vs. size of particle
(w= 0.57x10⁴N/m, u,=8.0m/s, d,=2.0μm, s=0.1)